Navigability of the river Waal
A stochastic approach

by

Steffen Hetzer

A thesis presented to the
Universität Stuttgart in fulfillment of
the requirements for the degree of
"Diplom-Ingenieur Umweltschutztechnik"

Delft, The Netherlands, May 2005

I hereby declare that I am the sole author of this thesis.
I authorize the Technische Universiteit Delft and the Universität Stuttgart to reproduce this thesis by photocopying or other means, in total or in part, at the request of other institutions or individuals for the purpose of scholarly research.

Delft, 30st of May, 2005

Steffen Hetzer

Abstract

Aim This thesis addresses the stochastic modelling of river morphology and the consequences for the navigability of a 37 km long stretch of the river Waal in The Netherlands. It should primarily give insight into the capabilities and limitations of one- and multi-dimensional models in predicting navigability, especially if a one-dimensional approach is sufficient or a multi-dimensional model has to be used to stochastically assess the navigability of a river.

Furthermore, it aims to give valuable advice for two groups of interest: (1) the river manager, who is interested in the navigability of the complete stretch, possible restrictions in space and time and the fulfillment of the minimum navigation requirements; (2) the modeller, who is interested in important sources of uncertainty for the navigability as well as an efficient setup of the simulations in terms of necessary number and time duration of the model runs.

Method The navigability of the river is assessed with the help of two morphodynamic models: a one-dimensional model based on the program SOBEK and a quasi-3D model based on the modelling package Delft3D. Both numerical models are used in a Monte Carlo Analysis (MCA) to take account of the uncertainty involved in the discharge, and compared to data of Least Measured Depth (LMD).

The principle of a MCA is to conduct a large number of model runs with statistically equivalent inputs. For each model run, a discharge time series of five years duration is statistically generated according to a prescribed probability distribution. On the basis of 100 simulations, the navigability is assessed in terms of the statistics of these model outputs.

Five characteristics of the navigability are defined: (1) the navigable percentage of time of the complete stretch; (2) the navigable percentage of time of each location along the river; (3) the navigable percentage of locations along the river as a function of time; (4) the percentage that a location forms the bottleneck location; (5) the probability that the navigation requirements are not given. Those characteristics are used in different approaches of analysis of the models and the data comparison to answer the questions of the river manager.

A method to estimate the number of required model runs to reach a certain accuracy of the model output as well as the behaviour of the uncertainty related to the number and duration of the simulations are presented to satisfy the needs of the modeller.

Results The 1D model leaves only one parameter to estimate navigability: the cross-sectionally averaged water depth. The quasi-3D model gives new possibilities as the navigability can be assessed in two dimensions, depth and width. An alternating behaviour of the channel in bends can be reproduced. Several additional morphologic phenomena like the evolution of a transverse bed slope in bends are included.

Both models show similar results in the prediction of the navigability for the first four of the five defined characteristics. The prediction of the restricting location per timestep, the "bottleneck location" differs. A correction for the transverse bed slope in bends shows to be essential and is successfully applied in the 1D model, in a parametric form. The comparison with the data of Least Measured Depth is not satisfying, due to several influences that are not included in the models (e.g. buoy placement and dredging). Furthermore, the criterion used is very sensitive.

For both models, the required number of simulations can be predicted very well beforehand. The effort for a MCA can thus be reduced. The uncertainty shows a strong dependency on the duration of the model runs. Higher uncertainties are found for short periods in order of one single year. This leads to the conclusion that a Monte Carlo Analysis is especially required for shorter model periods, as in this case the uncertainty related to the discharge is high. The discharge is found to have a large influence on the average navigability of the river, as well as on the resulting uncertainties.

Conclusions and recommendations The 1D model is applicable for a wide range of assessments of the navigability. For most of the assessed characteristics of navigability, the two-dimensional morphological effects that are not included seem to be of minor importance. The 1D model is able to predict the large-scale morphology (in the order of several kilometers) similar to the quasi-3D model. Furthermore, the range of uncertainty of the navigability estimated by both models shows a high agreement. The uncertainty included in the discharge time series seems to have a similar effect on both model outputs.

The quasi-3D model offers the opportunity to investigate the morphology and its effects on the navigability in two dimensions, including the corresponding morphologic effects as well as the shifting behaviour of the navigation channel in bends. This becomes important when locations that form restrictions for the navigation traffic should be identified. Even if the comparison with the LMD data is not completely satisfying, the results of this approach give the impression to be more trustworthy.

New data is necessary to validate the findings of the models. The available data of Least Measured Depth proves to be insufficient; it is not recommendable to identify one single location as being limitative to navigation. A new data set should be established: for a single stretch of the river, the water depth and the related channel width has to be measured and entered into a database for several permanent locations along the river on a daily basis.

The influence of the uncertainty in the discharge on the uncertainty of the navigability is large. Monte Carlo Analysis proves to be a possibility to assess these uncertainties. Nonetheless, the dependency of the uncertainty on the time duration shows that stochastic modelling is not always reasonable. For long modelling periods, a deterministic modelling approach still has its justification.

The same conclusion accounts for the model choice. A multi-dimensional model is not always necessary. For many of the relevant questions, a one-dimensional model can give sufficient insight with considerably lower effort.

Further research is necessary to assess the time dependency of the uncertainties and to investigate the influences of other uncertainties and their relative importance for different model durations. Finally, this kind of analysis should be applied to practical measures within the framework of the Dutch "Room for the River" program.

Keywords Navigation, Navigability, Morphology, Waal, Stochastic Modelling, Probabilistic, Monte Carlo Analysis, MCA, Uncertainty, Delft3D, SOBEK.

Acknowledgements

This thesis on the navigability of the river Waal has been carried out at the Department of Hydraulic Engineering of the Technische Universiteit Delft/ The Netherlands and submitted to the Universität Stuttgart/ Germany in fulfillment of the thesis requirements for the degree of "Diplom-Ingenieur Umweltschutztechnik".

The committee of supervisors consisted of:
Prof. Dr. Ir. H.J. de Vriend (TU Delft; WL|Delft Hydraulics)
Ir. S. van Vuren (TU Delft)
Ir. K. Sloff (TU Delft; WL|Delft Hydraulics)
Ir. H. Havinga (TU Delft; Rijkswaterstaat Directie Oost Nederland)
Prof. Dr.-Ing. S. Wieprecht (Universität Stuttgart)

I would like to thank Saskia van Vuren for her great help during the whole time of my thesis work as well as all my committee members for their valuable advice.

I especially would like to thank my girlfriend Ulla for her daily support which carried me through my time in Delft as well as my friends who helped with their phone calls and visits.
Special thanks to my parents who made my studies possible in the first place.

Contents

List of Tables

List of Figures

List of Symbols and Abbreviations

a	distance of the buoy from the bank	[m]
a, b	parameter of the sediment transport formula	[-]
A	secondary-flow direction coefficient	[-]
A_f	cross sectional flow area	[m^2]
A_S	sediment transporting cross-sectional area	[m^2]
B_n	normal channel width	[m]
B_{nav}	navigation channel width	[m]
B_S	sediment transporting width	[m]
B_{S_1}	security distance from the bank	[m]
B_{S_2}	security distance from the buoy	[m]
c	propagation speed of a morphological feature	[m/s]
c_α	accuracy interval for the Gaussian distribution	[-]
C	Chézy roughness coefficient	[$m^{1/2}$/s]
C_g	Chézy roughness of the grains	[m]
C_{bf}	Chézy roughness of the bedforms	[$m^{1/2}$/s]
d_a	correction of water depth	[m]
d_{min}	corrected water depth	[m]
$\bar{d}$	cross-sectional averaged water depth	[m]
D	deposition of suspended sediment	[m/s]
D_*	dimensionless grain diameter	[-]
D_{10}	grain size where 10% of the bed material is finer	[m]
D_{50}	median grain diameter	[m]
D_{90}	grain size where 90% of the bed material is finer	[m]
E	entrainment of suspended sediment	[m/s]
f_s	shape factor for the grains	[-]
Fr	Froude number	[-]
g	gravitational acceleration	[m^2/s]
h	water depth	[m]
i_b	transverse bed slope	[-]
k	bed roughness height	[m]
K	diffusion coefficient	[-]
L	morphologic length scale	[m]
m	sample size	[-]
N	number of simulations	[-]
p	fractile of the distribution	[-]
q_{lat}	lateral discharge per unit width	[m^2/s]
Q	discharge	[m^3/s]
r	bend radius	[m]

R	hydraulic radius	[m]
s	sediment transport per unit m width	[m^2/s]
s_b	bed load sediment transport per m width	[m^2/s]
s_{lat}	lateral sediment influx per unit river length	[m^2/s]
S	sediment transport through the cross-section	[m^3/s]
S_1, S_2	sediment distribution at a bifurcation	[m^3/s]
t	time increment	[s]
T	dimensionless bed-shear parameter	[-]
T_W/T_D	morphologic time scales	[s]
T_{xx}, T_{xy}, T_{yy}	horizontal exchange of momentum	[kg/ms^2]
u_*	bed shear velocity	[m/s]
u, v	depth averaged velocity in longitudinal and transversal direction	[m/s]
x, y	coordinates in longitudinal and transversal direction	[m]
x_i, x_k	upper and lower boundary of the confidence interval	[-]
z_b	bed level	[m]

α_b	Boussinesq constant	[-]
δ	height of bedforms	[m]
Δ	relative sediment density	[-]
ϵ_p	sediment porosity	[-]
κ	Von Karman coefficient	[-]
λ	length of bedforms	[m]
μ	mean value	[-]
ν	kinematic viscosity	[m^2/s]
Θ	dimensionless Shields parameter	[-]
Θ_{cr}	critical Shields parameter	[-]
ρ	water density	[kg/m^3]
σ	standard deviation	[-]
τ_x, τ_y	shear stress in x,y direction	[N/m^2]
τ'	shear stress without bedforms	[N/m^2]
τ_b	bed shear stress	[N/m^2]
τ_{cr}	critical shear stress	[N/m^2]

1D	One-dimensional
2D	Two-dimensional
3D	Three-dimensional
Delft3D	Two- and three-dimensional numerical modelling package
ECTM	European Conference of Ministers of Transport
LMD	Least Measured Depth
MCA	Monte Carlo Analysis
MHW	Maatgevand Hoogwater (critical flood condition)
NAP	Nieuw Amsterdams Peil (New Amsterdam Datum)
NVVP	Nationaal Verkeer en Vervoersplan (National Traffic and Transportation Plan)
OLA	Overeengekomen Lage Afvoer (Agreed low water discharge)
OLR	Overeengekomen Laagwater Referentieniveau (Agreed low water condition)
SOBEK	One-dimensional numerical modelling package

Chapter 1

Introduction

1.1 Problem identification

Most important factors for the navigability of a river are the available water depth and channel width, which both depend on the bed topography and the water level. In order to guarantee safe navigation on a river, locations and time periods where the navigation channel dimensions are restricted have to be determined.

In practice the navigability is examined with the help of single- or multi-beam soundings and Geographic Information Systems (GIS). On the Dutch Rhine, daily measurements of the water depth are used to inform the navigation traffic about temporal bottlenecks. The channel width is, especially in narrow bends, delineated by the placement of buoys.

Another way of investigating navigability is numerical modelling, using one- or multi-dimensional (2D or 3D) modelling packages to get an impression about problematic locations at different spatial and temporal scales, which can be used to give advice to the river manager for the application of short- or long-term and small- or large-scale river training measures.

The use of morphodynamic models is always associated to uncertainties. One reason for these uncertainties is a lack of knowledge in the modelling parameters and boundary conditions. A possibility to assess the involved uncertainties is the use of stochastical modelling. An attempt to examine the navigability of the Dutch Rhine branches with a one-dimensional model used in stochastic mode was made by Van Vuren [60]. In this research, the uncertainty related to the discharge hydrograph was taken into account: Each one of the simulations was driven by a different statistically derived discharge time series. This resulted, in contrast to deterministic modelling, not in only one model outcome, but in a different outcome for every model realisation, each representing one possible state of the navigability of the river. A one-dimensional model approach was used due to the high computational effort related to stochastic modelling. Thereby, the impact of several two-dimensional morphological phenomena were neglected.

It now has to be questioned whether a one-dimensional model is sufficient for an assessment of the navigability or if a multi-dimensional model has to be used. One-dimensional models can only give insight into the cross-sectional averaged water depth, while multi-dimensional models can provide additional information about effects like transverse slopes in bends and the influence of strongly alternating river geometry that could play an important role for navigability. Beyond that, multi-dimensional models also allow an examination of the navigable width in combination with the water depth and thus can represent a better view of navigability in reality.

1.2 Research objective

The objective of this thesis project is to develop methods for assessing the navigability of the river Waal for ships of various draughts, taking into account the spatial and temporal variability of the river morphology and hydraulics. Because modelling is related to several uncertainties, a stochastic Monte Carlo approach is chosen. Due to the high number of required model runs, a Monte Carlo Analysis (MCA) is very computationally intensive. Using a two-dimensional morphodynamic model may lead to an extreme increase of the computational effort. Therefore, it has to be carefully determined to what extent a one-dimensional model is sufficient for the assessment of navigability and for which questions a more detailed, but also more complicated and computationally intensive two-dimensional model has to be used.

Research questions

This thesis now compares the findings of a one- and a quasi-three dimensional model, both used in a Monte Carlo Analysis, with measured data of navigation channel depth and width. It should primarily give answer to the question whether a one-dimensional model approach is sufficient or if a three-dimensional model has to be used to stochastically assess the navigability of a river.

The results of this study should give advice to two different groups of interest:

1. The river manager, who is interested in the navigability of the river, the identification of critical locations for navigation, the capability of each model in predicting navigability as well as the agreement of the models with the measurement data and the possible need for new data for validating the model results.

2. The modeller, who is interested in the influence of the uncertainty in the discharge on the results, the efficient use of Monte Carlo Analysis in the assessment of navigability, in terms of how many simulations are required to reach a certain accuracy of the statistics, and how the time duration of those simulations influences the uncertainty in the results.

The interests of the river manager and the modeller can be formulated as concrete questions. These questions and a reference to the relevant sections of the thesis are given in Figure 1.1.
In addition to answers to these questions, this thesis work should give the following insights:

- Insight into the capabilities and limitations of one- and multi-dimensional models in predicting navigability
- Insight into post-processing methods for one-dimensional models to account for two-dimensional morphologic effects
- Insight into the impact of two-dimensional morphological features on navigability
- Insight into the influence of the uncertainty in the discharge on the navigability
- Insight into new data needed for the validation of the numerical models

- Insight into further features that need to be included in the models as well as the future model setup
- Insight into the efficient use of Monte Carlo Analysis in the assessment of navigability

Group of interest	Question	Answer	
		SOBEK	Delft3D
River manager	1. What is the navigability of the complete stretch? 2. What is the navigability of each location? 3. Which time periods are critical for navigation? 4. Which locations are critical for navigation? 5. What is the chance of not fulfilling the navigation requirements?	Section 4.1 to 4.3	Section 5.2 to 5.3
	6. To what extent can a 1D model be used ? 7. Do the models represent the reality?	Section 6.1 Section 6.2	
Modeller	1. What is the influence of the uncertainty in the discharge on the navigability?	Section 5.4	
	2. How many simulations are necessary to reach a certain accuracy of the model output? 3. How does the uncertainty behave for a changing duration/ number of model runs?	Section 7.1 Section 7.2	

Figure 1.1: Overview of the questions of the river manager and the modeller

1.3 Research area

A 37 km long stretch of the Waal between km 886 (at Nijmegen) to km 923 (downstream of Tiel) (see Figure 1.2) is chosen to compare the results of two numerical models and measured data. This stretch shows geometrical features like bends with rather moderate radii and wide and narrow floodplains arranged alternating on the left and right side of the river. The effect of bends on the river morphology is the cause of a transverse slope with the formation of pool/ point bars, while geometrical complex reaches like alternating floodplains can cause shoals and erosion pits. These features may be reason for nautical bottlenecks that constitute problems for navigation. Table 1.1 and Table 1.2 give an overview of the bends and floodplains in this stretch. This stretch is from here on referred to as Midden-Waal.

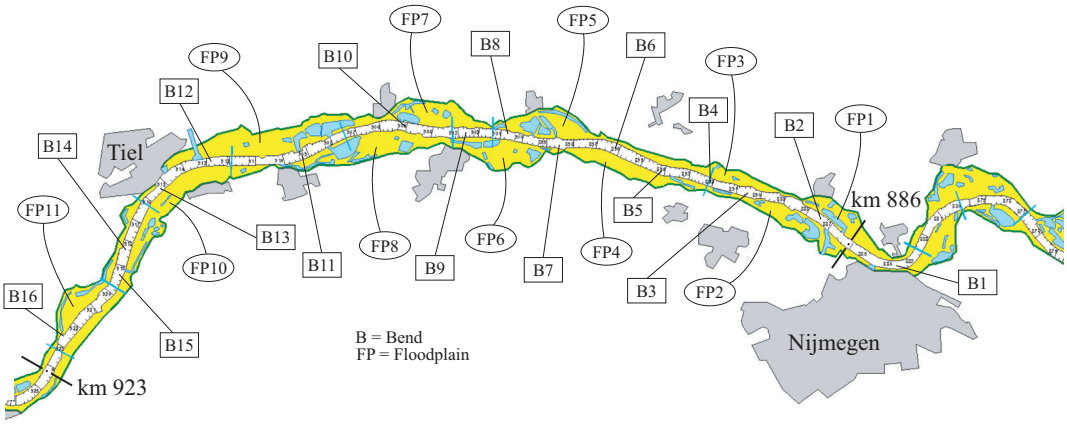

Figure 1.2: Area of research, the Midden-Waal

No.	Name	Type	From km	To km	Length [km]	Radius [m]
1	Nijmegen	bend	882.35	884.85	2.50	700
	Nijmegen Crossing	crossing	884.85	886.35	1.50	
2	Slijk-Ewijk	bend	886.35	889.75	3.40	4070
	Slijk-Ewijk Crossing	crossing	889.75	890.30	0.55	
3	Loenen	bend	890.30	891.55	1.25	6120
	Loenen Crossing	crossing	891.55	892.20	0.65	
4	Ewijk	bend	892.20	893.00	0.80	4870
	Ewijk Crossing	crossing	893.00	893.60	0.60	
5	Winssen	bend	893.60	894.70	1.10	3370
	Winssen Crossing	crossing	894.70	895.40	0.70	
6	Wely	bend	895.40	896.90	1.50	3870
	Wely Crossing	crossing	896.90	897.70	0.80	
7	Deest	bend	897.70	899.45	1.75	6870
	Deest Crossing	crossing	899.45	900.10	0.65	
8	Hooge Waard	bend	900.10	901.20	1.10	6870
	Hooge Waard Crossing	crossing	901.20	902.10	0.90	
9	Druten	bend	902.10	903.90	1.80	5870
	Druten Crossing	crossing	903.90	904.50	0.60	
10	Ochten	bend	904.50	906.20	1.70	4170
	Ochten Crossing	crossing	906.20	907.70	1.50	
11	Beneden Leeuwen	bend	907.70	910.75	3.05	4620
	Beneden Leeuwen Cross.	crossing	910.75	911.65	0.90	
12	Wamel	bend	911.65	914.95	3.30	2370
	Wamel Crossing	crossing	914.95	915.60	0.65	
13	Passewaay	bend	915.60	916.35	0.75	2370
	Passewaay Crossing	crossing	916.35	916.70	0.35	
14	Zennewijnen	bend	916.70	917.65	0.95	2370
	Zennewijnen Crossing	crossing	917.65	918.15	0.50	
15	Ophemert	bend	918.15	920.45	2.30	3620
	Ophemert Crossing	crossing	920.45	921.00	0.55	
16	Varik	bend	921.00	922.40	1.40	4870
	Varik Crossing	crossing	922.40	923.00	0.60	

Table 1.1: Location of bends and crossings along the Midden-Waal

No.	Name	From km	To km	Side
1	Oosterhoutsche Waarden	885	888	right
2	Weurt	887	890	left
3	Loenensche Buitenpolder	890	893	right
4	Winssensche Waarden	894	898	left
5	Hiensche Uiterwaarden	898	901	right
6	Afferdensche&Deestsche Waarden	899	903	left
7	Ochtensche Buitenpolder	902	906	right
8	Drutensche Waarden	905	910	left
9	Willemspolder	910	914	right
10	Wamelsche Uiterward&Dreumelsche Waard	911	918	left
11	Stiftsche Uiterwaarden	920	922	right

Table 1.2: Location of floodplains along the Midden-Waal

1.4 Report outline

The report is organised as follows:
In Chapter 2 the factors which influence river morphology and navigability are explained.
In Chapter 3 an overview of the method and tools is given: the used models, the stochastic method and the data used for comparison are described in detail.
In Chapter 4 the results of the one-dimensional model SOBEK are presented, while in Chapter 5 the results of the two-dimensional model Delft3D are shown.
Chapter 6 follows with a comparison of the model results with the available data.
In Chapter 7 different aspects of stochastic modelling like the required sample size and the influence of the number and the duration of the model runs on the uncertainty are discussed.
Chapter 8 finishes with the conclusions and recommendations.

Chapter 2

Morphology and Navigation

2.1 The river Rhine

Topography The Rhine is an important river in Western Europe. With a catchment area of around 252,000 km^2, the Rhine-area is one of the largest river catchments in Europe. The Rhine rises as a snowmelt-fed river in the Swiss Alps and ends as a rain- and snowmelt-fed lowland river in the North Sea. During its 1,320 km-long journey it flows through six countries namely Switzerland, Lichtenstein, Austria, Germany, France and The Netherlands. Its most important tributaries are the Aar, Neckar, Main, Moselle, and Ruhr rivers; canals also link the river with the Maas, Rhône-Saône, Marne, and Danube (via the Main) valleys.
The Rhine-area can be divided into the following parts:

- Alpenrhein from the source to Lake Constance (Switzerland)
- Hochrhein from Lake Constance to Basel (km 0-150)
- Oberrhein from Basel to Bingen (km 150-530)
- Mittelrhein from Bingen to Bonn (km 530-660)
- Niederrhein from Bonn to the bifurcation Pannerdensche Kop in The Netherlands, with the German-Dutch border at Lobith (km 660-868). At the Pannerdensche Kop the river splits into two branches: the Waal and the Pannerdensch Kanaal, latter again splits into two branches at the IJsselkop: the Nederrijn-Lek and the IJssel [15] (see Figure 2.1).

This research focuses on the river Waal in The Netherlands.

Hydrology The sub-basins of the Rhine have different hydrological characteristics and show a certain opposing behaviour. For this reason the discharge of the Rhine is less fluctuating than that of other European rivers of the same dimension [29]. The upper course in Switzerland has a lower discharge in winter than in summer, because a large part of the winter precipitation is stored as snow and thus only contributes to the discharge in the warm season. For the Niederrhein this relation is reversed, because in the low mountains and the lowland the precipitation during winter is not stored as snow and summer precipitation largely evaporates. The relation between the OLA-discharge (Overeengekomen Lage Afvoer - agreed low water discharge) and the MHW-discharge (Maatgevand Hoogwater - critical

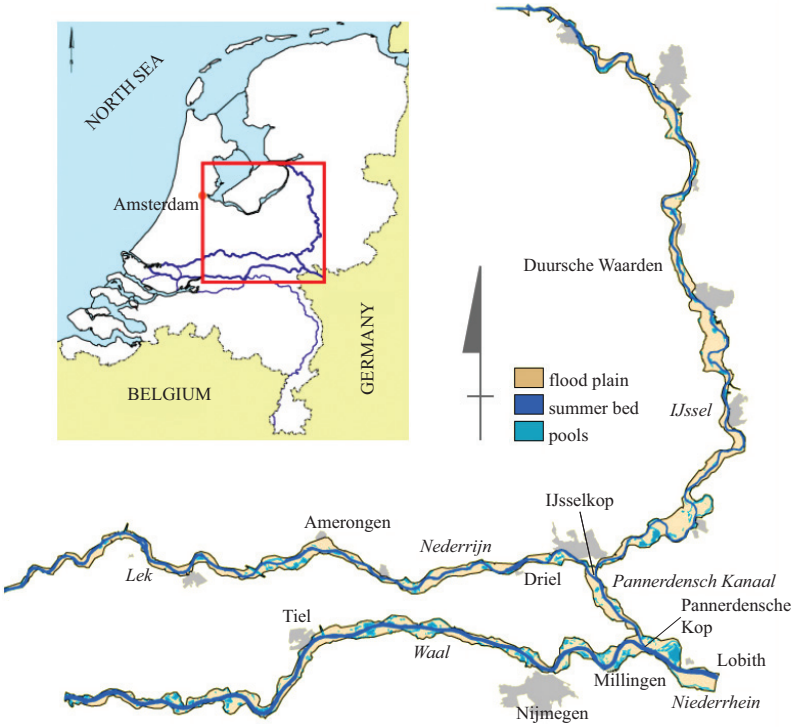

Figure 2.1: Rhine branches in The Netherlands

flood condition) for the Rhine at the German-Dutch border is 1:16 [7]. The high water season for the Rhine in The Netherlands is between January and March; the dry period can be expected from August to October.

The future changes in climate are of importance for the discharge regime of the Rhine. Several scenarios project an increase in temperature between 1°C and 4°C in the next 100 years. These forecasts are of course subject of discussion, but possible effects still should be considered. For a temperature increase of 4°C the Rhine is expected to change to a predominantly rainfed river and the sum of the annual discharge will increase by 10% for the year 2100 [37]. Also the intra-annual variation of the discharge will increase. This means that there will be more water during the winter (causing higher floods) and less water during the summer, leading to more severe and longer lasting droughts.

The Rhine in The Netherlands At Lobith (km 868) a mean discharge Q_{mean} of 2,220 m^3/s is measured. From Lobith on, the river flows another 170 km until it empties into the North Sea. At the Pannerdensche Kop, the Rhine diverts into the Waal and the Pannerdensch Kanaal, which itself diverts into the Nederrijn-Lek and the IJssel at the IJsselkop. The local morphology condition of the bifurcation at the Pannerdensche Kop controls the discharge distribution between the Pannerdensch Kanaal and the Waal while the weir at Driel in the Nederrijn controls the discharge distribution between the Nederrijn and the IJssel under low and intermediate flow conditions. The flow is distributed following a pattern that was agreed upon a convention between the provinces of Gelderland, Overijssel, Utrecht and Holland in 1771: At the Pannerdensche Kop approx. 2/3 of the discharge goes into the Waal, while approx. 1/3 goes into the Pannerdensch Kanaal. At the IJsselkop the flow of the Pannerdensch Kanaal is divided to approx. 2/3 into the IJssel and approx. 1/3 into the Nederrijn.

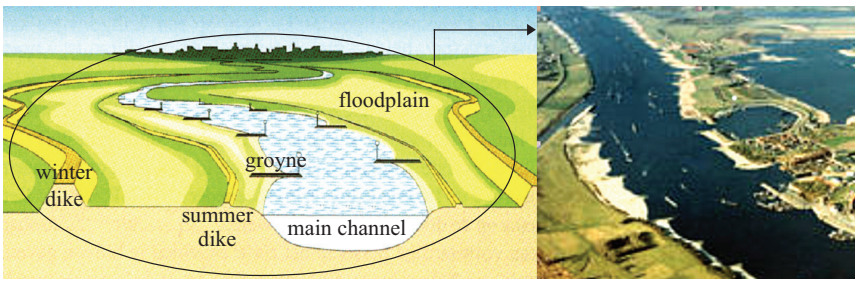

Figure 2.2: Outline of the Rhine in The Netherlands, courtesy of Rijkswaterstaat

The Rhine in The Netherlands underwent a large number of river training measures in the 19th and 20th century. Today it appears as a river with a fixed planform, non-permeable groynes, a single main channel intensively used for navigation, summer dikes that protect the floodplains from frequent inundation, silted-up flat floodplains used as meadows and winter dikes (major levees) forming a flood defense to protect a dense population living in low lying polders behind them [61] (see Figure 2.2) . The tidal influence of the North Sea is largely suppressed. The barrier at Hagenstein regulates the tidal influence in the Nederrijn, while the barriers at Haringvliet and Volkeraksluizen regulate the tidal influence in the Waal. This study focuses on the part of the Waal without tidal influence.

Despite of the spatial variability within the branches, Table 2.1 shows rough approximations of the dimensions and the characteristics of the Niederrhein, Waal and IJssel.

Characteristic	**Symbol**	**Rhine branch**			**Unit**
		Niederrhein	**Waal**	**IJssel**	
Length	L	5	83	93	km
Width main channel[1]	B_m	330/440	260/370	90/120	m
Width floodplain	B_f	850	550	550	m
Bed slope	i	0.13	0.12	0.10	m/km
Chézy coefficient main channel	C_m	40	40	40	$\sqrt{\text{m}}$/s
Chézy coefficient floodplain	C_f	35	35	35	$\sqrt{\text{m}}$/s
Grain size of bed material	D_{50}	0.005	0.001	0.001	m
Mean discharge	Q_{mean}	2,220	1,480	317	m^3
Agreed low water discharge	Q_{OLA}	1,020	818	172	m^3
Annual sediment load	S_{yr}	570,000	507,000	37,000	m^3/yr

[1] width of main channel excluding and including groyne section

Table 2.1: Dimensions and characteristics of the Rhine branches, after Van Vuren [57]

2.2 Navigation on the Rhine

Transportation on the Rhine underwent a rapid growth in the second half of the last century [33]. Today pusher trains with 2,000 to 6,000 horsepowers with 2 or 6 barges are sailing on the Rhine. Several important technical innovations have been made, for example the LASH barges (Lighter Aboard SHip, with barges that can directly be loaded into special oversea-ships), the distri-ship (which is able to carry pallets) and roll-on/roll-off traffic (ships carrying trailers)[17]. Ship size has still been increasing in the recent years. The mode value for tank ships on the Rhine increased from 1,000-1,500 t in 1980

to 1,500-3,000 t in 2001, for ships carrying dry goods this value increased from 650-1,000 t to 1,500-3,000 t [41] [42].

The European Conference of Ministers of Transport (ECMT) defined design vessels and their dimensions in 1954 [14]. The Western European waterways were divided into six classes. The Rhine is classified in the following categories:

Branch	Category
Niederrhein	VIc
Waal	VIc
Pannerdensch Kanaal	Va
Nederrijn	Va
Lek	Va
IJssel	Va

Table 2.2: Classification of the Rhine according to ECTM [14]

Thus, pushing units with a length of up to 280 m and a gauge of up to 34.2 m have to be able to navigate on the Niederrhein and the Waal safely. The range for the draught of those ships varies from 1.8 m up to 2.8 m for motorships and from 2.5 m to 4.5 m for pushing units.

Navigation is the most important transport form in The Netherlands. About 40% of all international and 20% of all national transport is carried by ship. In 1998, 368 million tons freight were transported, of which 46% by ship, 39% by truck, 4% by train and 11% via pipeline. 220 million tons were carried on the Waal in this year, with a provided traffic service of 55 billion kilometertons. Especially the container shipping is getting more and more important. Currently 40% of all containers from and via Rotterdam travel on the Waal. With 165,000 ships crossing the Dutch-German boarder each year, the Waal is the most densely sailed river in Western Europe [36].

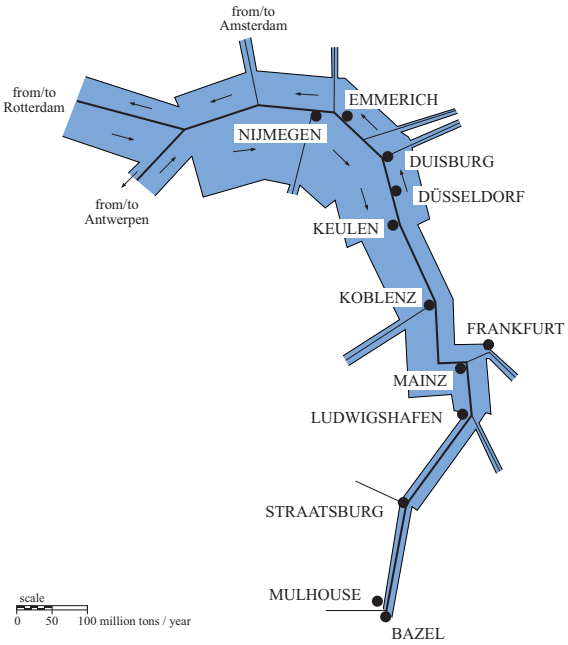

Figure 2.3: Transport between The Netherlands and Germany, after Middelkoop [36]

The traditional strength of inland navigation is that it is safe and cheap. These advantages still hold good and in recent times the environmental aspect has been added. Most important for further development of inland navigation is the integration into the transport chain (the transport chain involves the interaction between four factors: price, punctuality, flexibility and care of the cargo) and so the effective linking with rail and road transport. This demands that inland navigation is capable of "just in time" delivery and a high reliability [18]. This requires a river with a high capacity that is navigable on its whole length all the time without physical obstructions.

Safe, efficient and profitable inland shipping requires a deep and wide navigation channel. The National Traffic and Transportation Plan (in Dutch: Nationaal Verkeer en Vervoersplan, NVVP [67]) gives guidelines with respect to the navigation channel requirements. According to this plan, during discharges above a threshold value of 1,020 m^3/s at Lobith (equals 818 m^3/s for the Waal), the navigation channel in the Niederrhein and the Waal should have a guaranteed width of 150 m and a depth of 2.8 m. This threshold value is called Agreed Low Water Discharge (in Dutch: Overeengekomen Lage Afvoer, OLA) and has a probability of exceedance of 95%. The associated water depth of 2.8 m is called Agreed Low Water Level (in Dutch: Overeengekomen Laagwater Referentieniveau, OLR).

In the 20^{th} century several severe droughts occurred in The Netherlands that had influence on navigation [11]. Table 2.3 shows the ten most severe droughts during this time including the lowest discharge and the number of days with low discharges.

Year	Duration[1] [days]	Minimal discharge at Lobith [m^3/s]
1947	115	620
1949	148	635
1921	201	670
1954	81	680
1959	104	715
1971	62	760
1943	65	780
2003	65	780
1976	78	782
1991	48	794

[1] number of days with discharges lower than 1000 m^3/s at Lobith

Table 2.3: Most severe droughts of the Rhine, after De Wit [11]

2.3 Requirements for navigation

2.3.1 Channel dimensions

Save navigation needs a river channel that is sufficient in depth and width dimensions over the length of the river and over continuous periods of time.

The water depth at a certain location depends on the variation in water level and in bed level in time. The variation of water depth at dominant locations is of great importance for shipping companies and the river manager, as it gives an impression of the navigability of the river. It is further important to know during which periods of a year a certain water depth is available and also on how many consecutive days.

The actual depth required for efficient navigation must be larger than the draught of the ship. It was shown in experiments that the manoeuvrability of ships decreases rapidly

when the keel clearance is less than 30% of the draught [26]. In the case of irregularities in the river bed the manoeuvrability decreases even further. A second need for extra depth is the tilting of sailing ships in longitudinal direction (squat). A third reason is that a sailing ship induces a return current in the opposite direction which causes a lowering of the water level in order to produce the necessary acceleration of the flow. The ship therefore sails in a depression which extent depends on the ship's speed as well as on the cross-section of the ship and the channel [68]. The effects of this return flow induced by navigation are discussed in detail in Bhowmik et al. [2].

The required width depends on the space two encountering ships need. An encounter as well as a passing should be possible without reducing the sailing speed. Especially in sharp curved bends and on densely sailed rivers the channel width can form a problem for navigation.

2.3.2 Bottlenecks

Goldsteen&Glansdorp [19] distinguish between two kind of bottlenecks to assess the navigability of a river: traffic bottlenecks and nautical bottlenecks. The latter is defined as: "a location or area where the safe navigation of the vessel concerned will be impeded by the conditions which prevail at the time the vessel passes through that area or location". Havinga [21] defines the term bottleneck as a "location where the fairway dimensions are not met" referring to the low water depth and width for the river Waal defined in the Dutch National Traffic and Transportation Plan (NVVP) [67].

After Goldsteen&Glansdorp the parameters that are important to locate nautical bottlenecks are the dynamic sailing characteristics of a vessel as well as the channel configuration, external effects like wind and tide and aids for navigation. The analysis of nautical bottlenecks thus divides into seven steps from defining the keel clearance over the calculation of required width and depth to the calculation of locations and time intervals where those requirements are not given, even including meteorological effects [19].

In this research the navigability of the Waal is assessed on a simplified level. Ships with draughts between 1.5 m and 5.0 m are assumed to be sailing on the river. The under keel clearance and the above mentioned effects of sailing ships are neglected. Additionally, the adherence of the minimal channel dimensions of 2.8 m in depth and 150 m in width set by the NVVP is assessed.

2.3.3 Present state of the river Waal

The Waal underwent a large number of river training measures that resulted in a highly navigable river. The first regulation works were carried out in the middle of the 18^{th} century; two further stages followed end of the 19^{th} and beginning of the 20^{th} century. An example of the history of the river works on the Waal from km 913 to km 930 is shown in Figure 2.4.

The river training was first conducted to improve the flood protection, only in the last stage the navigability was considered. The low-water bed was enhanced by longitudinal dikes (summer dikes) and perpendicular groynes as well as bed protection measures like armoured layers in bends. Today the Waal has a normal channel width of 260 m, where the navigation channel dimensions during low flow conditions are 150 m in width and 2.8 m in depth. In order to improve the navigability of the Rhine, the low water depth has been increased from 2.5 m to 2.8 m only in the recent years. An increase of the low water width

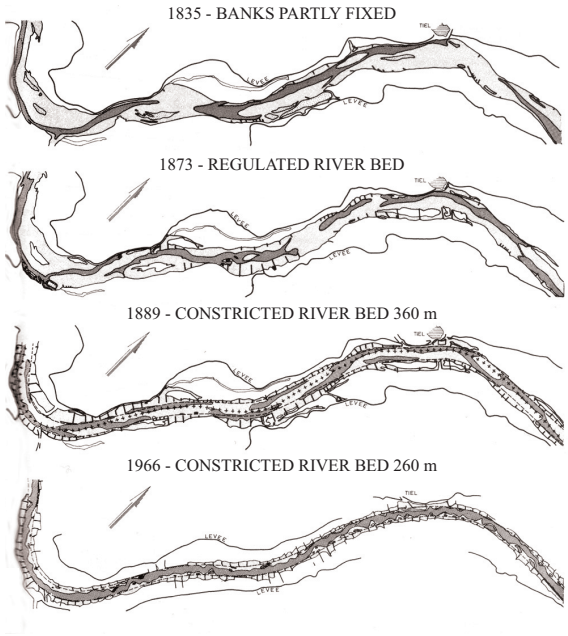

Figure 2.4: History of improvements of the Waal, km 910-930, after Jansen et al. [26]

up to 170 m is planned according to the National Traffic and Transportation Plan (NVVP) [67], but not achieved yet.

Maintaining a deep and wide navigation channel is of great economical relevance. For a standard pushing unit with 6 barges, every additional cm draught means an extra freight capacity of 8.2 t per barge. The 30 cm gained from rising the OLR-depth from 2.5 m to 2.8 m thus lead to an increase of the capacity of $6 * 30 * 8.2 = 1,476$ tons. The economical savings of this measure are estimated with 178 million Euro. The increase in navigation channel width is of similar importance. A width that is not sufficient can lead to delays at bottlenecks and raises the risk of accidents [36].

The following section gives an overview over the morphologic processes at different scales that have influence on the bed evolution and thus on the navigability of the river. Large parts of this section are based on the work of Van Vuren [57].

2.4 Morphological processes

A wide variation of morphological changes, from individual grain motion to the evolution of the entire river system, can be observed in an alluvial river. Those changes can be divided into classes following the different spatial and temporal scales at which they take place (Figure 2.5). As shown in Section 2.3, the Waal today is river with a fixed planform; meandering, braiding and alternating bars do not appear due to fixed river banks, continuous groynes and dykes.

The Waal is an alluvial river, it's sediment consists of sand and gravel with a mean diameter of 2 mm [26]. Velocities vary between 0.5 m/s and 1.5 m/s, during floods velocities up to 2 m/s occur. Froude numbers stay in the low range, subcritical flow is predominant. Morphological effects at the following spatial and temporal scales can be observed in the Waal [6]:

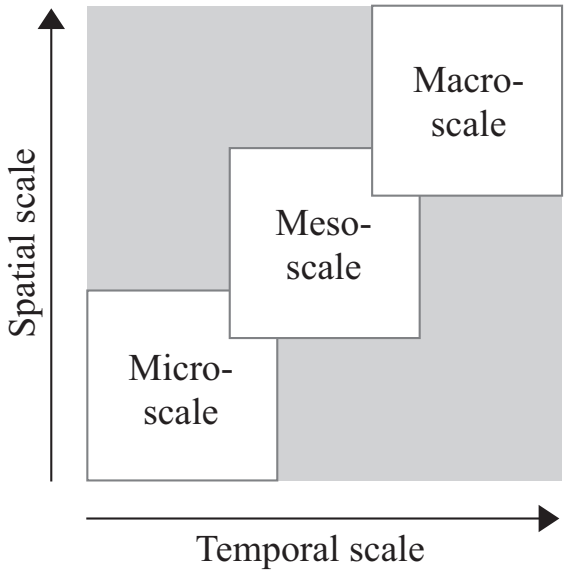

Figure 2.5: Morphologic scales in the Waal, after De Vriend [6]

Scale levels	**Morphological phenomena**
Micro	- bedforms, such as ripples and dunes - lateral and vertical segregation of sediment fractions
Meso	cross sectional profile evolution: - transverse bed slope and pointbar/pool formation in bends - crossings between opposite bends - formation of shallow and deep parts in geometrically complex reaches - bank erosion - overbank sand deposition - local scour in groyne fields and formation of so-called groyne flames - local scour e.g. around bridge piers
Macro	- longitudinal profile evolution - evolution of geometry at river bifurcations

Table 2.4: Morphodynamic scale levels in the Rhine in The Netherlands [57]

2.4.1 Micro-scale

Micro-scale effects are very much dependent on the interaction between the river bed and the flow [55], thus the flow velocity (and therefore the discharge) and the grain size of the bed have great influence. With the help of the Van Rijn bedform predictor [54] the type and the dimension of bedforms can be estimated depending on two parameters: the excess skin friction T and the dimensionless grain size D_*.

$$T = \frac{\tau' - \tau_{cr}}{\tau_{cr}} \tag{2.1}$$

in which:
T is the excess skin friction, τ_{cr} is the critical shear stress and τ' is the shear stress without the bedforms, with $\tau' = \rho g \left(\frac{u}{C'}\right)^2$ and $C' = 18 \log \frac{12h}{3D_{90}}$.

$$D_* = D_{50} \left(\frac{\nu^2}{\Delta g}\right)^{-1/3} \tag{2.2}$$

in which:
D_* is the dimensionless grain diameter, D_{50} is the median grain diameter, ν is the kinematic viscosity, Δ is the relative sediment-density and g is the gravitational acceleration.

Ripples Ripples are short crested bedforms that tend to develop at flow conditions with small Froude numbers. The height of ripples compared to the water depth is very low. The dimensions of ripples are (for $1 \leq D_* \leq 10$ and $0 \leq T \leq 3$):

$$\text{height} \quad \delta = 10D_{50} \tag{2.3}$$

$$\text{length} \quad \lambda = 100\frac{\nu}{u_*} \tag{2.4}$$

in which:
u_* is the shear velocity.

In the Waal, ripples of the dimension of several centimeters in height and length can be observed. The formation of ripples is much more related to the grain size than to the discharge condition. For higher flow velocities ripples first develop into mega-ripples with a height and length proportional to the water depth and finally evolve into dunes. The dimension of mega-ripples can be estimated (for $1 \leq D_* \leq 10$ and $3 \leq T \leq 10$):

$$\text{height} \quad \frac{\delta}{h} = 0.02(1 - \mathrm{e}^{-0.1T})(10 - T) \tag{2.5}$$

$$\text{length} \quad \lambda = 0.5h \tag{2.6}$$

in which:
h is the water depth.

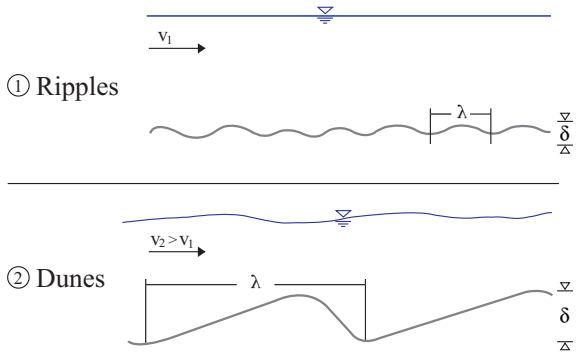

Figure 2.6: Bedforms in alluvial rivers

Dunes Dunes are asymmetrical transverse bedforms with a low luv slope and a steep lee slope. Dunes can develop into large bedforms in the order from 1 m up to hundreds of meters long and 10 cm to several meters high. Unlike with ripples the grain size is less important for the formation of dunes, but the more are water depth and flow velocity. Dimensions of dunes are (for $D_* \geq 10$ or $1 \leq D_* \leq 10$ and $10 \leq T \leq 15$)

$$\text{height} \quad \frac{\delta}{h} = 0.11\frac{D_{50}}{h}(1 - \mathrm{e}^{-0.5T})(25 - T) \tag{2.7}$$

$$\text{length} \quad \lambda = 7.3h \tag{2.8}$$

In the Waal, ripples and small dunes are superposed on larger dunes. The growth and damping of dunes is imposed by the discharge variation. Dunes increase in length and in height as a function of discharge. The maximum dune dimensions are reached some days after the peak discharge.

Lateral and vertical sediment segregation [57] Wilbers [69] observed differences in the bedforms on the north and the south side of the river Waal. He found that the mean grain diameter on the downstream right (north) side is 1.5-2 mm, while the mean diameter on the left (south) side is 0.6-1 mm. It is supposed that the fully loaded and thus heavier navigation traffic upstream to Germany is the reason for this lateral segregation. Both vessels sailing up- and downstream induce currents in between groynes that are strong enough to erode fine-grained sediments and transfer these into the main channel. These currents are stronger for loaded vessels that are sailing against the current, resulting in a left bank that is finer grained than the right. Furthermore, navigation seems to have influence on the bedforms by flattening the top of the dunes [69].

In the Rhine significant downstream fining and vertical segregation of fine and coarse sediment are observed (see e.g. [30], [28] and [4]). Bend effects, bifurcation points, bedforms and navigation cause lateral variation in grain size. Vertical grain sorting and bed armouring, with coarser particles covering the finer ones, are important segregation processes in the Niederrhein, Pannerdensch Kanaal and the areas close to the bifurcations [27].

2.4.2 Meso-scale

At the meso-scale the focus lies on different features that influence the development of the cross sectional profile: the flow in bends and crossings leads to lateral bed slopes thus to point bar and pool combinations; the development of shallow and deep parts at crossings between two opposing bends; local erosion zones around groynes and bridge piers and the formation of so-called groyne flames; lateral sediment transport into the floodplains during floods and shallow and deep parts in geometrical complex reaches. The discharge and the river geometry proof to be the dominating factors.

Flow in bends The flow pattern in bends and the effect on the morphology of the bend and the following straight river part is shown in Figure 2.7. It can be seen that in the straight section (cross-section A) before the bend two eddies are present. At the entrance of the bend, the water flow tries to keep its direction due to the inertia of the water particles. This leads to a shifting of the water masses, a larger right and a smaller left eddy develop (cross-section B). By colliding with the river bank the flow is redirected to the center. The line with the highest flow velocity is shifted to the left side. In cross-section C only one large eddy is present. The superstition of the high velocity, the energy dissipation at the collision with the bank and the large eddy lead to erosion and so to the formation of a pool. At the other bank the small flow velocity and the upward directed secondary flow lead to sedimentation.
The area after the bend is characterized by shallow and deep areas alternating on the left and the right side of the river. This is due to the inertia of the water that gets deflected at the bend. The resulting development would be a meandering of the river, which in the river Waal is prevented by groynes and dykes.

To avoid the point bar/pool formation and so the restriction of the navigation channel width, bed protections in form of armoured layers have been placed in the bends of Nijmegen (km 885) in 1985 and St. Andries (km 925) in 1998. Bend-weirs with the same effect have been placed in the bend at Erlecom (km 876) in 1996. The measures showed a good success in the way that they increase the channel width. However the bend armouring at Nijmegen induces an erosion pit that travels downstream with an average rate of 1.5 km/year. The effects of the protection structures at Erlecom and St. Andries cannot be

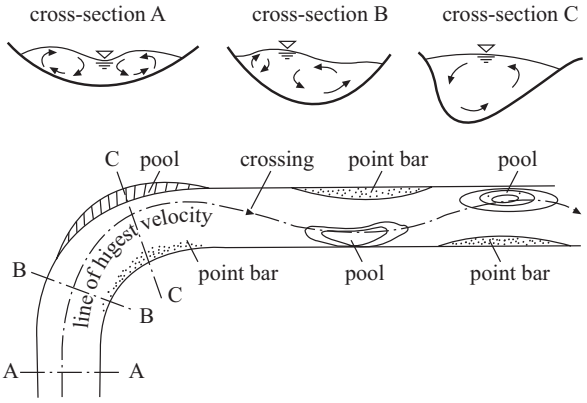

Figure 2.7: Flow in bends and crossings, after Lattermann [34]

evaluated due to the short time that they are installed [21].

Several research projects have been conducted to assess the extent of the bed deformation in bends: Struiksma et al. [48] investigated the large-scale bed deformation in alluvial rivers with relatively stable banks with the help of laboratory experiments. Before that it was assumed that the lateral bed slope is determined by local parameters only (water depth, bed shear stress, bend curvature and sediment properties), thus the balance between upslope drag force (caused by spiral flow) and the downslope gravitational force. A review on these former investigations is given by Odgaard [39].

Struiksma et al. [48] found that the point bar height and pool depth in the inner and outer bends cannot be predicted only from local conditions. The transversal bed slope is influenced by transitional effects resulting from the different conditions upstream of the bend and in the bend itself. An overshoot effect induced by the redistribution of the water and sediment motion in the first part of the bend is observed. This leads to an increase of the lateral bed slope in the same order of magnitude as the slope resulting out of the local conditions. The lateral bed slope in this research was approximated with:

$$\frac{\delta z_b}{\delta y} = -A f_s \Theta \frac{h}{r} \tag{2.9}$$

in which:
$\frac{\delta z_b}{\delta y}$ is the lateral bed slope, A is the secondary flow direction coefficient, f_s is a shape factor for the grains (with a value between 1 and 2), Θ is the Shields parameter ($\Theta = \frac{u^2}{\Delta D_{50}}$), h is the water depth, and r is the bend radius.

The secondary flow direction coefficient is defined as [5]:

$$A = \frac{2\epsilon}{\kappa^2}(1 - \frac{\sqrt{g}}{\kappa C}) \tag{2.10}$$

in which:
ϵ is a tuning coefficient, κ is the Von Karman constant, g is the gravitational acceleration and C is the Chézy roughness.

It was found that more experimental evidence is needed to achieve a correct formulation for the sediment transport direction and so to create a quantitavely correct model.

In a following research, Talmon et al. [49] conducted laboratory experiments to provide data for the modelling of the sediment transport on a transverse sloping bed. The

experiments were carried out with a straight flume with an initial transverse bed slope to assess the influence of the slope without the spiral flow effect. Lab experiments and natural behaviour were found to differ by a factor of 2 for bed load transport. Talmon et al. considered this effect to result from relatively large ripples and dunes in the laboratory experiments.

Experiments for suspended load indicated that the transverse slope effect is also a function of a characteristic flow velocity-scale and the fall velocity of the sediment. They concluded that a distinction between laboratory and natural conditions should be made. From the numerical modelling of large scale river bed deformations it was concluded that the transverse slope effect for a natural river and laboratory conditions with bed load transport can best be estimated by:

$$\frac{\delta z_b}{\delta r} = -f(\Theta)\beta\frac{h}{r} \tag{2.11}$$

with:

$$\beta = \frac{2}{\kappa^2}\left(1-\frac{\sqrt{g}}{\kappa C}\right)$$

$$f(\Theta) = 9\left(\frac{D_{50}}{h}\right)^{0.3}\sqrt{\Theta}$$

in which:
$\frac{\delta z_b}{\delta r}$ is the lateral bed level slope, h is the water depth, r is the bend radius, κ is the Von Karman coefficient (≈ 0.4), g is the gravitational acceleration, C is the Chézy roughness, D_{50} is the mean grain diameter and Θ is the Shields parameter.

A detailed description of the flow in bends and the resulting transversal slope is given in Blanckaert&De Vriend [3]. They describe two secondary flow phenomena appearing in river bends (see Figure 2.8): A helical motion in the center, and a weaker and smaller, counterrotating circulation on the outer bend, which is responsible for bank erosion.

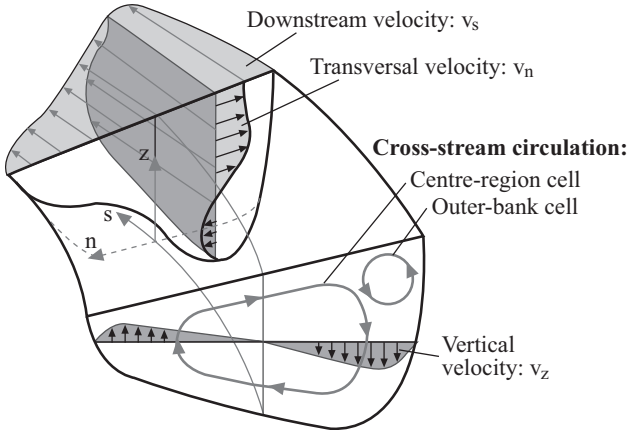

Figure 2.8: Flow pattern in bends, after Blanckaert&De Vriend [3]

Flow in crossings At the crossing between two opposite orientated river bends the evolution of the bed is influenced by the flow conditions of both, the upstream and the downstream bend, due to the slowly adapting flow pattern. In a river crossing shallow parts that restrict the navigability are likely to occur in the middle of the river. Those depend on the discharge and to a large extend on the local geometry. Winkley [70] developed

empirical relationships between the geometry of a river crossing to the crossing depth for the Mississippi river. Although the formulae may not be transferable to other alluvial rivers he points out that the local geometry of the two adjacent bends and of the crossing in between them has a very high influence on the available water depth and thus on the navigation. The size of the shoals forming in the middle of the channel is dependent on the discharge and the hydraulic roughness. At low discharges the scour occurs at crossings, resulting in an increase of the water depth. At high discharges the opposite is observed.

Formation of shoals and pools in geometrically complex reaches [57] The river Waal contains several geometrically complex reaches like reaches with a high variation of floodplain width or man made structures that may influence the water motion, causing spatial gradients in the sediment transport and so induce morphological changes. The Midden-Waal for example contains wide and narrow floodplains arranged alternating on the left and right side of the river. The regular inundation of these floodplains could lead to a transversal flow that has influence on the sediment transport.

Overbank sand deposition [57] Sediments that accumulate in the floodplain area during periods where high water is flowing or standing outside the main channel are called overbank deposits.

Using aerial photographs and field measurements, sandy overbank deposits formed by the large-magnitude floods of 1993/94 and 1995, were quantified along the Waal [50]. Deposits were observed at patchy sand splays on the top and landward slope of the natural levees, and covered about 4% of the embanked floodplain on the Waal.

The total volume of sand deposits were 169,000 m^3 and 217,000 m^3 for the Waal in 1993/94 and 1995, respectively. This is a rather large volume compared to the averaged yearly transport of bed material in the Waal, which is roughly 500,000 m^3. The overlap of the deposition areas in both years was between 55% and 70%. The volumes on the left bank of the Waal were larger than the volumes of the right bank [46]. The volumes of overbank deposits on the inner bend are much larger than the volumes of the outer bend.

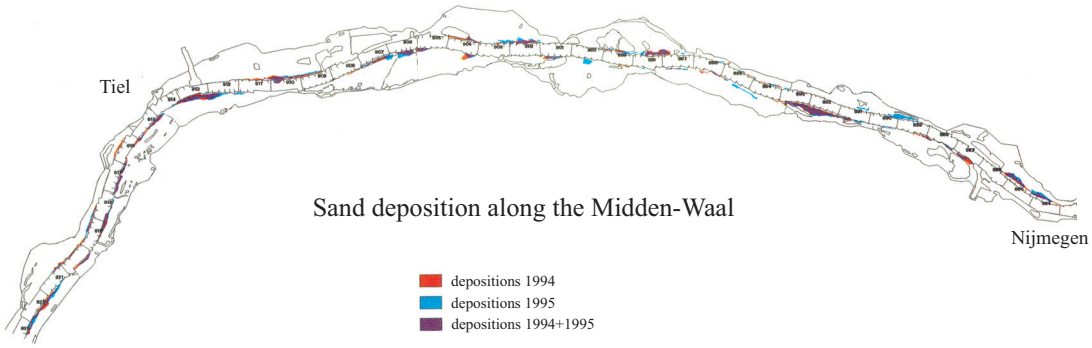

Figure 2.9: Sand depositions along the Midden-Waal 1994/95, after Sorber [46]

The controlling mechanisms of overbank deposition are pointbar formation and lateral flow exchange between main channel and floodplains. Curvature-induced secondary flow in river bends results in sediment transport from the outer bend to the inner bend. During large-magnitude floods these helicoidal currents are important for overbank sand transport.

The flux of overbank sand is much larger in a sinuous section of the river when compared to straight reaches. Moreover, high frequency and magnitude of overbank flows induced at geometrically complex locations in combination with large amounts of suspended material leads to (almost entirely) spatially discrete overbank deposits. Erosion of sandy sediments in the groyne fields due to the navigation traffic on the Waal, appears to be more significant at the left bank. This leads to larger amounts of suspended fine sediments there.

Groyne flames [57] Groynes are constructed perpendicular to the flow direction to delineate a deep navigation channel. They have an impact on the flow and the river bed morphology: At the groyne heads a turbulence is introduced that causes erosion which extends and fades in direction of the river axis in downstream direction. Downstream of this erosion zones deposition areas are found that are called "groyne flames". These groyne flames are found to reach for some ten meters in the transversal direction and may so cause problems for navigation during low flow conditions [71].

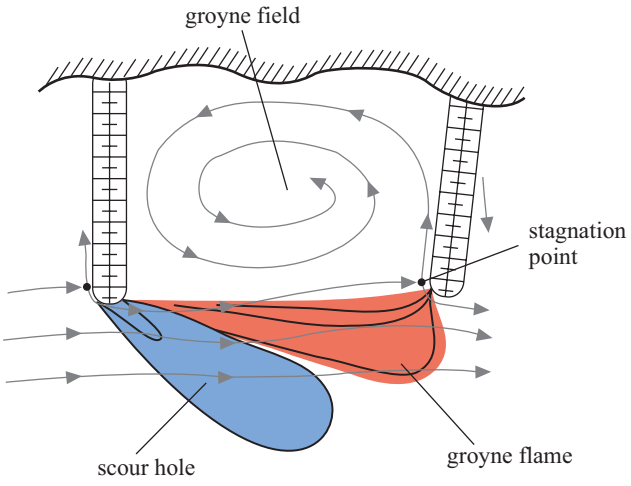

Figure 2.10: Flow in groyne fields and formation of groyne flames

2.4.3 Macro-scale

At the macro-scale, the longitudinal profile development of the river in response to natural changes or training works is observed. The training works in the 19^{th} and 20^{th} century had large effect on the profile of the Waal.

Longitudinal profile evolution [57] Cutting of meanders and rectifying the channel in the upstream part lead to a higher sediment transport capacity. The mean width of the Waal was reduced from over 500 m to 260 m today. This resulted in large-scale erosion in the upstream part (0.8 m over a period of 50 years [64]). Near Tiel (km 915) a hinge point can be observed, downstream of which long-term sedimentation takes place. The bed slope of the Waal is thus reduced. Furthermore, the river training lead to a silting-up of the floodplains. The induced morphological response has several negative effects, such as: the risk of undermining and destabilising the foundation of hydraulic structures (for example bridge piers or groynes); necessary dredging in the downstream part of the Waal to maintain the navigation channel depth; a redistribution of the river discharge between the main channel and the floodplains, which tends to enhance the tilting effect.

Dredging [57] Large-scale dredging activities have been conducted in the Waal from the end of the 19$^{\text{th}}$ century onwards. The dredging was aimed to realise the desired goal of the river regulation works (a bed level degradation to obtain a larger navigation depth in the river) faster. Most of this dredging took place without control by authorities and without permits and regulation. This, in combination with poor registration, resulted in the fact that the impacts of the regulation works on the longitudinal profile evolution cannot be estimated sufficiently. It is not known whether the river system has already adjusted to the regulations or if they still affect the bed evolution [64].

2.4.4 Time scale

Figure 2.5 assumes that changes in river morphology not only take place at different spatial scales but also at different time scales. Formulae for the morphological time scale for large-scale changes in river morphology have been developed by De Vries [9]. With the help of these formulae an estimate can be given of the speed at which large scale river morphology reacts to changes. The morphological response to changes has both a wave character (propagation of disturbances) and a diffusion character (smoothing and spreading of disturbances). For short distances the wave character is dominant, for large distances the diffusion character.

The time-scale for the wave character of morphological responses is:

$$T_w = \frac{L}{c} \tag{2.12}$$

with:

$$c = \frac{b}{(1-\epsilon_p)}\frac{s}{h}$$

in which:
T_w is the morphological time scale, L is the length scale, c is the characteristic propagation speed of the morphological feature, b is the degree of non-linearity depending on the used transport formula, s is the sediment transport per m width, h is the water depth and ϵ_p is the sediment porosity.

The time-scale for the diffusion character can be estimated with:

$$T_d = \frac{L^2}{K} \tag{2.13}$$

with:

$$K = \frac{bs}{3i_b}$$

in which:
T_d is the morphological time scale, L is the length scale, K is the diffusion coefficient and i_b is the bed slope.

The morphological diffusion time scale T_d is approximately equal to the time needed for a lowering or aggrading of the river bed by 50% of the total erosion or aggradation due to the change in river regime at a downstream location with the distance L.

This derivation contains a number of assumptions, most important that the equations are only valid for $L > 3h/i$. Nonetheless they can give an impression of the speed with that degradation and aggregation take place. For the Waal this time scale is very high. For a length scale of 100 km the morphological time scale is estimated with approx. 700 years [63].

2.5 Modelling river morphology

Flow and sediment transport in rivers are characterized by turbulence, variation in the free-surface, change in the river bed and phase interaction. A model capable of including all of these effects accurately has not been developed yet. So far, most of the sediment transport models include the following assumptions [65]:

1. The sediment concentration is very low, meaning that the interaction between flow and sediment movement can be neglected. For this reason the clear-water flow and the sediment advection-diffusion equations can be solved separately.
2. The change in the bed level is much slower than the flow movement. Therefore, at each time step the flow can be calculated assuming a fixed bed level.
3. The hiding and exposure mechanisms in the bed material are included by correction factors in the nonuniform sediment transport capacity formulae. The interactions among different size classes of the moving sediment are not considered. Thus, the transport of each size class of the sediment can be handled individually.

Nonetheless can river models give valuable insight into the hydraulic and morphologic behaviour of a river. They can give a schematized picture of reality, based on a simplified representation of the real river system. In the most models the river is considered as a morphodynamic system, based on dynamic feedback between water motion, sediment transport and changes in the river bed (Figure 2.11).

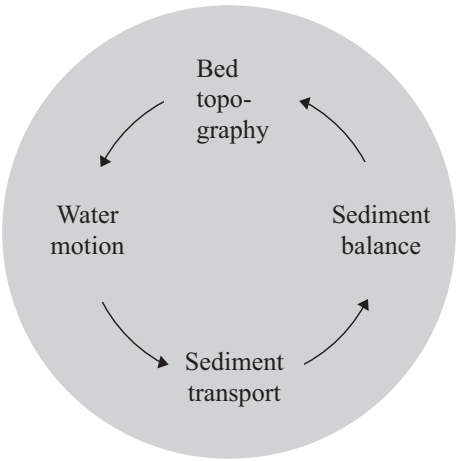

Figure 2.11: Morphodynamic approach in modelling, after De Vriend [6]

For sub-critical flow the propagation speed of a disturbance in the water surface is larger than the flow velocity and very much larger than the propagation speed of a bed disturbance. Disturbances of the water surface travel at a speed of $u \pm \sqrt{gh}$, while one group travels downstream and one upstream. The bed disturbances only travel downstream. In the morphodynamic approach for sub-critical flow it is assumed that the water motion drives the sediment transport without noticeable feedback effect. Using this assumption, water flow, sediment transport and bed level changes can be decoupled and a quasi-steady approach can be used (see Figure 2.12).

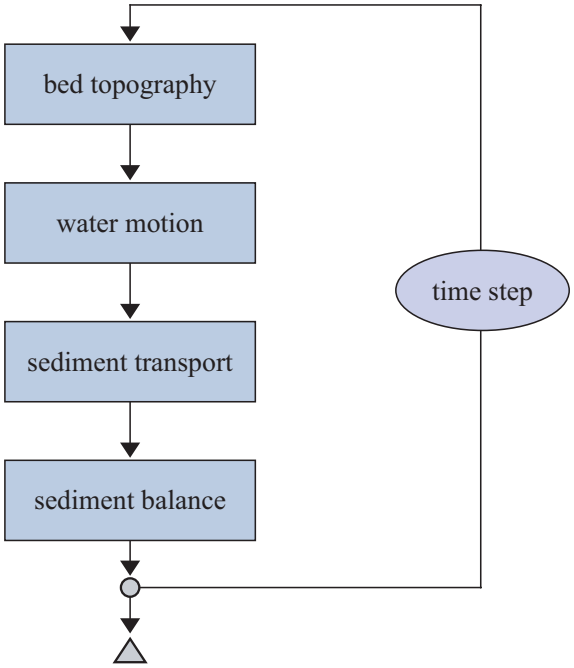

Figure 2.12: Quasi-steady modelling approach, after De Vriend [6]

Shortcomings in present day modelling Deterministic models that are well calibrated have the capability to reproduce the morphological change in a river in the past [47]. The calibrated models are then used for large-scale, long-term predictions of the river morphology. Long-term morphological computations are subjected to the following constraints [58]:

1. The morphological changes are generally assessed in a deterministic way. The calculated morphological response is therefore based on one single model run using a set of carefully chosen deterministic input parameters. It is assumed that this single model run represents the temporal and spatial changes correctly. The stochastic nature of a river is not considered.

2. The statistical characteristics of the model input are not constant, but change with time, which has impact on the morphological changes.

3. The non-linear character of the system does not only lead to dynamic interactions between different scale levels, but it also includes the possibility of multiple equilibrium states and deterministic chaos. Internal dynamic processes may result in a chaotic behaviour. The stochastic variations in the external forcing complicate the estimation of the morphological behaviour.

4. The chronology of events has great influence on the morphological response.

5. Uncertainties in the model schematisation and the model input, but also uncertainties in the data used for calibration and verification of the model lead to uncertainties in the model results.

The contribution of these different sources of uncertainties to the overall uncertainty in the model results is seldom clarified. Instead of a range of possible states, each with its own probability of occurrence, only one future state is estimated and believed to be true.

To take account of uncertainties involved in the model process this research uses a stochastic approach in modelling. In the following chapter the numerical models as well as the used stochastic approach are presented.

Chapter 3

Methods and Tools

In order to assess the navigability of the river Waal two different numerical model packages (used in a stochastic mode) and two measured data sets are used, namely:

- A one-dimensional SOBEK model of the Niederrhein and the Waal
- A quasi-3D Delft3D model of the Midden-Waal
- Data of the Least Measured Depth (LMD) to estimate the navigation channel depth
- Data of the placement of buoys to estimate the navigation channel width

In this chapter the detailed model setup and the used stochastic method are described, followed by an explanation and analysis of the available data. The description of the models given in Sections 3.1.2 to 3.1.4 are largely based on the work of Van Vuren [57].

3.1 Rhine models

3.1.1 Types of numerical models

Numerical models are useful tools to assess problems in river engineering. They have become more and more sophisticated with increasing computer capacity and the ongoing development of numerical methods. Three classes can be distinguished [56]:

1. One-dimensional models are suitable for river and channel networks. They use cross-sectional integrated equations for flow and sediment transport, are easy to apply and can give good insight into long term morphology. Yet, one-dimensional models cannot predict lateral morphology and flow effects.

2. Two-dimensional models (vertically or horizontally averaged). Two-dimensional horizontal models include the depth-averaged mass and momentum equations and the depth-averaged suspended sediment equations. They are also relatively easy to apply and give reliable insight into long term estimates on the price of higher computational effort. The partial disadvantage that these models do not account of secondary flow can be solved by applying a parameterisation for this effect.

3. Three-dimensional models include mass and momentum conservation in all three dimensions and use a curvi-linear grid for efficient computations. All effects of stratified, non-stratified and secondary flow can be included in detail. The disadvantage of this models is the very high computational effort.

In contrast to physical scale models, numerical models do not suffer from scale effects, but the results need careful interpretation as they use simplified model formulations and boundary conditions. Care has to be taken about the most important parameters and sources of uncertainties which have influence on the model results.

All models are based on physical conservation laws which have to be solved numerically. Those conservation laws are:

- The conservation of water mass (CW)
- The momentum equation for the water motion (MW)
- The dynamic equation for the sediment motion (MS)
- The conservation of sediment mass (CS)

The first two laws describe the water motion, while the third includes the sediment transport and the last one the morphologic bed evolution.

In this research two different numerical model packages are used to investigate the river morphology and the resulting effects on navigation: the one-dimensional model package SOBEK and the two- and three-dimensional model package Delft3D. In the following sections the equations used by these two models, as well as the setup of the models for the river Waal are described.

3.1.2 One-dimensional SOBEK model

In this study a one-dimensional morphodynamic Rhine model based on the SOBEK modelling package developed by WL|Delft Hydraulics and Rijkswaterstaat (RIZA) in The Netherlands is used [25]. The specific "Rijntakken" (Rhine branches) model was developed by Jesse&Kroekenstoel [27] and adjusted for the use in this research.

3.1.2.1 SOBEK model package

In SOBEK the quasi-steady approach (decoupled water flow, sediment transport and bed level changes) is used for modelling the interaction between water flow and bed morphology. This approach is valid for flow with a moderate Froude number as present in the river Waal. The morphodynamic process is then approximated by the interaction between a steady water motion and a non-steady bed evolution. The flow chart shown in Figure 2.12 is run through at every time step.

Flow equations The water flow in one dimension is described by the one-dimensional cross-sectionally integrated shallow-water equations: the continuity equation and the momentum equation (also called St. Venant-equations). They read as follows:

$$\frac{\delta A_f}{\delta t} + \frac{\delta Q}{\delta x} = q_{lat} \tag{3.1}$$

$$\frac{\delta Q}{\delta t} + \frac{\delta}{\delta x}\left(\alpha_b \frac{Q^2}{A_f}\right) + gA_f \frac{\delta(h + z_b)}{\delta x} + A_f \frac{\tau_b}{\rho R} = 0 \tag{3.2}$$

in which:
A_f is the cross-sectional flow area, Q is the discharge, q_{lat} is the lateral discharge, α_b is the Boussinesq constant, g is the gravitational acceleration, h is the water depth, z_b is the

bed level, τ_b the bed-shear stress and R is the hydraulic radius. In this equation t is the time and x is the distance along the river axis.

The bed-shear stress τ_b is expressed by the Chézy formula:

$$\frac{\tau_{\mathrm{b}}}{\rho} = \frac{gQ\,|Q|}{C^2 A_{\mathrm{f}}^2} \tag{3.3}$$

in which:
C is the Chézy-coefficient.

Transport&morphology equations In addition, the sediment transport and the sediment balance equation have to be solved to estimate the morphological changes. The momentum equation for the sediment transport rate is an empirical equation of the form

$$s = au^b \tag{3.4}$$

in which:
s is the sediment transport per unit time and length, u is the flow velocity and a and b are parameters specified by the used sediment transport formula.

Different sediment transport formulae, each with a different field of application, can be used: Meyer-Peter&Müller (for bed load [35]), Van Rijn (for suspended load [55]) or Engelund-Hansen (for total load [16]). The sediment transport capacity depends on the flow conditions and sediment characteristics such as density, grain size distribution, shape and uniformity. Spatial gradients in the sediment transport will lead to morphological changes. These changes are incorporated in SOBEK via the continuity equation for bed material:

$$\frac{\delta A_s}{\delta t} - \frac{\delta S}{\delta x} = -s_{lat} \tag{3.5}$$

in which:
A_s is the sediment transporting cross-sectional area, S is the sediment transport through the cross-section expressed in deposited volume including pores and s_{lat} is the lateral sediment influx per unit river length.

Boundary&initial conditions The fully time-dependent morphodynamic system has three bundles of characteristics: two characteristics belonging to the propagation of flow disturbances and another describing the propagation of bed disturbances. In a fully dynamic system, the characteristics of water and bed will mutually influence each other and are generally too complex to be separated.

In systems with sub-critical flow (low Froude numbers), the propagation speed of a disturbance in the water surface is larger than the flow velocity and much larger than the propagation speed of a bed disturbance. Therefore, a decoupled system is applicable: when computing the water motion, the bed is held fixed, and when computing the bed level changes, the water motion is kept invariant to changes in the bed level. The water surface disturbances propagate at a speed

$$u \pm \sqrt{gh} \tag{3.6}$$

in which:
u is the flow velocity, g is the acceleration due to gravity and h is the water depth.

One group of disturbance travels downstream and one group travels upstream. The approximation of the celerity of a small disturbance of the river bed is:

$$c_b = \frac{b \cdot s_b}{h} \frac{1}{1 - Fr^2} \tag{3.7}$$

in which:
b is the exponent in the transport formula when written as an exponential function of the flow velocity, s_b is the bedload sediment transport per unit width, h is the water depth, and Fr is the Froude number.

In order to have a mathematically well-posed system, fixed-bed flow computations require one boundary condition at the upstream boundary (usually the discharge) and one at the downstream boundary (often the water level or a stage-discharge relationship). Two initial conditions are needed, which are usually given in terms of the dependent variables h and Q. If the bed is mobile, one extra condition is required at the upstream boundary, usually given in terms of bed level or sediment transport rate. Furthermore, one extra initial condition is necessary and usually given in terms of bed topography at the beginning of the model run.

Further model parameters In addition, the hydraulic roughness, the empirical sediment transport formula, the grain size and the geometry of the river, like cross-sectional profiles and longitudinal slope have to be defined.

3.1.2.2 Rhine model in SOBEK

The SOBEK Rhine branches model was developed by Jesse&Kroekenstoel [27] and adjusted for this study. As a one-dimensional approach is used, the computed hydraulical and morphological output is cross-sectional averaged. The quasi-steady approach is used, meaning that the flow module iterates until the flow pattern reaches a steady state solution, after which the sediment transport rates are estimated and the bed levels are updated. The model is used to conduct dynamical simulations, with a morphological time step of ten days and a grid size of 500 m. The modelled period is five years. The model is calibrated on the basis of hydraulic and bathymetric data and data on sediment transport rates during the period 1987-1997. The hydraulic roughness, the nodal-point relation (describing sediment distribution at bifurcations), the sediment transport formula and the parameters in the sediment transport formula are used as tuning parameters in the calibration process of the model.

Model schematization The model schematically represents the river as a network of nodes and branches. The original Rhine branches model included the six main branches of the Rhine: Niederrhein, Waal, Pannerdensch Kanaal, Nederrijn, Lek and IJssel. Because of the high computational effort to conduct Monte Carlo Simulations the model was simplified: All branches but the Waal were cut at the Pannerdensche Kop.
The adjusted model now consists of four branches, one branch for the Niederrhein, two branches for the Waal and one short branch for the Pannerdensch Kanaal. These branches are connected by four nodes, two of them are boundary nodes (Ruhrort and Werkendam) and one a bifurcation point (Pannerdensche Kop), see Figure 3.1.

The grid size and the defined cross-sections were maintained from the original model, cross-sections are approximately every 500 m. At each grid point a cross-section profile

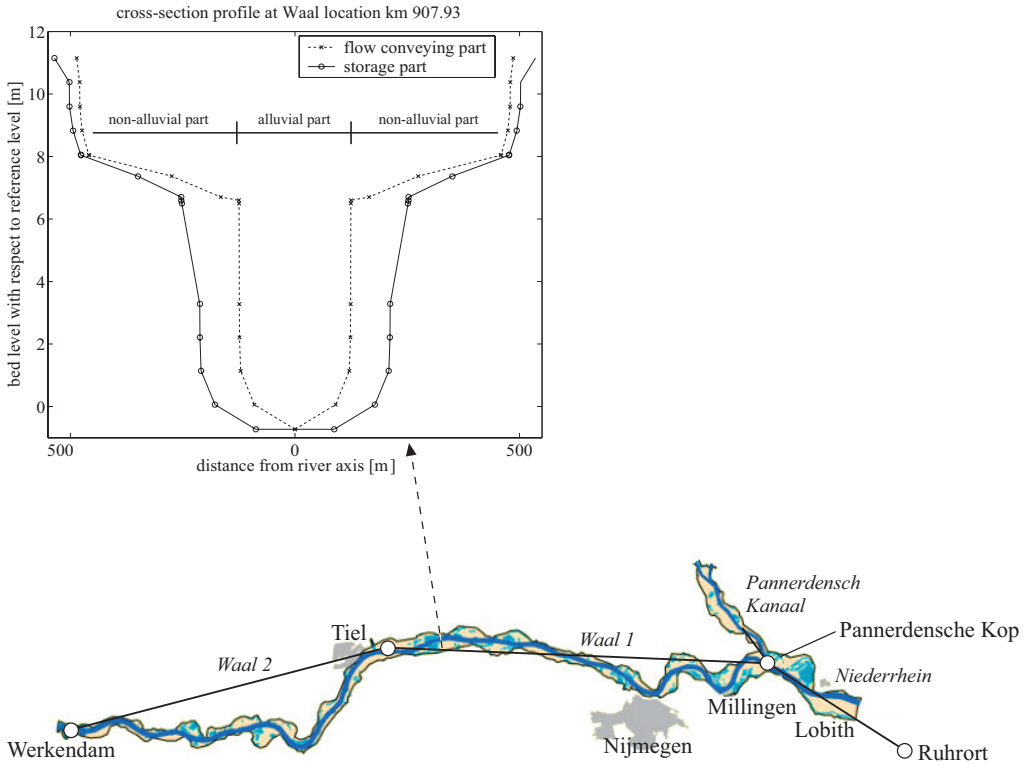

Figure 3.1: Adjusted Rhine model with cross-sectional profile, after Van Vuren [57]

dividing the river into main channel, groyne section, flow-conveying floodplain and storage area is set. Digital elevation maps and bathymetric soundings were used for this.

All cross-sectional profiles included in the SOBEK model are axis-symmetrical. Two-dimensional features like asymmetrical cross-sections in river bends are therefore neglected. A cross-section is defined by 15 points (5 for the main channel, 3 for the groyne section and 7 for the floodplain), where for each point the bed level, the total width and the flow conveying width are specified (see Figure 3.1). The height of summer levees and the flow-conveying and storage area behind the summer levees are defined separately in the model.

Due to gradients in the sediment transport, the bed level in the alluvial part of the cross-sections will change. Erosion and sedimentation are distributed proportional to a local reference depth across the sediment transport width of the cross-section.

The bottom protection structures at Erlecom (km 873-876), Nijmegen (km 882-885) and St. Andries (km 925-928) have been constructed to prevent the river bed from erosion and so to enhance the navigation profile of the Waal. Those structures are included in the model as fixed bed layers with an enhanced hydraulic roughness.

Boundary conditions The model needs a hydraulic and a morphological boundary condition at the upstream boundary and a hydraulic condition at the downstream boundary, as well as initial conditions for bed level, water level and discharge distribution at the bifurcation point. A discharge hydrograph and a fixed bed level (due to a natural unerodable clay layer) are used on the upstream boundary at Ruhrort (km 868) and a rating curve and a fixed bed level at the downstream boundary at Werkendam (km 964). The end of the downstream model area is placed at Vuren (km 952), because the tidal influence at

this location is known to be zero. At the Pannerdensche Kop a linear function is used for the sediment distribution at the bifurcation of Waal and Pannderdensch Kanaal.

As in this research the discharge is the parameter assumed to be uncertain, the discharge hydrograph used as upstream boundary condition was statistically derived. This is shown in detail in Section 3.2.2. The rating curve used at the downstream boundary is included in Figure 3.2.

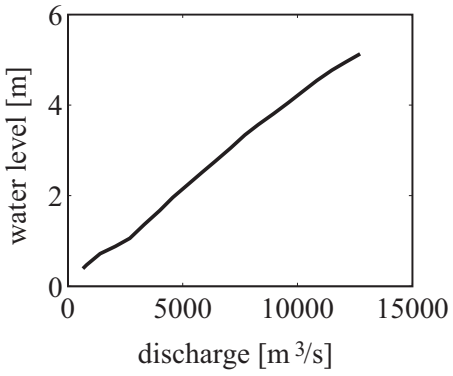

Figure 3.2: Rating curve at downstream boundary condition at Werkendam [57]

For the branch Waal 2 (starting at km 913) an additional morphologic condition was imposed: A dry load is specified to be extracted as a function of the time to take account of regular dredging happening in this section.

Condition at the bifurcation At the bifurcation point at the Pannerdensche Kop the discharge distribution fully depends on the conveyance and the available total difference in head at the outflowing branches to the base of the river.

The distribution of sediment at the bifurcation is expressed by means of the following nodal-point relation:

$$\frac{S_1}{S_2} = \alpha \frac{Q_1}{Q_2} + \beta \tag{3.8}$$

The ratio of sediment load of the two outflowing branches, S_1/S_2, is expressed as a linear function of the water distribution over these branches, Q_1/Q_2. The coefficient α is used as a tuning coefficient in the calibration process of the model, and equals 3 for the Pannerdensche Kop. The coefficient β equals zero [27].
This relation can be rewritten in the following format:

$$\begin{aligned} S_1 &= \frac{F}{1+F} S_t \\ S_2 &= \frac{1}{1+F} S_t \\ \text{which leads to:} \qquad F &= \alpha \frac{Q_1}{Q_2} \end{aligned} \tag{3.9}$$

in which:
S_t is the total sediment volume entering the bifurcation.

Thus, assuming that at the Pannerdensche Kop bifurcation 66% of the Rhine discharge is directed into the Waal and the remaining 34% flow into the Pannerdensch Kanaal, then 85% of the sediment load is directed into the Waal and 15% goes towards the Pannerdensch Kanaal. This ratio corresponds more or less with the ratio derived by Wilbers [69].

Transport formula The model uses the Meyer-Peter&Müller sediment transport formula with a reduced critical Shields parameter θ_c. The formula reads:

$$s = A \cdot \frac{8\sqrt{g\Delta D_{50}^3}}{1-\epsilon}\left(\frac{u^2}{C_{90}^{3/2}C^{1/2}\Delta D_{50}} - \theta_c\right)^{\alpha} \tag{3.10}$$

in which:
s is the bedload sediment transport rate per unit width, expressed in deposited volume (including pores), A is a multiplier used for calibration purposes, g the acceleration due to gravity, Δ the relative density of the sediment, D_{50} the median grain size of the bed material, ϵ the porosity of the bed, C_{90} the hydraulic roughness Chézy coefficient related to the bed material, C the Chézy coefficient, u the depth averaged flow velocity in the main channel, θ_c the critical Shields parameter (equal to 0.047) and α a constant exponent (equal to 1.5).

The Rhine is characterised by non-uniform sediment. Nonetheless, uniformity in the bed material is assumed in the model. When significant vertical segregation of fine and coarse sediment occurs, sediment particles finer than the uniform grain size characteristics (D_{50} and D_{90}) will be in motion at low flow, whereas no motion is predicted by the transport formula. To account for the transport of fine sediment under low flow conditions, the critical Shields parameter θ_c is reduced to 0.025 to enhance the sediment transport. Justification of the assumptions regarding the uniformity in the bed material and the reduction of the critical Shields parameter, is shown by Jesse&Kroekenstoel [27].

Hydraulic roughness The hydraulic roughness of the main channel composes itself out of contributions from the grains of the bed material and the bedforms present at the river bed. In the model this is estimated by the roughness predictor of Vanoni and Wang [62]:

$$C^{-2} = C_g^{-2} + C_{bf}^{-2} \tag{3.11}$$

in which:
C_g is the Chézy roughness of the grain size and C_{bf} is the Chézy roughness of the bedforms. The Chézy coefficient for the grain size is given by the White-Colebrook formula [26]:

$$C_g = ln\,(10)\,\kappa^{-1}g^{1/2}log\frac{12R}{k} \approx 18\log\frac{12R}{k} \tag{3.12}$$

in which:
κ is the Von Karman coefficient (≈ 0.4), g is the acceleration due to gravity, R is the hydraulic radius and k is the roughness height. The roughness height k is expressed as $3.5D_{90}$ in the model, in which D_{90} is the grain size diameter where 90% of the bed material is smaller. The Chézy coefficient related to the bed forms can be estimated as follows [62]:

$$C_{bf} = (8g)^{1/2}\left(3.3log\frac{Lh}{H_d^2} - 2.3\right) \tag{3.13}$$

in which:
g is the acceleration due to gravity, L is the dune length, H_d is the dune height and h is the water depth.
The model was divided into several units. For each of those, the Chézy hydraulic roughness values are included as a function of the river discharge by the Vanoni and Wang [62] roughness predictor (see Figure 3.3(a)). The roughness of the floodplains is represented by

an extrinsic Nikuradse parameter k, according to the various existing ecotypes and their spatial occurrence in the floodplains (see Figure 3.3(b)). Those values were chosen with the help of roughness tables.

Subsequently, all "estimated" Chézy coefficients are used as tuning parameters in the calibration process of the model. As a consequence, these coefficients are slightly adjusted, thus lose part of their physical meaning. This may have impact on the computed transport rates.

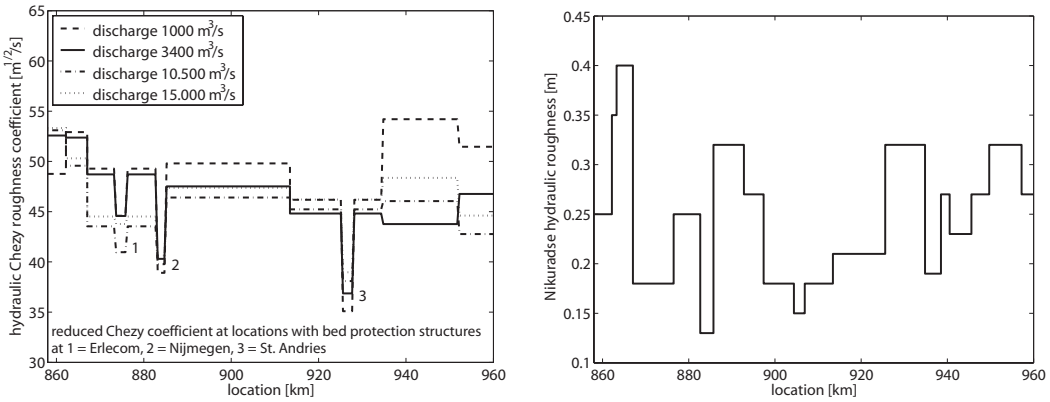

(a) Chézy hydraulic roughness coefficients of the main channel for different discharges at Lobith

(b) Nikuradse hydraulic roughness coefficients of the floodplains

Figure 3.3: Hydraulic roughness coefficients of the main channel and the floodplains [57]

Grain size As mentioned above, the Rhine is characterised by non-uniform sediment (see e.g. [30] and [28]). In the Rhine significant downstream fining and vertical segregation of fine and coarse sediments are observed. Bend effects, the bifurcation points, bedforms and navigation traffic cause lateral variation in grain size. Vertical grain sorting and bed armouring, with coarser particles covering the finer ones, are important segregation processes in the Niederrhein, Pannerdensch Kanaal and areas close to the bifurcations [27].

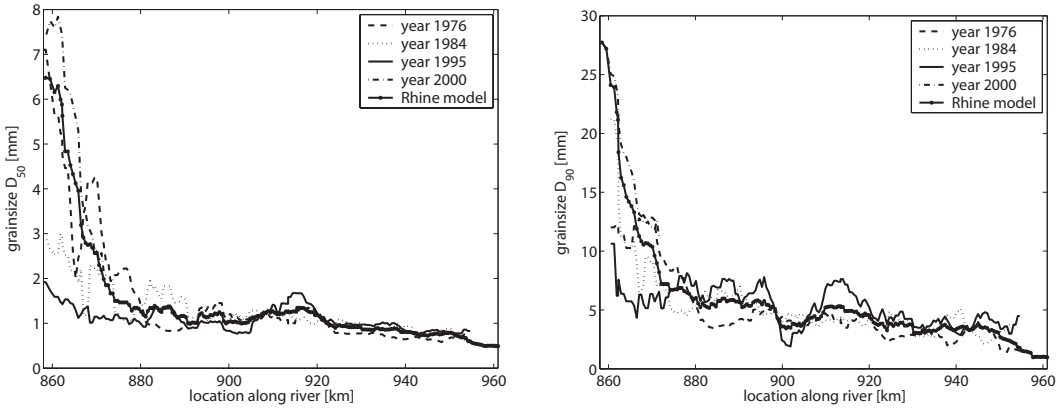

(a) grain size characteristics D_{50}

(b) grain size characteristics D_{90}

Figure 3.4: Spatial distribution of grain size characteristics in Niederrhein and Waal [57]

In a morphodynamic model system for non-uniform sediment, the bed could be schematised into homogeneous top layer, the active layer (of a certain thickness and sediment size

fraction) and a non-moving homogeneous substrate [22]. In this kind of model system, detailed information on sediment layers, their thickness and size fractions is required. This data is not available for the Dutch Rhine. Moreover, the vertical sorting processes are less important in the Waal. Therefore, uniformity of the bed material is assumed in the model. The model accounts for the longitudinal sorting process (downstream fining) by specifying the uniform grain size of the bed material at each location. Four sediment measuring campaigns between 1976 and 2000 are used as data source. The characteristic grain sizes D_{50} and D_{90} (diameter where 50% respectively 90% of the bed material is finer) are used in the model (see Figure 3.4).

3.1.3 Quasi-3D Delft3D model

The modelling package Delft3D can be used for meandering and braided rivers and accounts for sediment transport and its feedback on the flow. Floodplains with different kinds of vegetation and bottom vanes, spurs, groynes, levees and weirs can be simulated. The morphological module integrates the effects of waves, currents, and sediment transport on morphological development, related to grain sizes from silt to gravel. Rivers including bars, river bends (with spiral flow), bifurcations, non-erodible layers as well as dredging operations can be modelled. In this research, Delft3D is used in a quasi-3D mode (2D depth-averaged with parameterised curvature-induced secondary flow). The model of the above described reach of the Waal was developed by WL|Delft Hydraulics [45] .

3.1.3.1 Delft3D model package

The morphology program of the Delft3D package is called Delft3D-MOR [24]. It is able to simulate the morphodynamic behaviour of rivers, coasts and estatuaries on time scales of days to years by considering the interaction between waves, currents, sediment transport and bed evolution. Each of these processes are treated in separate modules which are run in succession and make use of each others results. Delft3D-MOR works with a finite-difference system in which the processes are simulated on an orthogonal curvilinear grid that allows an efficient and accurate representation of the complex model domain. The computational grid is staggered, meaning that not all quantities are defined at the same location in the numerical grid. The used modules are Delft3D-FLOW, Delft3D-TRAN and Delft3D-BOTT which treat water flow, sediment transport and bed evolution.

Flow equations The hydrodynamic module Delft3D-FLOW solves the unsteady shallow water equations in two- or in three dimensions. The 2D depth-averaged flow mode is applicable in vertical well-mixed flow regimes and is often combined with a parametrisation of the secondary flow (quasi-3D). Delft3D-FLOW solves the continuity equation and the equation of momentum. The depth-averaged continuity equation reads [23]:

$$\frac{\partial (h + z_b)}{\partial t} + \frac{\partial hu}{\partial x} + \frac{\partial hv}{\partial y} = 0 \tag{3.14}$$

The depth-averaged equations for conservation of momentum in x- and y-direction read:

$$\frac{\partial u}{\partial t} + u\frac{\partial u}{\partial x} + v\frac{\partial u}{\partial y} + g\frac{\partial (h + z_b)}{\partial x} + \frac{\tau_{bx}}{\rho h} = \frac{1}{\rho h}\frac{\partial (hT_{xx})}{\partial x} + \frac{1}{\rho h}\frac{\partial (hT_{xy})}{\partial y} \tag{3.15}$$

$$\frac{\partial v}{\partial t} + u\frac{\partial v}{\partial x} + v\frac{\partial v}{\partial y} + g\frac{\partial (h + z_b)}{\partial y} + \frac{\tau_{by}}{\rho h} = \frac{1}{\rho h}\frac{\partial (hT_{xy})}{\partial x} + \frac{1}{\rho h}\frac{\partial (hT_{yy})}{\partial y} \tag{3.16}$$

in which:
h is the water depth, z_b is the bed level, τ_x, τ_y are the shear stress components, g is the gravitation acceleration, u is the depth averaged velocity component in x direction, v is the depth averaged velocity component in y direction and z_b is the bed elevation. T_{xx}, T_{xy} and T_{yy} represent the horizontal exchange of momentum through viscosity, turbulence, spiral flow, wave action and non-uniformity of the velocity distribution.

The components of the shear stress in the momentum equations are related to the depth-averaged velocity using the relation by Chézy:

$$\tau_x = \frac{\rho g u \sqrt{u^2+v^2}}{C^2} \quad \text{and} \quad \tau_y = \frac{\rho g v \sqrt{u^2+v^2}}{C^2} \tag{3.17}$$

in which:
C is the Chézy roughness coefficient.

Transport&morphology equations Several empirical sediment transport formulae can be incorporated in the Delft3D-TRAN module, which takes account of the sediment transport. The bed level evolution is calculated by the Delft3D-BOTT module. It is based on the conservation of sediment mass:

$$\frac{\partial z_b}{\partial t} + \frac{\partial s_{b,x}}{\partial x} + \frac{\partial s_{b,y}}{\partial y} + E - D = 0 \tag{3.18}$$

in which:
$s_{b,x}$ and $s_{b,y}$ are the bed-load sediment transport rates per unit width in x and y direction, D is the deposition of suspended sediment and E is the entrainment of suspended sediment. These transport components are computed from the bedload transport magnitude S and the transport direction, indicated by an angle α_s relative to the x direction, as:

$$s_{b,x} = s_b cos\,(\alpha_s) \quad \text{and} \quad s_{b,y} = s_b sin\,(\alpha_s) \tag{3.19}$$

Secondary flow For time-dependent two-dimensional river bed deformation, the formulation of the direction of bed load sediment transport is divided into two components:
(1) the influence of the spiral motion (due to the curvature of the flow) and (2) the influence of the sloping bed.
The flow direction near the bed, and thus the bed shear stress direction, deviates in river bends from the depth-averaged flow direction due to spiral flow. This effect is modelled as follows:

$$tan\,(\alpha_\tau) = \frac{v - \alpha_I \frac{u}{|u|} I}{u - \alpha_I \frac{v}{|u|} I} \tag{3.20}$$

in which:
u is the flow velocity in direction of the streamline, v is the flow velocity perpendicular to the streamline, $|u|$ is the depth-averaged velocity magnitude and I is the spiral motion intensity. α_I is given by:

$$\alpha_I = \frac{2}{\kappa^2} E_s \left(1 - \frac{1}{2}\frac{\sqrt{g}}{\kappa C}\right) \tag{3.21}$$

in which:
E_s is a calibration coefficient.

Van Bendegom [51] gives the following direction formula for sediment grains moving along a sloping bed:

$$tan\left(\alpha_s\right) = \frac{sin\left(\delta\right) - \frac{1}{f(\theta)}\frac{\partial z_b}{\partial y}}{cos\left(\delta\right) - \frac{1}{f(\theta)}\frac{\partial z_b}{\partial x}} \tag{3.22}$$

in which:
$f\left(\theta\right)$ is the transverse slope effect that is assumed to be a function of the Shields parameter θ, α_s is the direction of the sediment transport and δ is the angle of direction of the flow near the bed, or the bed shear stress.

The transverse slope effect is given as:

$$f\left(\theta\right) = a_s \theta^{b_s} \tag{3.23}$$

in which:
a_s and b_s are calibration parameters.

The function was approximated by Talmon et al. [49] (see Section 2.4.2). In practice the function is often written as $f\left(\theta\right) = 0.85\sqrt{\theta}$ for natural channels.

3.1.3.2 Waal model in Delft3D

The quasi-3D (2D depth-averaged with parameterised curvature-induced secondary flow) Delft3D model has been developed by Sloff [45]. It can be used to simulate morphodynamic behaviour of the river at meso- and macro-scale. The formation of bedforms, such as dunes and ripples, is not included. The hydraulic roughness, the parameters in the transport formula and those related to the direction of bedload sediment transport are used as tuning parameters in the model.

Model schematization The area of research is a 37 km long stretch from Nijmegen (km 886) to Varik (km 923). This stretch of the Waal is characterised by large variations in geometry (e.g. floodplains widening and constricting alternately on the left and right side of the river) and a high number of bends with rather moderate radii and crossings between two bends of opposite orientation. This can be seen in Figure 3.5, showing the model topography.

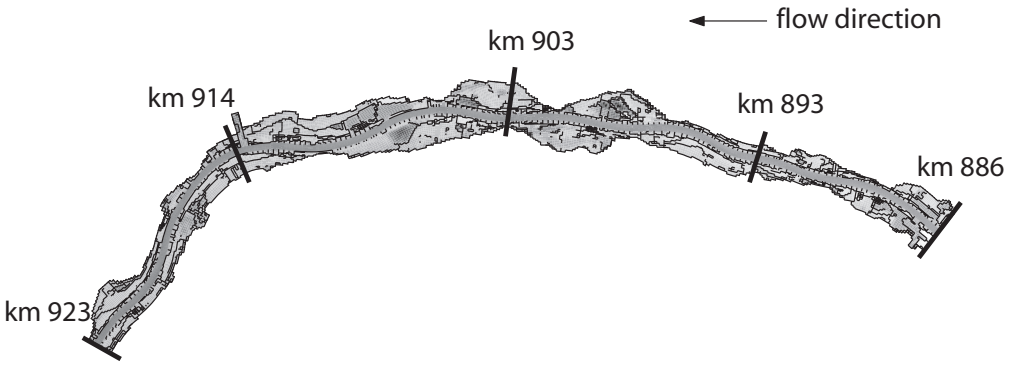

Figure 3.5: Bed topography of the Waal model in Delft3D [57]

The computation grid consists of 370 cells in y-direction (along the river axis) and 70 cells in x-direction (perpendicular to the river axis), with the gridlines (almost) perpendicular

to each other. The topography is based on bed elevation maps and bathymetric sounding data. The river is divided into main channel, groyne section and floodplains. The main channel (cell rows 29-40) is the only alluvial part of the river, thus morphologic processes in the floodplains are neglected. The averaged cell width and length in the main channel are 90-110 m longitudinal and 22-27 m transversal. The groyne fields, summer levees and steep obstacles in floodplains are schematised as 2D-weirs. The formation of groyne flames is not included.

Figure 3.6 shows the initial bed topography for different locations along the river. It can be seen that each cross-section shows a certain degree of asymmetry. Deep ponds (usually sand mining pits) are located in the floodplains at the left and right side of the river. An alternation between narrow and wide cross-sections can also be found.

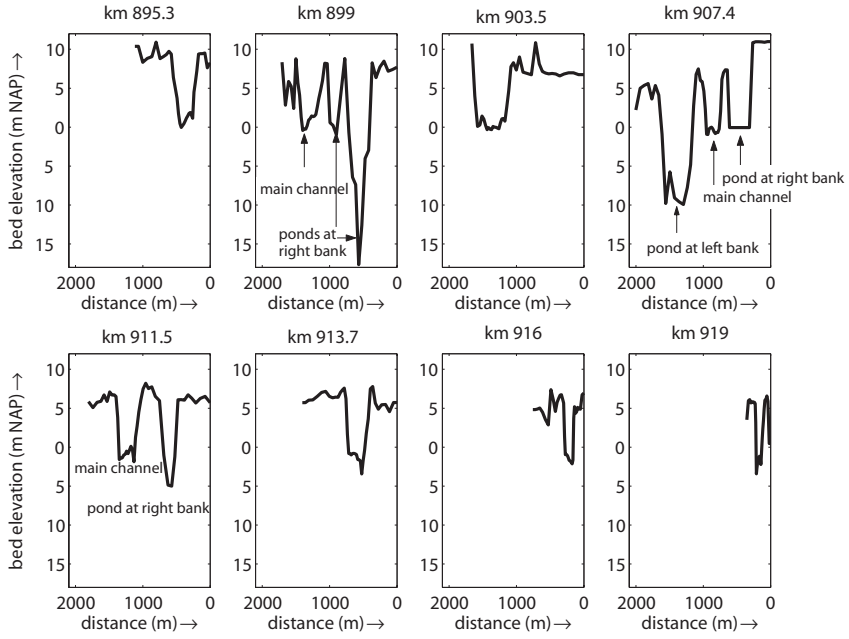

Figure 3.6: Initial bed topography at eight different cross-sections in Delft3D [57]

The curvilinear grid for four subsections (km 893-903, km 903-913, km 913-918, km 918-923) is shown in Figure 3.7. The bold lines represent the groyne fields, summer levees and steep banks; the dashed lines indicate the boundaries of the main channel.

Boundary conditions The boundary conditions consist of a hydraulic and morphologic condition at the upstream boundary and a hydraulic condition at the downstream boundary. The derivation of the discharge time series used at the upstream boundary is shown in Section 3.2.2. For each of the discharge states, a discharge distribution over the grid cells of the upstream boundary is required. For discharges lower than 1,693 m^3/s all water flow happens only in the main channel. Thus only grid cells 29-40 are active flow cells. At discharges higher than this threshold value, the floodplains are inundated and the discharge is distributed over the entire cross-section. The morphological boundary condition upstream was set so that the incoming sediment transport is equal to the local transport at the boundary. The hydraulic condition at the downstream boundary consists of a rating curve computed with the one-dimensional SOBEK model.

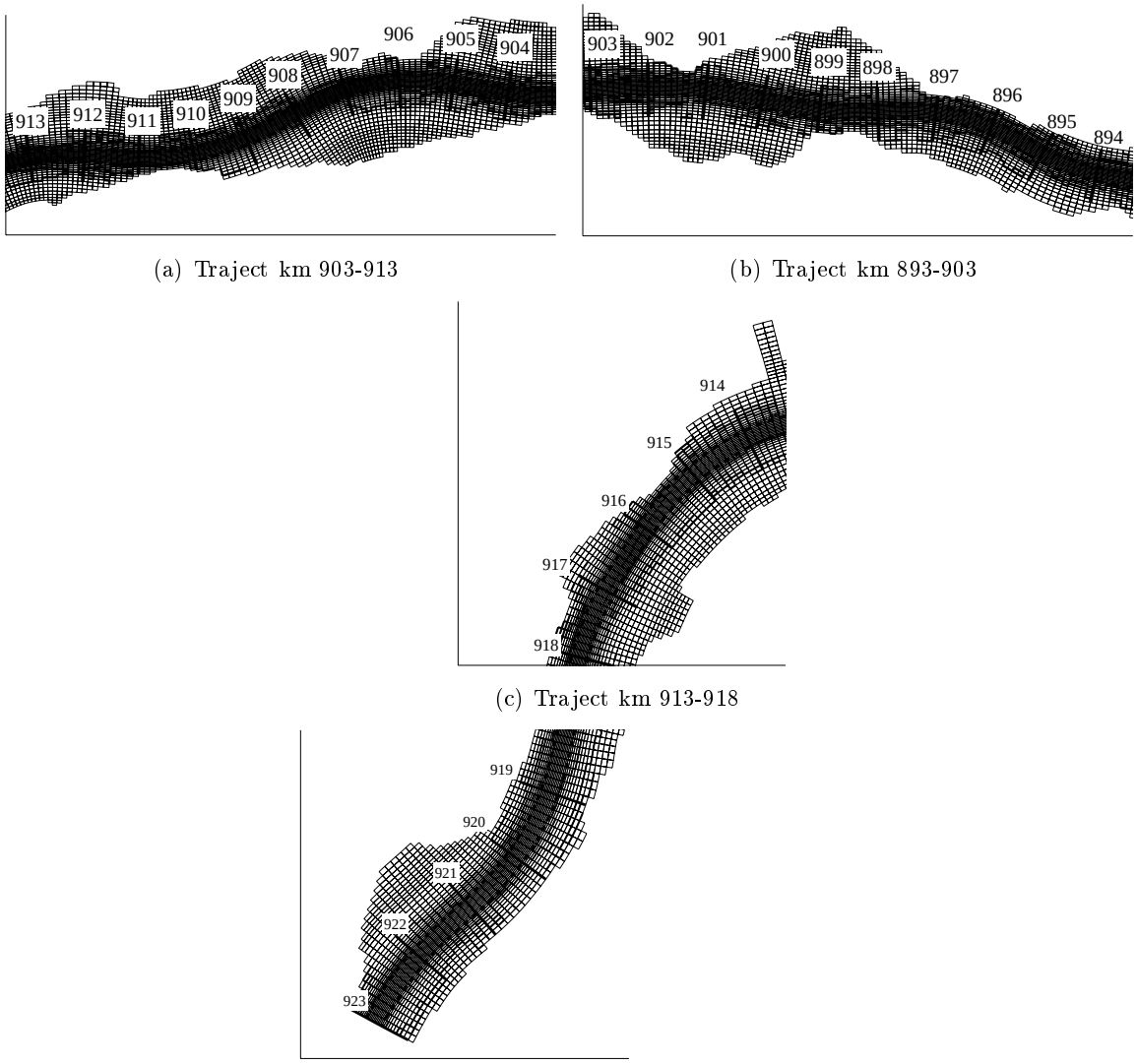

(a) Traject km 903-913

(b) Traject km 893-903

(c) Traject km 913-918

(d) Traject km 918-923

Figure 3.7: Curvilinear computation grid of four subsections in Delft3D [57]

Transport formula&model parameters The Meyer-Peter&Müller [35] formula has been extensively tested and used for rivers with coarse bed material in which suspended load was absent. The Engelund-Hansen [16] formula has been found to give a fair prediction for fine sandy rivers with substantial suspended load. The formula of Engelund-Hansen concerns the total load, with bed and suspended load, and reads:

$$s = A \frac{0.05 u^5}{(1-\epsilon)\sqrt{g} C^3 \Delta^2 D_{50}} \tag{3.24}$$

in which:
s is the sediment transport rate per unit width (i.e. including pores), u the depth-averaged flow velocity in the main channel, ϵ the porosity of the bed, g the acceleration due to gravity, C the Chézy coefficient, Δ the relative density of the sediment and D_{50} the median grain size of the bed material. A is a multiplier used for calibration purposes, and is chosen equal to 0.5.

In the calibration process of the model, the Engelund-Hansen formula was found to be

more appropriate than the Meyer-Peter&Müller formula. Sediment segregation processes are significant in the upstream regions of the Rhine system, but are of minor importance in the Waal branch. As a consequence of downstream fining of sediment, suspended load is of major importance in the Waal.

In the study area uniformity of the bed material is assumed. Lateral sorting of sediment is neglected. The bed material is characterised using the D_{50} characteristic, which is taken equal to 0.001 m.

In the quasi-3D model, the direction of the bedload sediment transport is split into two components, viz. the influence of the spiral motion and the sloping bed. The calibration coefficient E_s in the spiral flow effect on the transport direction (Eq. 3.21) is taken equal to 1. The coefficients for a_s and b_s in the bed slope effect (Eq. 3.23) are chosen 0.6 and 0.5, respectively.

Hydraulic roughness The model includes an adapted version of the Van Rijn-roughness predictor [54] to impose Nikuradse roughness values in the main channel. The hydraulic roughness varies in longitudinal and transversal direction. The predictor accounts for variation in hydraulic roughness at different flow conditions, since bedforms tend to develop dependent on the discharge and so affect the bottom roughness.

The hydraulic roughness of the floodplains is related to the ecotypes and their spatial distribution over the floodplains. Extrinsic Nikuradse parameters k are determined with the help of roughness tables. In some situations the roughness of the floodplain depends additionally on the inundation depth of the floodplain. For floodplain shrub, forest ecotypes and fencings, for instance, this dependency on the inundation depth is significant and may even turn the Chézy coefficient from an increasing into a decreasing function of the water depth [1]. An analytical model for hydraulic roughness of submerged vegetation is incorporated in the model [31].

Morphodynamic process tree The different modules Delft3D-FLOW, Delft3D-TRAN and Delft3D-BOT are all operated sequentially, but use each others results. The main module controls the interaction between these modules, known as the process tree. Only one module is active at a time, which results in a decoupling of the various physical processes. The modules are executed consecutively in a loop, where the user can specify the order and which time step is used in each module. That way, the use of the model can be varied from an almost fully coupled approach to a quasi-steady approach.

For this research a quasi-steady approach is used. Each time first the flow module iterates towards a steady state solution, that is then used to predict the sediment transport on with the bottom module operates. The computation-effort of a numerical simulation mostly depends on the effort required in the flow module. A reduction of the computation effort is obtained the following way:

1. The scaled version of the historical discharge hydrograph is discretised using a step of 500 m^3/s, resulting in a range of 16 discharge stages to be computed, varying from 500 up to 8,000 m^3/s (see Figure 3.8).

2. For each of these discharge stages, using the initial morphological state, the flow module is iterated until the flow pattern reaches an equilibrium. The resulting flow patterns are stored in a database.

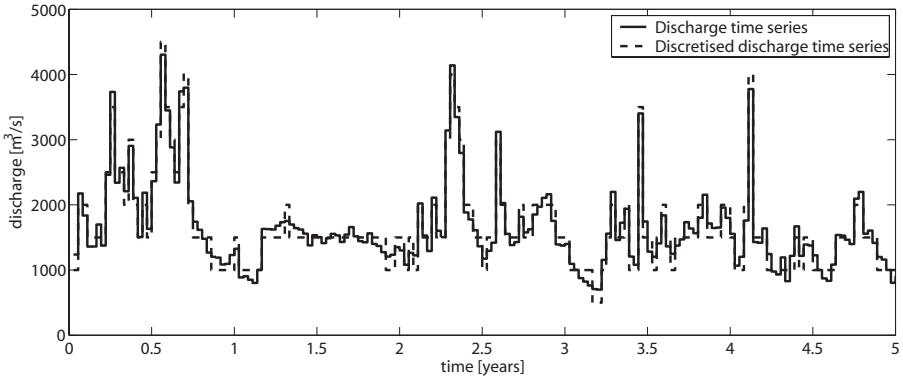

Figure 3.8: Discretization of the discharge time series used in Delft3D [57]

3. During the morphodynamic simulation the steady flow conditions in the database form the starting point for each discharge level in the discharge time series, while using the most recent morphological state. In this way, the flow pattern iterates quickly towards its new steady state.

The computation comprehends a period of five years. Figure 3.9 shows the switching between modules as a process tree. For the discharge time series a stepwise approximation is taken, with a new discharge level every 10 days. Each level starts with the stabilised hydrodynamics corresponding with the initial morphological state. The flow conditions are updated next, while using the most recent morphological state. The internal time step in the flow module is 6 seconds. The transport and bottom modules are updated after every 100 time steps of the flow computation. The transport and bottom modules are executed five times with a morphological step of 1 day.

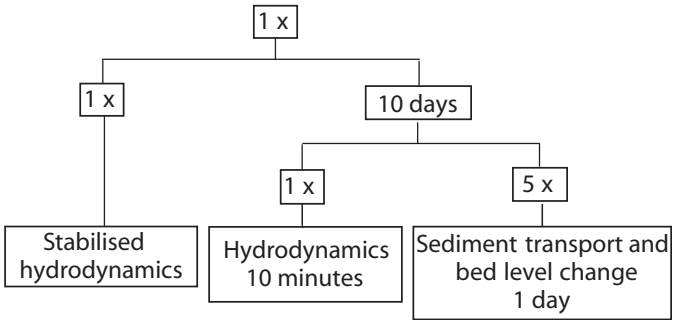

(a) Process tree

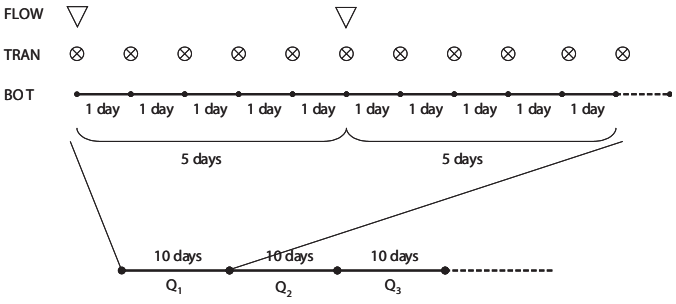

(b) Time management

Figure 3.9: Process tree and time management for the Delft3D model [57]

As long as the bed level changes are relatively small, one can assume that the spatial distributions of water level and discharge remain unaffected. This means that it is possible to compute new flow velocities using $\vec{u} = \vec{q}/h$, where $\vec{q}$ is the local unit discharge vector and h is the local adjusted water depth. This "continuity correction" allows to continue with another morphological step without running the flow module in between the transport and bottom module. After executing the transport and bottom modules five times, an update of the hydrodynamics follows. This loop is repeated two times thus covering a period of 10 days. For the computation period of five years, the entire flow chart is run through 180 times.

3.1.4 Overview of the model features

As summary of the model description, this Section gives a short overview of the morphological phenomena that are included in the models as well as the used parameter settings.

Table 3.1 gives an overview of the model inputs and parameter settings used in the SOBEK and the Delft3D model.

Description	**SOBEK model**	**Delft3D model**
Flow equations	◦ shallow water equation solved in one-dimension	◦ shallow water equation solved in two-dimensions ◦ parametrisation for curvature-induced secondary flow
Grid size Δx	◦ 500 m	◦ 90-110 m
Time step Δt	◦ 10 days	◦ 1 day
Upstream boundary	◦ discharges per interval of $\pm$10 days	◦ discharges per interval of $\pm$ 10 days, which are discretised into constant values 500 m^3/s apart
Downstream boundary	◦ stage-discharge relationship	◦ stage-discharge relationship
Roughness main channel	◦ Vanoni&Wang roughness predictor [62]	◦ Van Rijn roughness predictor [54]
Roughness floodplain	◦ constant values from roughness table	◦ constant values from roughness table ◦ analytical model for submerged vegetation
Grain size bed material	◦ uniform at each location	◦ uniform in entire model
Sediment transport formula	◦ Meyer-Peter&Müller [35] with a reduced critical Shields parameter	◦ Engelund and Hansen [16]

Table 3.1: Overview of the model inputs and parameter settings of the models [57]

A Monte Carlo Analysis is characterized by a high computational effort. Especially the use of computationally intensive numerical models in combination with a large number of simulations can make MCA a laborious operation. It is therefore important to use a one-dimensional modelling approach as far as possible, and only use the more computational intensive two-dimensional approach if two-dimensional morphologic phenomena are dominant.

Table 3.2 gives an overview over the morphological phenomena included in the models and shows how those phenomena are treated. The theoretical background to this table can be found in Section 2.4.

The calibrated one-dimensional SOBEK Rhine model is valuable to gain insight into the morphological processes at macro-scale level, thus the longitudinal profile evolution. Moreover, the geometrically induced bed variability along the river is incorporated.

Scale levels	Morphological phenomena	SOBEK model	Delft3D model
Micro	- bedforms, such as ripples and dunes	±	±
	- vertical segregation of sediment fractions	-	-
Meso	cross sectional profile evolution:		
	- transverse bed slope and pointbar/pool formation in bends	-	+
	- formation of shallow and deep parts in geometrically complex reaches	a	+
	- crossings between opposite bends	-	+
	- bank erosion	-	-
	- overbank sand deposition	-	-
	- local scour e.g. around bridge piers	-	-
	- local scour in groyne fields and formation of so-called groyne flames	-	-
Macro	- longitudinal profile evolution	+	+
	- evolution of geometry at river bifurcations	±	+

- = not dealt with; + = dealt with; ± = dealt with parametrically;
a = formation of shallow and deep parts is width-averaged

Table 3.2: Overview of the implemented morphologic phenomena in the models [57]

The SOBEK model gives a width-averaged representation of the morphodynamics of the river bed, meaning that two-dimensional phenomena, such as cross-sectional profile evolution imposed by the river alignment, are neglected. This means that two-dimensional features, such as alternate bars, or transverse slopes in bends, are not considered. Neither is the fact that large floodplain areas are located alternately at the right and left side of the river, which under flood conditions may lead to strong three-dimensional cross-flows over the main channel (see [32] and [43]). For those effects analytically based post-processing should be applied (see Section 4.2 and 4.3), or the step to two- or three-dimensional modelling has to be done.

In principle, river morphology constitutes a three-dimensional process. However, most problems do not need to be tackled by means of a "complete" three-dimensional description [10]. Therefore, a quasi-3D Delft3D model (2D depth-averaged with parameterised curvature-induced secondary flow) is used for comparison with the results of the one-dimensional model.

The quasi-3D model of the Waal [45] is appropriate for the purpose of validating the 1D approach, since the model area considered is characterised by large variations in geometry (such as floodplain widenings and constrictions alternately located left and right of the river axis), bends of moderate curvature and crossing between opposite bends. Morphodynamic phenomena at meso- and macro-scale are considered in this model, see Table 3.2. This includes the simulation of transverse bed slope formation (pointbar and pool combinations in bends) and the formation of shallow and deep parts alternately at the left and the right side of the river. The formation of bedforms, such as dunes and ripples, is not explicitly simulated in the Delft3D model, but is included parametrically via an alluvial bed roughness predictor.

3.2 Uncertainties and stochastic method

Modelling river morphology is associated with different kinds of uncertainties. To assess these uncertainties several stochastical methods have been developed. This section explains the uncertainties in modelling that have to be taken into account and shows which stochastic method is used in this research. It also describes the use of the models in a stochastic mode.

3.2.1 Uncertainties in modelling

Recent state of the art is the deterministic modelling of river morphology. This approach presents the bed level at a certain time and location as one discrete value. For several reasons the modelling of river morphology contains uncertainties that are not considered in this deterministic approach [52]. The input parameters like discharge hydrograph, grain size of the bed material, roughness of the river bed as well as the model code introduce uncertainties. The deterministic approach therefore represents only one of many potential states of the river.

De Vriend [8] distinguishes between the following effects that have to be considered in numerical modelling:

- Sensitivity: Sensitivity describes the sensibility of model results to variations in the model input parameters. The relative influence of one parameter can be assessed by modelling with different values for this parameter while holding all other parameters constant.
- Variability: Variability describes the variation of a parameter in time. Variability of a parameter can be assessed by analysing its behaviour over time.
- Uncertainty: Uncertainty is a different dimension than the two former mentioned effects; it is introduced through different scenarios of input parameters. The range of uncertainty should be larger than the variability. Uncertainty has to be treated with care. Uncertainties have to be labeled, categorised, analysed, quantified, if possible reduced and if necessary lived and worked with.

This research focuses on the uncertainties introduced by the model input parameters.
An uncertainty analysis consisting of the following steps is necessary to gain insight into the temporal and spatial variability of morphological processes:

- Inventory of the involved uncertainties
- Identification and quantification of the uncertainties with a large effect on the model results
- Interpreting the uncertainty in the model results

Figure 3.10 shows the uncertainties that are introduced during the modelling process [58]: Those uncertainties can be distinguished with respect to the model structure (1), boundary structure (2), initial conditions (3), model parameters (4), input scenarios (5) and numerical parameters (6).

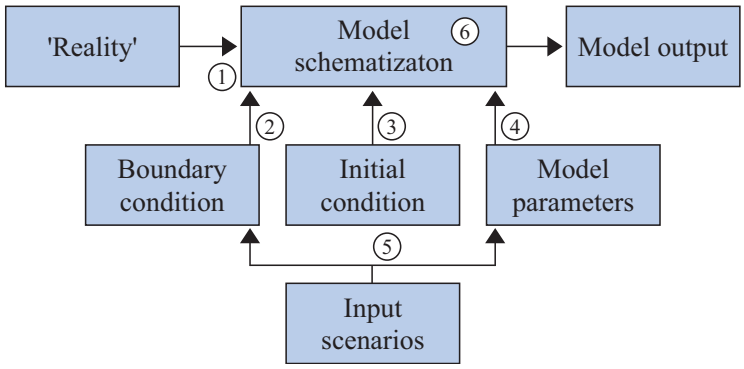

Figure 3.10: Uncertainties related to the modelling process, after Van Vuren [58]

The uncertainties shown in Figure 3.10 can be further divided into two classes [53]: inherent and epistemological uncertainties (see Figure 3.11). Inherent uncertainty results out of the unpredictable variation of nature and cannot be treated by further research. Epistemological uncertainty results from the lack of knowledge about physical processes, missing data or statistical uncertainty. This types of uncertainty can be reduced by additional research.

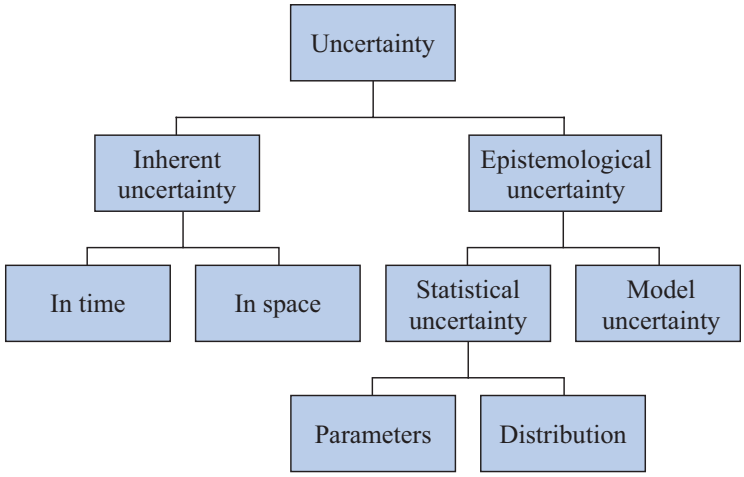

Figure 3.11: Different kinds of uncertainties, after Van Gelder [53]

3.2.2 Monte Carlo Analysis

Different stochastic methods to assess uncertainties in modelling exist, like Numerical Integration, First Order Reliability Method (FORM), Response Surface Replacement, Stochastic Differential Equations and Monte Carlo Analysis. A Monte Carlo Analysis (MCA) was found to be the most appropriate method to assess uncertainties in river morphology [52]. A large number of simulations with randomly generated uncertain model input according to prescribed probability distributions are used [20]. The statistical properties of the model output are then estimated with standard statistical tools (see Figure 3.12). MCA proofed to be very computational intensive, thus the number of simulations has to be limited to a minimum.

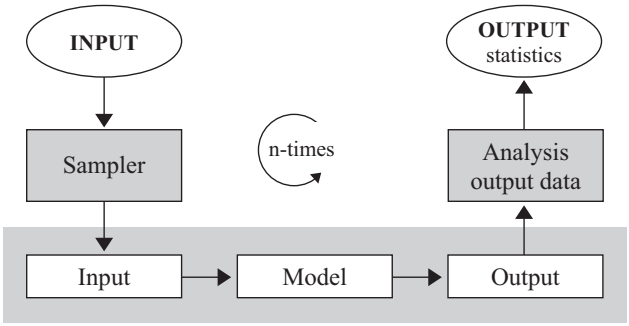

Figure 3.12: Flow chart Monte Carlo Analysis, after Van Vuren [58]

Van der Klis [52] and Van Vuren et al. [61] have shown that the discharge hydrograph is one of the important sources of uncertainty. Therefore, uncertainties introduced by the model schematization and the specification of model inputs, other than the river discharge, are not considered in this research.

Model use in Monte Carlo Analysis In this study both models are run 100 times, each time with a different discharge time series of five years duration. A flow chart is presented in Figure 3.13. The output of all model runs are analysed in terms of mean values, standard deviations, percentile values and confidence intervals. With the help of those characteristics the navigability of the river is assessed in statistical terms.

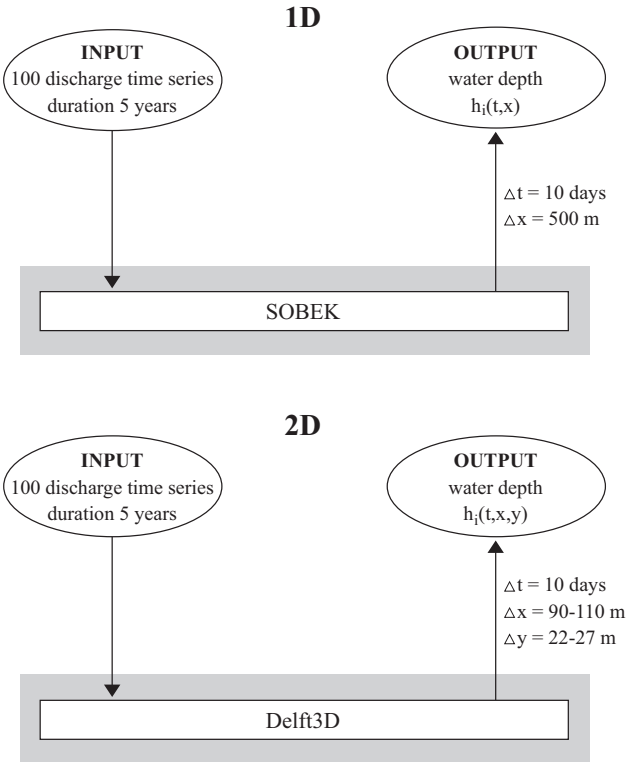

Figure 3.13: Flow chart of the SOBEK and Delft3D model in MCA

The output of the SOBEK model consists of cross-sectional averaged values for the water depth for cross-sections every 500 m, while the output of the Delft3D model consists of water depth values approx. every 100 m in longitudinal and approx. 25 m in lateral direction. For both models an output value is given every ten days.

Synthesis of the discharge time series [57] One hydraulic and one morphologic condition for every single run are needed as boundary conditions at the upstream boundary at Ruhrort. The used hydraulic condition is a discharge time series, while the morphologic condition was set in a way that at any point in time the incoming sediment transport rate equals the local transport capacity at the boundary. The discharge time series were synthesised by Van Vuren [61] with the help of the Bootstrap Re-sampling Technique [13] on the basis of 100-year daily measurements taken near Lobith (from 1900 to 2000).

Regarding the hydraulic boundary condition at the upstream boundary, the quasi-steady approach allows the discharge time series to be represented by a piecewise constant function, such that during one computational time step the discharge is constant. The measured discharge data was averaged over periods of approximately ten days, so that 36 periods form one year. For each period the weighted average Q_w of the daily discharge Q_d was estimated, such that the expected total sediment volume V in each period T_w remains unchanged:

$$V = T_w \cdot S\left(Q_w\right) = T_w \cdot E\left(S\left(Q_d\right)\right) = T_w \cdot \frac{\sum_{d=1}^{N} S\left(Q_d\right)}{N} \tag{3.25}$$

in which:
S is the sediment transport volume per second, and N the number of daily discharges averaged (10 or 11).

If the sediment transport formula is a general function of the depth averaged flow velocity u to the power n, the following calculation for the sediment transport and representative discharge can be made:

$$S\left(Q_w\right) = B_s m u^n = m B_s^{1-n} Q_w^n h^{-n}, \text{ so that } Q_w = B_s h \left(\frac{E\left(S\left(Q_d\right)\right)}{m B_s}\right)^{1/n} \tag{3.26}$$

in which:
B_s is the sediment transporting width, m a multiplier and h the water depth.

If in the definition of Q_w the bed slope would be set constant, instead of using the water depth, the equation would read:

$$S\left(Q_w\right) = m B_s^{1-n/3} Q_w^{n/3} i_b^{n/3} C^{2n/3}, \text{ so that } Q_w = \left(\frac{E\left(S\left(Q_d\right)\right)}{m B_s}\right)^{3/n} \frac{B_s}{C^2 i_b} \tag{3.27}$$

Thus, for the conversion from daily discharge to discharges per intervals of approximately 10 days, either Eq. 3.26 or Eq. 3.27 can be used. The conversion results in 36 intervals of 100 data points.

With the help of the Bootstrap Re-sampling technique a one-year discharge series is randomly selected. Then, with the help of a flood event predictor, a yearly flood event Q_H with a discharge peak described by a Weibull probability distribution function is created:

$$f(Q_H) = ab Q_H^{b-1} e^{-a Q_H^b} \tag{3.28}$$

in which:
a and b are scale and shape parameters equal to $8.5 * 10^{-4}$ and 3.5.

A corresponding flood wave with a standard wave shape is constructed. This is done by amplifying historical flood waves to a standard peak value and taking the mean of all these normalised shapes. The constructed flood wave is then placed instead of the highest flood event in the selected one-year discharge series using the Bootstrap Re-sampling technique. The synthesized one-year discharge series are connected to build a new discharge hydrograph of five years duration. For illustration, the resulting discharge series for each year in the period 1900-2000 and its statistics are shown in Figure 3.14(a) to (d).

In order to save computation time of the Delft3D model the discharge hydrograph was discretized in steps of 500 m^3/s, resulting in 16 discharge stages. The discharge time series used in the Delft3D model is shown in Figure 3.8.

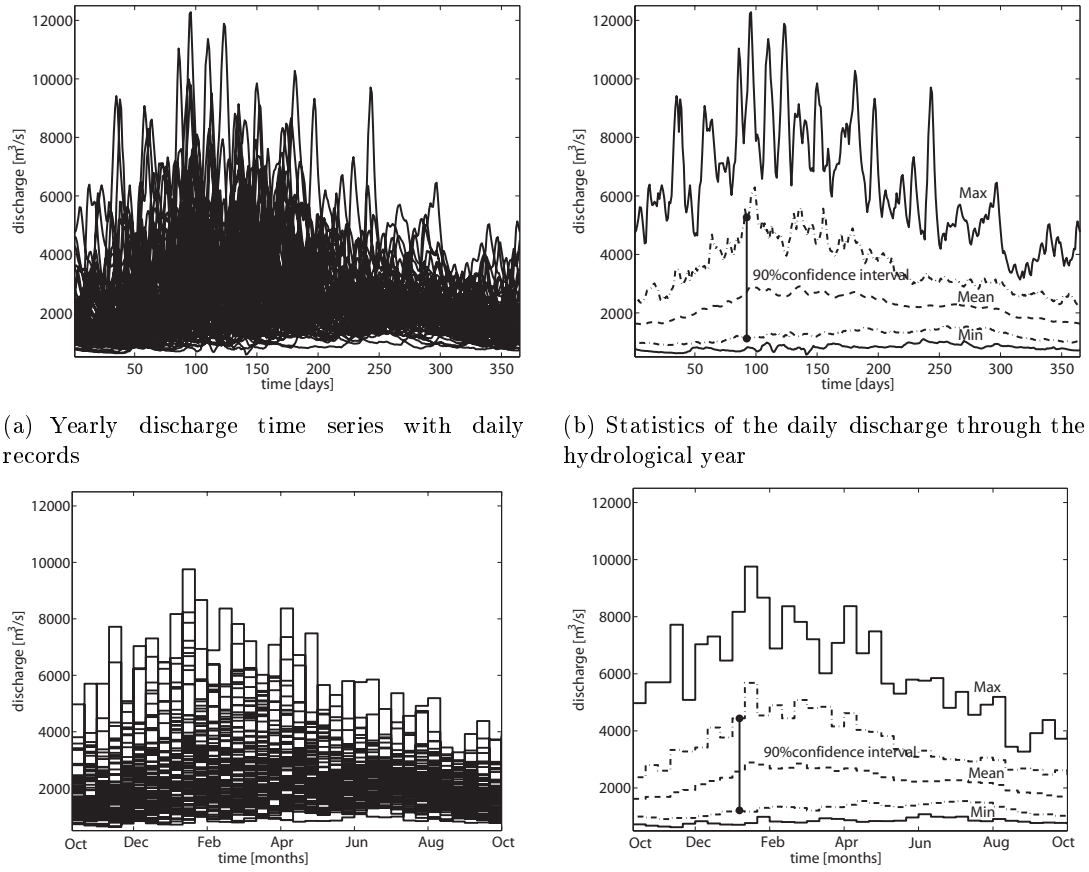

(a) Yearly discharge time series with daily records

(b) Statistics of the daily discharge through the hydrological year

(c) Yearly discharge time series, averaged over intervals of approximately 10 days

(d) Statistics of the discharge over 36 intervals through the hydrological year

Figure 3.14: Discharge record and statistics at Lobith for the period 1900-2000 [57]

About two third of the Rhine discharge flows in the Waal. A more accurate scaling-factor for different discharge regimes, determined on the basis of (1) discharge measurements at Pannerdensche Kop and (2) Rhine model computations, is shown in Figure 3.15.

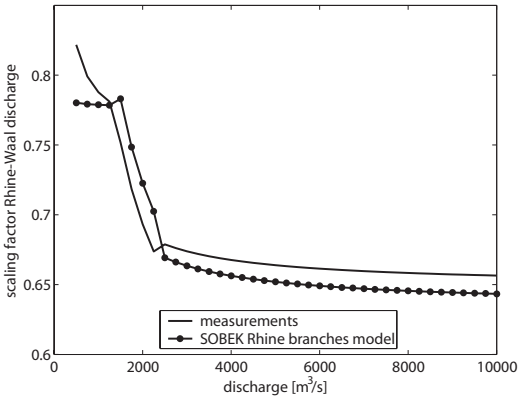

Figure 3.15: Scaling-factor Rhine-Waal discharges for different discharge regimes [57]

3.3 Data for comparison

Two different sets of data are available to get an impression of the navigability of the river and locations that form bottlenecks in means of restricting the navigation channel in depth and width in reality:

1. Data of the Least Measured Depth on the Niederrhein and Waal
2. Data of the placement of buoys on the Midden-Waal

3.3.1 Least Measured Depth

The Least Measured Depth (in Dutch: Minst Gepeilde Diepte), from here on referred to as LMD, identifies the location with the minimum water depth in the Niederrhein and the Waal. It is used to inform the navigation traffic about the limitations of the navigation channel and hence is an important parameter to judge the navigability of the river in means of navigation depth. In practice, the LMD is measured on different locations along the Niederrhein and Waal on a daily basis, when the water level at Nijmegen (km 885) drops below 9 m+NAP. Above this water level no restrictions for the navigation traffic on the river exist. Only the one location with the lowest water depth is defined as the Least Measured Depth and transfered into the database. The values of the LMD are determined as a function of the river location (the position along the river axis) and the distance from the left or right bank. With this data, the dimension of the navigation channel in terms of water depth can be estimated. Special attention has to be paid to locations where the designated minimum depth of 2.8 m is violated (see NVVP [67]). Daily values are available for the period from 1993 to 2003, in total 11 years.

Because only one LMD is defined per day on the complete Niederrhein and Waal, the interpretation of this dataset is complicated. Especially the view at only a part of the Waal (as this research does with the Midden-Waal) leads to problems. For this reason, the data for LMD is analysed both for the complete Niederrhein and Waal as well as for the Midden-Waal.

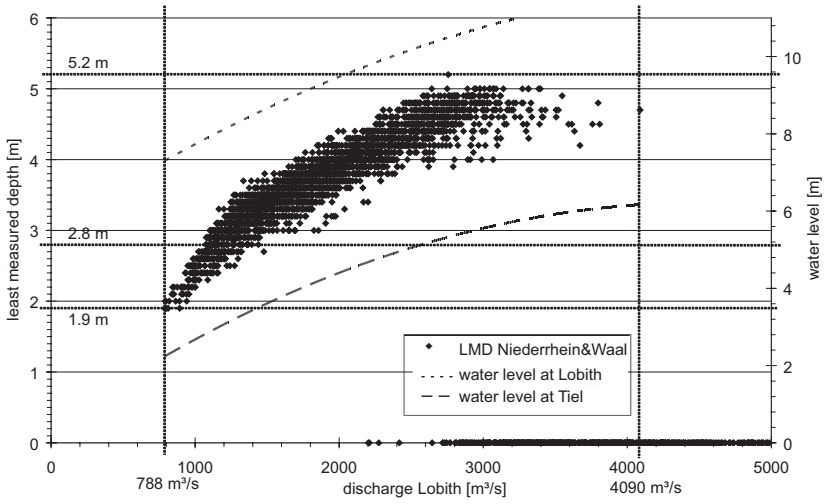

Figure 3.16: LMD on the Niederrhein&Waal versus the discharge at Lobith

Figure 3.16 shows the LMD on the Niederrhein and Waal and the water level at Nijmegen as function of the discharge at Lobith. The LMD is only measured when the water level at Nijmegen drops below 9 m+NAP. From Figure 3.16 can be seen that the minimum discharge without LMD is 2,200 m^3/s (data points with the value zero represent that no LMD is existent), while the maximum discharge where a LMD occurs is 4,090 m^3/s. LMDs smaller than 2.8 m occur for a discharge of 1,439 m^3/s, LMDs smaller than 2.0 m for a discharge less than 942 m^3/s. A strong correlation between the discharge at Lobith and the LMDs can be found (the linear correlation coefficient is 0.93 for the Niederrhein and Waal, 0.94 for the Midden-Waal, respectively).

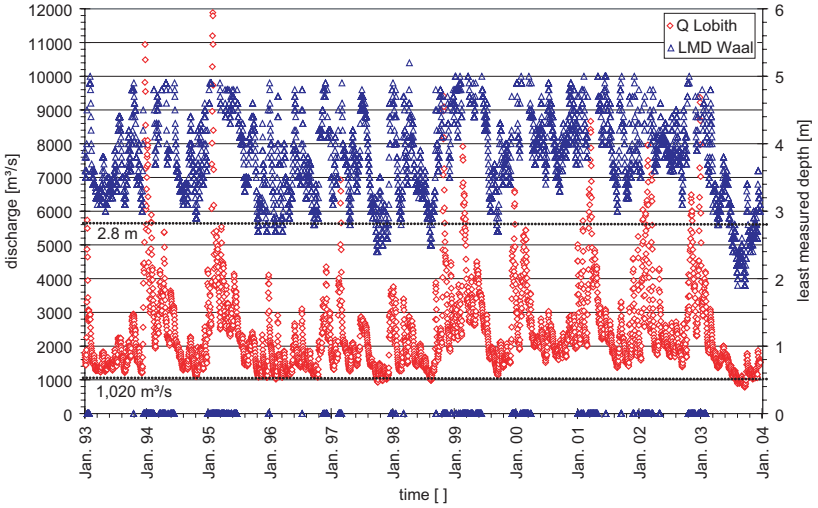

Figure 3.17: LMD for Niederrhein&Waal as function of time

Figure 3.17 shows the strong correlation between the discharge at Lobith and the LMD as well as the time periods where a smaller number or no LMD appears (indicated by the value zero). During the winter month with higher discharges less LMDs are measured. Critical values for the LMD (smaller than 3.0 m) occur during the low water period from August to October.

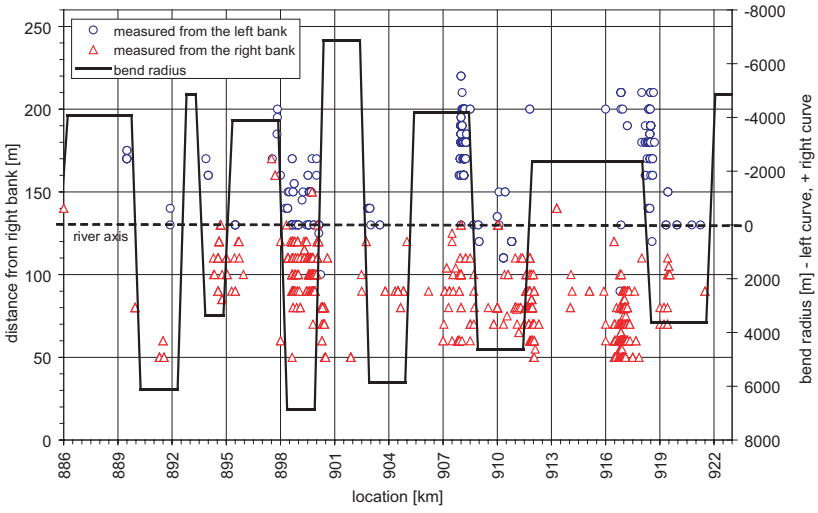

Figure 3.18: Distance of LMD from the right bank on the Midden-Waal

Figure 3.18 shows the location of the LMD in the river channel in terms of the distance from the right bank, including the bend radius. A positive bend radius means a right bend, while a negative radius stands for a left bend. Most LMDs are found to occur on the inner bend of curves. Only a small number are found close to the axis of the channel. It is supposed that the cross-sectional bed profile in a bend with a pool and a point bar is reason for this behaviour. In general, more LMDs (78.5%) are found on the right side of the river; only 21.5% of the LMDs are found on the left side of the river. The heavier navigation traffic going upstream to Germany might be an explanation for this as it flattens the top of the dunes [69] (see Section 2.4.1).

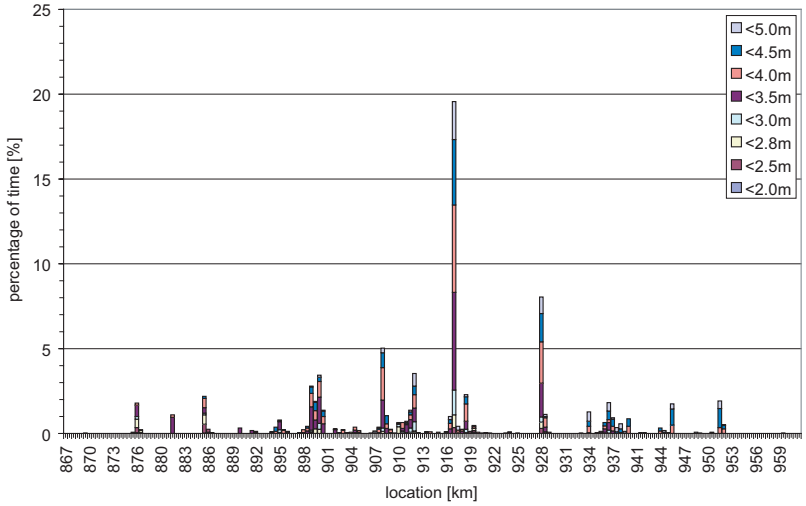

(a) Percentage of LMD per location for the Niederrhein&Waal

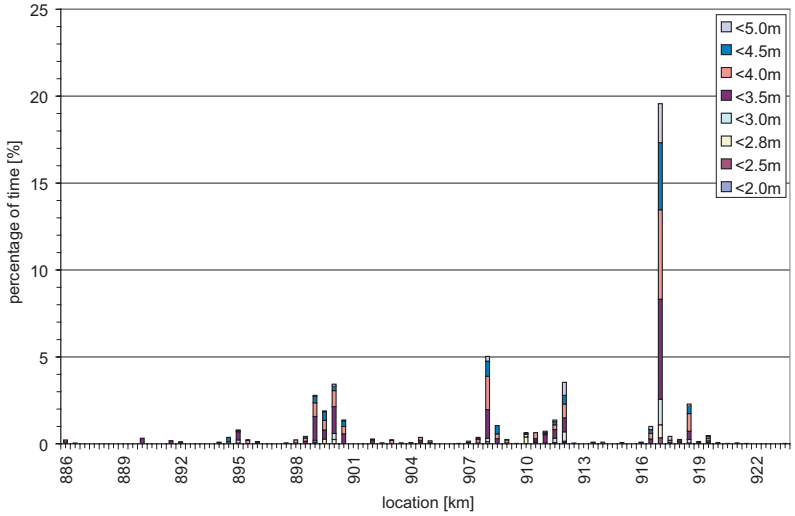

(b) Percentage of LMD per location for the Midden-Waal

Figure 3.19: Percentage of LMD for different water depth as function of the location

Figure 3.19(a) shows the percentage that a location forms the Least Measured Depth on the Niederrhein and Waal, Figure 3.19(b) shows the same percentage for the Midden-Waal only. In practice, LMD are noted with a longitudinal spatial precision of approx. 10 m. In order to make a comparison with the model results, the LMD are merged into reaches of 500 m length. The location Zennewijnen (km 917) shows to be the dominating bottleneck

location for the Niederrhein and the Waal. This location forms a bottleneck for about 19.8% of the time for a depth of 5.0 m. It is followed by Opijnen (km 928) with approx. 8%. On the Midden-Waal the location Ochten (km 908) with approx. 5%, as well as the areas around Dest&Hooge Waard (km 898-900) and Wamel (km 912) also frequently state problems for navigation. All other locations show LMD occurances lower than 1% of the time.

It can be clearly seen that, by only analysing the Midden-Waal, a large number of LMD are left out of consideration (see km 928-953 in Figure 3.19(a)). Therefore, the data set used in this research is not complete, and has to be integrated with care.

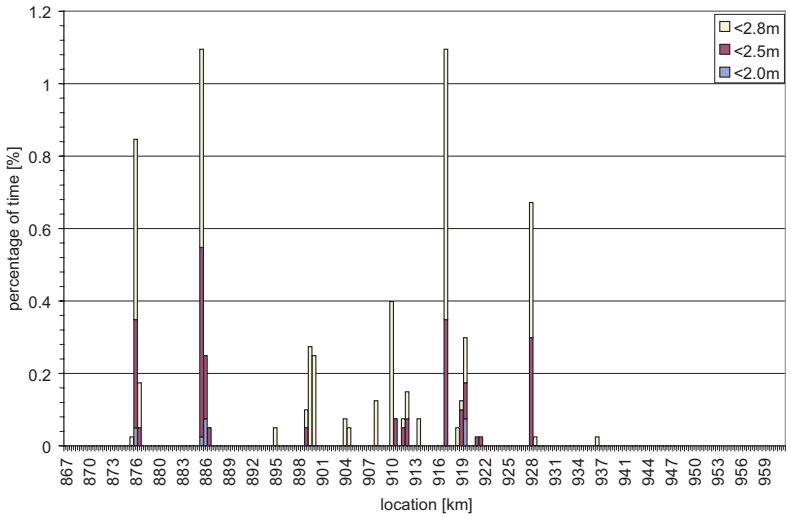

(a) Percentage of LMD lower than OLR for the Niederrhein&Waal

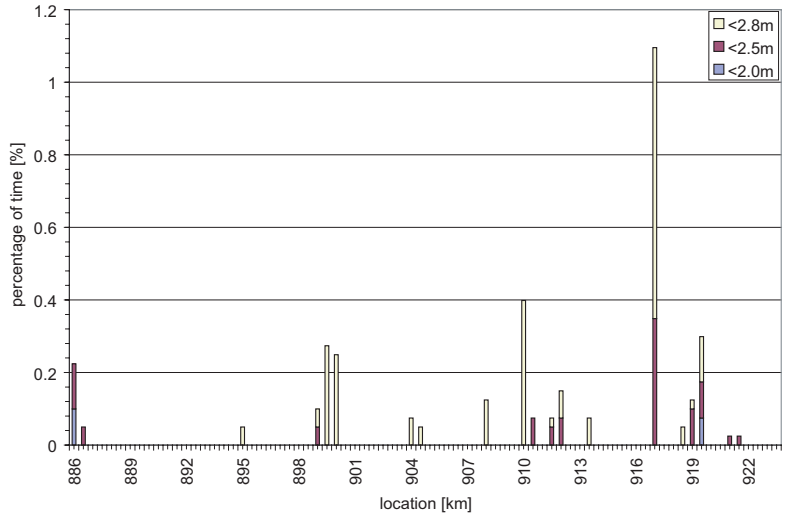

(b) Percentage of LMD lower than OLR for the Midden-Waal

Figure 3.20: Percentage of LMD lower than the OLR-criterion as function of the location

Figures 3.20 (a) and (b) show the locations where the OLR-criterion of a depth of 2.8 m is not fulfilled. During the period from 1993 to 2003, this criterion is not fulfilled for 6.36% of the time for the Niederrhein and the Waal. For the Midden-Waal this depth was not given for 3.61% of the time. For the Niederrhein and the Waal, four locations play an important role for this low water depth with percentages ranging from 0.7% to 1.1%: Er-

lecom (km 876), Nijmegen (km 885), Zennewijnen (km 917) and Opijnen (km 928), (Figure 3.20(a)). For the Midden-Waal, Dest&Hooge Waard (km 898-900), Ochten (km 908), Wamel (km 912) and Zennewijnen (km 917) are the four locations that constitute the most problems for a depth of 2.8 m (Figure 3.20(b)).

Of great importance is the question whether bends show a tendency to form locations with high occurrence of the Least Measured Depth. In Figure 3.21 the percentage that a location constitutes the LMD location related to the bend radius is plotted. A relation between the occurrence of a LMD and the bend radius cannot be seen.

This could be explained by the dynamic placement of buoys to enhance the navigation depth, which is explained in the following chapter. Especially in bends with narrow radii buoys are frequently placed in order to maintain a narrower but deeper navigation channel. In the bends at Nijmegen (km 885), Beneden-Leeuwen (km 909-911), Wamel (km 912), Winnssen (km 895) and Ophemert (km 919) buoys are positioned on a regular basis (indicated in the graph by arrows). This suggests that the interpretation of the LMD cannot be done properly without considering the placement of buoys in the Waal. At the location Nijmegen (km 885) additionally an armoured layer has been installed, which also enhances the navigation profile and so decreases the number of measured LMD. The locations Wamel (km 912) and Zennewijnen (km 917) have both the same bend radius, but only in the bend at Wamel buoys are placed. The resulting high percentage is hence mostly due to the frequent occurrence of a LMD at Zennewijnen.

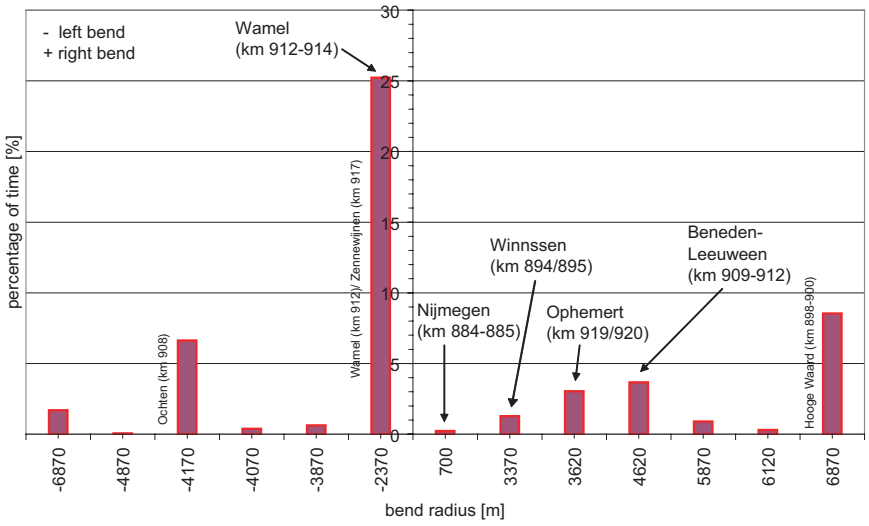

Figure 3.21: Percentage of LMD relative to the bend radius

Discussion Concluding it can be said that for the Midden-Waal four locations exist that very frequently form a nautical bottleneck. This statement is weakened by the fact that data for the LMD must be interpreted with great care, due to the following reasons:

- Only one LMD location is defined every day, which means that only the one minimum location for the complete Niederrhein and Waal for that day is noted. In reality several locations can form nautical bottlenecks at the same time, but only the one of those with the minimum water depth will appear in the LMD dataset. It can be

concluded that only the "top of the iceberg" is seen and in reality the in Figure 3.19 and 3.20 estimated percentages for each location should be a lot higher.

- By analysing only a part of the river, the Midden-Waal (37 km out of the 88 km of the Niederrhein and Waal), a large number of LMDs are neglected, as shown in Figure 3.19(a). Thus, the used dataset is not complete.
- In practice the Least Measured Depth does seldom occur in the section between the bifurcation Pannerdensche Kop and Nijmegen. At these locations, the navigation channel width is very often reduced by buoys.
- The same is valid for nine other locations on the Midden-Waal which are analysed in the following discussion of the navigation channel width. Buoys restricting the channel width are placed in order to maintain a higher navigation depth. This distorts the meaning of the LMD (see Figure 3.21). Least Measured Depth and Navigation Channel Width cannot be analysed separately.

3.3.2 Navigation Channel Width

The river manager economically prefers a navigation width reduction to a reduction in navigation depth. Thus on several locations, especially in river bends, buoys are placed in order to delineate a narrower but deeper navigation channel. The normal width of the Waal is 260 m. Subtracting a security distance of 25 m from both banks leaves a maximum navigation width of 210 m. In this case no buoys are placed. If the water depth drops, buoys are placed (and so the width is reduced) on a weekly basis to garantuee a channel depth of 3.5 m. This is done until a channel width of 100 m is reached, from then on the channel width is not further reduced and a LMD is measured [66].

Weekly values of the location (position along the river axis and distance from the bank) of these buoys are available for the years 1999 to 2003, in total five years.

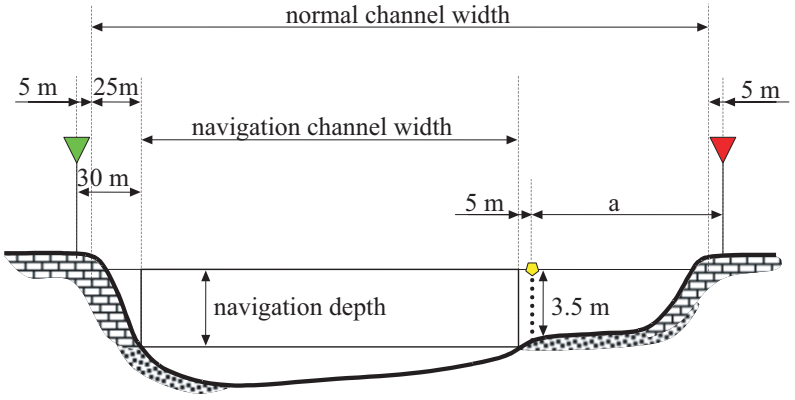

Figure 3.22: Channel width and buoy placement

The channel width was calculated the following way [12] (see Figure 3.22):

$$B_{nav} = B_n - a - B_{s1} - B_{s2} \tag{3.29}$$

in which:
B_{nav} is the resulting navigation channel width, B_n is the normal channel width (260 m for

the Waal), a is the distance of the placed buoy to the bank, B_{s1} is the security distance from the bank (25 m) and B_{s2} is the security distance from the buoy (5 m).

The resulting width is always related to a navigation depth of 3.5 m down to a minimum width of 100 m. At a lower width, a water depth of 3.5 m is no longer guaranteed, but an LMD is measured. Special attention has to be given to locations that show a navigation channel width lower than the by the National Traffic and Transportation Plan [67] intended minimum of 150 m.
In the Midden-Waal buoys are frequently placed in nine reaches:

No.	Reach	From km	To km
1	Bend Slijk-Ewijk	888.8	889.9
2	Crossing Ewijk	893.2	893.9
3	Bend&crossing Winssen	894.4	895.4
4	Bend&crossing Wely	896.4	897.5
5	Crossing Hooge Waard	901.2	901.4
6	Bend&crossing Druten	903.2	905.4
7	Bend&crossing Beneden-Leeuwen	909.0	911.7)
8	Bend Wamel	912.8	913.7
9	Bend&crossing Ophemert	919.0	920.9

Table 3.3: Reaches of the Midden-Waal with buoy placement

The channel width shows a dependency to the water level at Lobith (see Figure 3.23). The resulting channel width is very often around 200 m, a minimum width was found at the bend Winssen with 130 m. The channel width of 150 m was also violated at Wely and Ophemert.

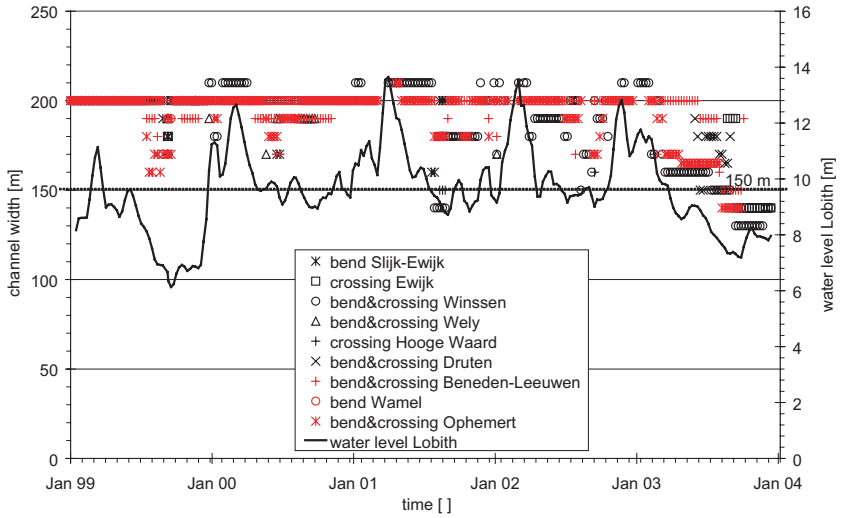

Figure 3.23: Estimated channel width as function time

Figure 3.24 gives an impression about the number of restrictions found at each location in relation to the discharge at Lobith. It can be seen that the three locations Winssen (km 894-895), Beneden-Leeuwen (km 909-912) and Ophemert (km 919-921) form restrictions for the navigation width nearly continuously. At the bend Wamel (km 912-914), buoys were placed only until the beginning of the year 2001, afterwards no more restrictions could be found at this location.

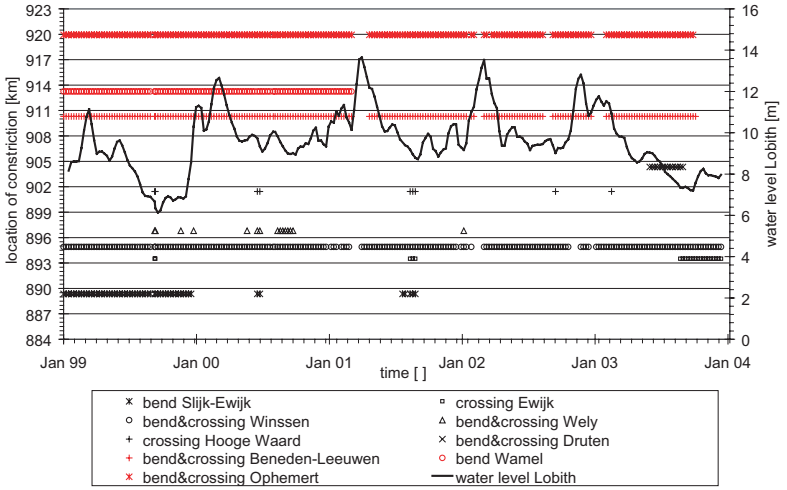

Figure 3.24: Location of width constriction as function time

Important for navigation are especially the cases where the navigation channel is less than 150 m. This percentage is included in Figure 3.25. The locations Winssen (with 7.7%), Ewijk (with 5.0%) and Ophemert (with 3.1%) form restrictions for the OLR-criterion.

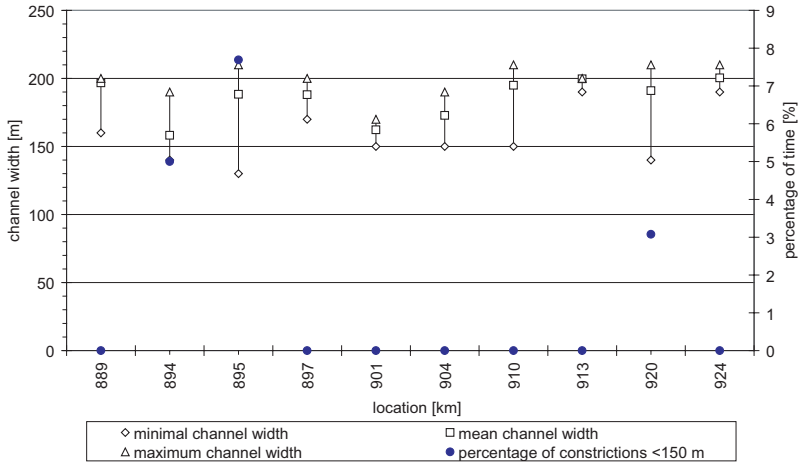

Figure 3.25: Restricted channel width as function the location

Discussion The following problems make an interpretation of the channel width difficult:

- For the Midden-Waal only at nine reaches buoys were set. Furthermore, the locations are only noted on a weekly basis, hence the data density is very low.
- Most of the time buoys are placed very close to the banks, delineating a navigation channel of 200 m. This forms only minor problems for the navigation, only restrictions lower than the OLR-criterion of 150 m are of high importance. According to the buoy data, this criterion is only violated at three locations.
- The nine reaches cover only 11.6 km of the 37 km long Midden-Waal. For 25.4 km no data to estimate the channel width exists. This does not mean that outside of the monitored stretches the channel width always stays above 150 m.

Chapter 4

Results of the one-dimensional Model

In this chapter the navigability of the Midden-Waal resulting out of the one-dimensional SOBEK Rhine model is described. For a period of four years the cross-sectional averaged bed level and the resulting water level for a spatial step of 500 m and and time step of ten days are computed. In total 100 model runs are conducted. Each model run results in one possible state of the river and its navigability. The results of these 100 simulations are presented in means of statistic characteristics of the navigability of the river, similar to the approach used in Van Vuren&Barneveld [59]. Only the years 2-4 are considered in the analysis to produce results comparable to the Delft3D model, which is found to be influenced by initial effects during the first year.
The navigability of the river is shown in means of five characteristics which should answer the questions of the river manager (see Section 1.2):

1. The navigable percentage of time of the complete Midden-Waal for four years
2. The navigable percentage of time of each location along the river for the period of four years
3. The navigable percentage of locations along the river as a function of time during these four years
4. The percentage of time that a location forms the bottleneck location (the location per time step with the smallest water depth) during four years
5. The probability (expressed in a percentage of time) that the navigation requirements set by the OLR-criterion for the complete stretch is not given during the four years

SOBEK is a one-dimensional model, hence only one parameter is left for the analysis of the navigability: the cross-sectional averaged water depth. Therefore, each of the above mentioned characteristics is shown for a draught from 1.5 m to 5.0 m, including the OLR-criterion of a water depth of 2.8 m. This analysis gives insight into the degree that certain locations form restrictions for the navigation traffic in means of the available water depth.

Special attention has to be given to the influence of geometrical features of the research area, especially the flow in bends and the alternating wide and narrow floodplains on the left and right side of the river. Since the SOBEK model cannot take account for the cross-sectional bed evolution in bends, two analytically based post-processing methods in form of parametrisations are used to incorporate the transverse slope effect on navigation.

The description of the navigability is thus divided into four parts:

1. The original SOBEK results without a transverse slope correction are presented
2. A correction for the transverse slope in bends after Talmon et al. [49] is explained and applied to the results
3. A correction for the transverse slope derived from the Delft3D model is applied to the results
4. All three results are compared with the LMD data and the agreement and differences are discussed

4.1 Results without transverse slope correction

Based on the 100 model runs with statistically generated discharge time series (see Section 3.2.2) the navigability of the Midden-Waal from km 886 to km 923 is assessed with statistical parameters. Each graph shows the statistics of the navigable percentage as a function of draught varying between 1.5 m and 5.0 m, including the OLR-depth of 2.8 m.

1. Navigability of the complete Midden-Waal Figure 4.1(a) shows the percentage of time that the complete 37 km long stretch is navigable for one single simulation (simulation number 20), arbitrary chosen out of the 100 computed simulations. It states that the river is navigable all the time up to a draught of 2.5 m, and e.g. for ships with a draught of 3.5 m, the complete stretch is navigable for 89% of the time during the four year long period. This result is equal to the outcome of a deterministic modelling approach. It can be regarded as one "picture of reality".

The following Figure 4.1(b) shows the percentage of time that the complete stretch is navigable for three arbitrary chosen simulations (simulations number 20, 50 and 90). The high differences between these three simulations give a first impression of the uncertainties involved in the modelling process. Each simulation is driven by a different discharge time series and thus represents only one possible state ("picture of reality") of the navigability of the river.

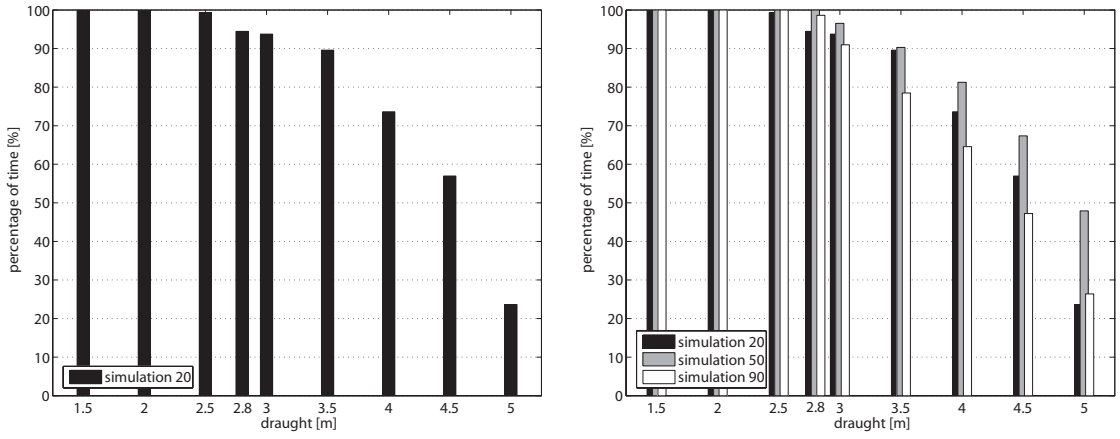

(a) Navigable percentage for one simulation (b) Navigable percentage for three simulations

Figure 4.1: Navigable percentage for single simulations, without correction

As in this research 100 simulations are conducted, the results for the navigability are from now on shown in terms of the statistics of those 100 outcomes. Figure 4.2 shows the statistics of the navigability of the complete Midden-Waal for all 100 simulations. It can be seen that for example for a draught of 3.5 m, over the period of four years, at least one simulation predicts a very low navigability, with approximately 72% of the time. On the other hand, there is at least one simulation which predicts the stretch to be navigable 100% of the time. The mean of all 100 conducted simulations estimates the navigability for a draught of 3.5 m with approx. 90%.

A characteristic often used in the statistics of distributions is the 90% confidence interval. In this research the size of the 90% confidence interval is used as a measure of the involved uncertainty, as it gives an impression of the variation in the predicted navigability. The size of the 90% confidence interval can be easily calculated as the difference between the 95^{th} percentile and the 5^{th} percentile of the distribution of the outcome of the conducted 100 simulations. For the case of a draught of 3.5 m in Figure 4.2, the size of the 90% confidence interval is approx. $99\% - 77\% = 22\%$.

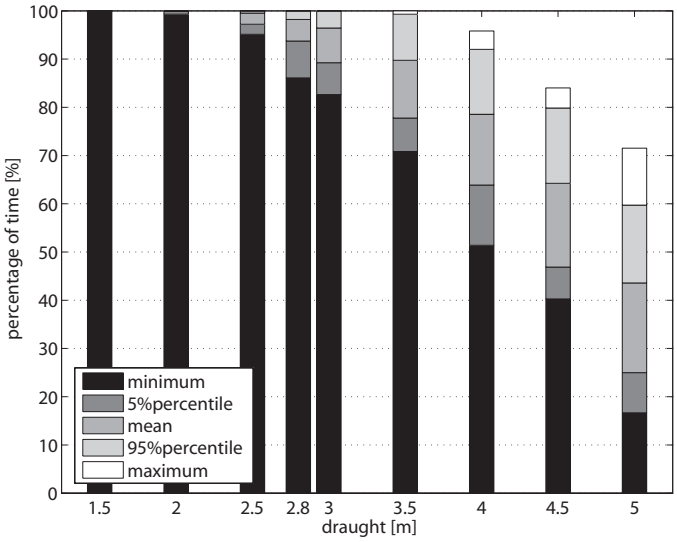

Figure 4.2: Navigable percentage for the complete Midden-Waal, without correction

2. Navigability of each location Figures 4.3 (a) to (h) show the navigable percentage of time as a function of the location along the river for draughts from 1.5 m to 5.0 m. This provides insight into locations that are restricting navigation. The size of the confidence interval gives an indication at which locations the uncertainty of the navigability is high.

The model predicts that all locations are navigable at any time for draughts up to 2.5 m. From then on, the navigability decreases at all locations more or less uniform as a function of the draught. On the other hand, the size of the 90% confidence interval increases, meaning that the involved uncertainty increases as a function of the draught.

Several locations, like the part after the bend at Nijmegen (km 886-891) and the locations Hooge Waard (km 900-901), Ochten (km 906), Beneden-Leeuwen (km 908-910), Wamel (km 912), Zennewijnen (km 917) and Ophemert (km 919) show a slightly lower navigability. Those locations also show a slightly larger confidence interval, which points out the higher uncertainty in water depth.

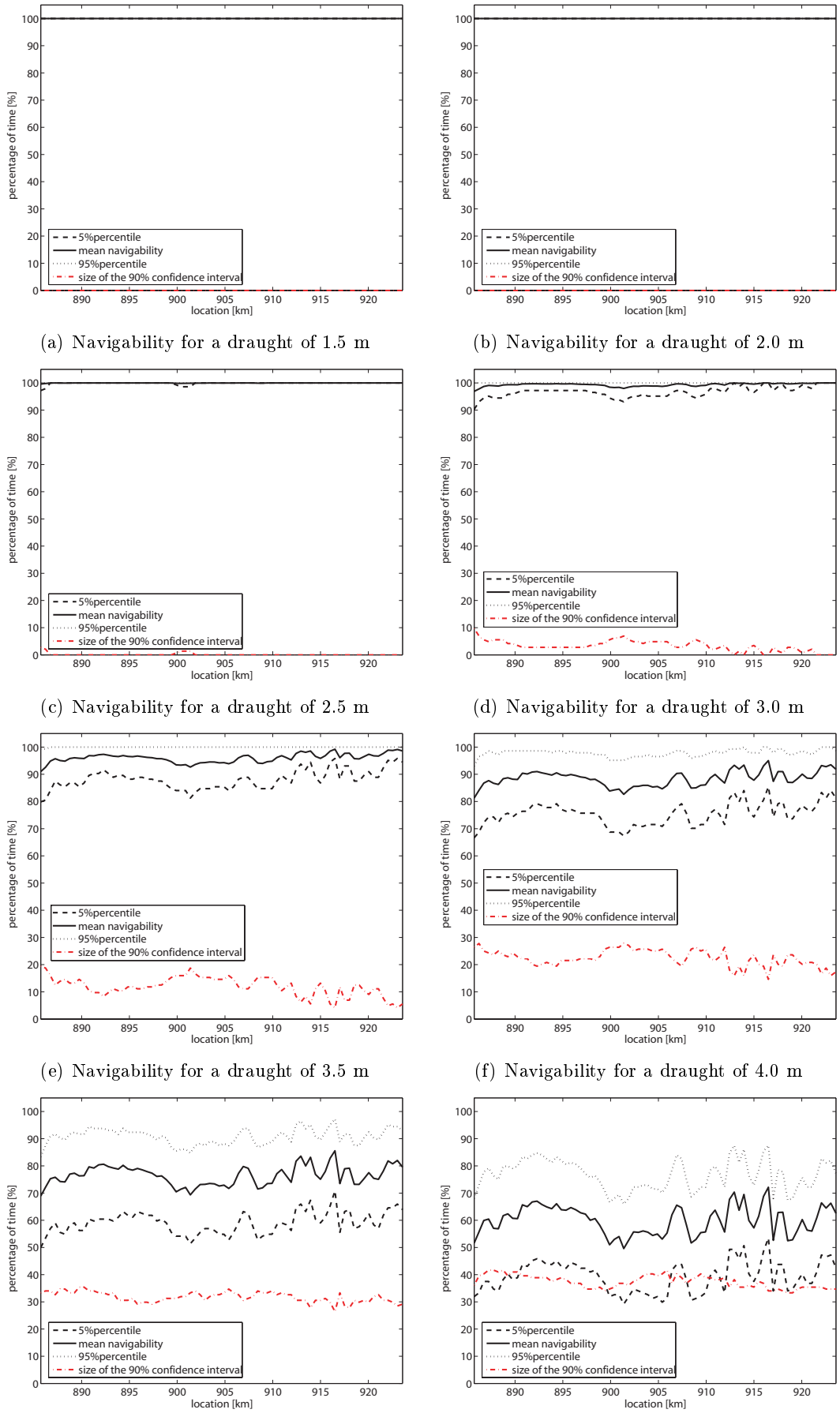

(a) Navigability for a draught of 1.5 m

(b) Navigability for a draught of 2.0 m

(c) Navigability for a draught of 2.5 m

(d) Navigability for a draught of 3.0 m

(e) Navigability for a draught of 3.5 m

(f) Navigability for a draught of 4.0 m

(g) Navigability for a draught of 4.5 m

(h) Navigability for a draught of 5.0 m

Figure 4.3: Navigable percentage as function of the location, without correction

3. Navigability as function of time Figure 4.4 gives insight into the time intervals over the four year simulation period where the river is navigable for ships of a draught of 3.5 m. It shows the percentage of locations that are navigable for this draught at each time step. The navigability is highly dependent on the discharge, so periods with restrictions in the navigability can especially be found during the low-water period from August to October (Start of the simulations is the month September).

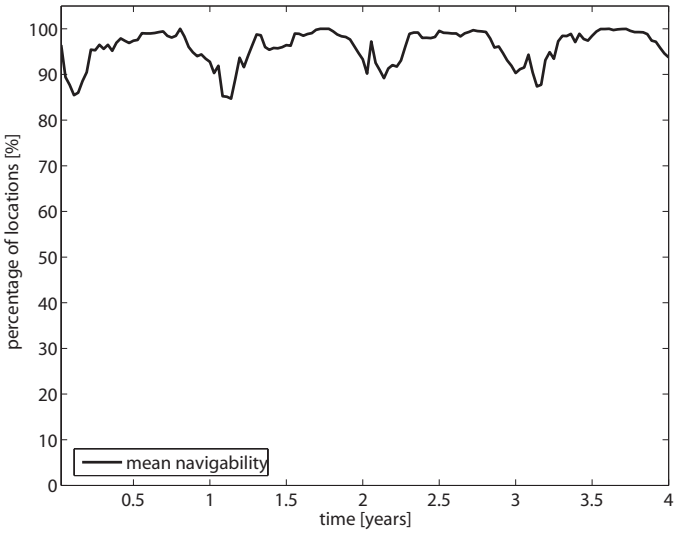

Figure 4.4: Navigable percentage as function of time, without correction

4. Bottleneck location An important parameter for the river manager and navigation is the location that is restricting the navigation traffic at a certain time step, meaning the location that shows the lowest water depth for the complete stretch at a certain time. This location is from now on called the "bottleneck location" and is equal to the definition of the in practice used Least Measured Depth location (see Section 3.3.1). Figure 4.5 shows the percentage of time that a location forms the bottleneck location.

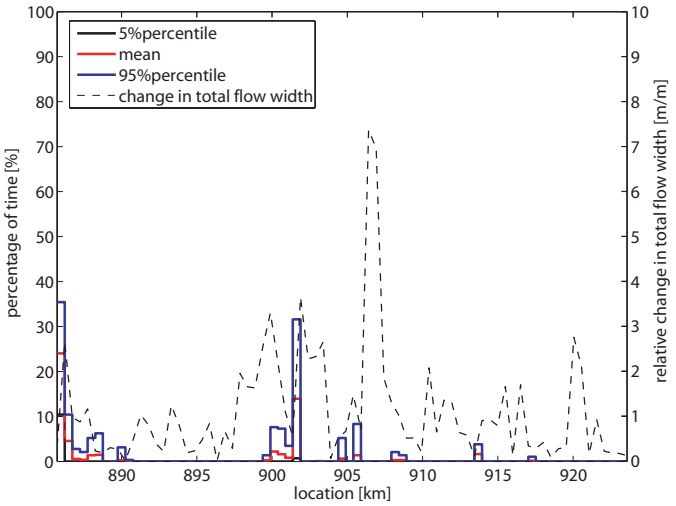

Figure 4.5: Percentage that a location forms a bottleneck, without correction

The narrowing and widening floodplains along the river are expected to have influence on the morphology and thus on the navigability. The same accounts for the transverse bed slope evolving in a river bend (see Section 2.4.2). As the latter effect is not included in the SOBEK model, only the relative change in total flow width is displayed in the picture. A relation between the relative change in total flow width and the percentage that a location forms a bottleneck can be seen with a lag of approximately 500 m to 1.0 km.

Locations that tend to form nautical bottlenecks are the area after the bend of Nijmegen (km 886) with an mean percentage of 24%, Hooge Waard (km 902) with 13% followed by several locations with percentages between 2% and 4%.

5. Fulfillment of the navigation requirements The National Traffic and Transportation Plan [67] sets the limit that a water depth of 2.8 m should be available for the navigation traffic on the river for discharges higher than 818 m^3/s (OLA-conditions). This discharge is in reality exceeded for 95% of the time. It is important to know that this criterion for the water depth is not fallen short for more than 5% of the time including all discharges. It is also interesting to know with which probability the navigation requirements are fulfilled for discharges that are larger than 818 m^3/s.

Figure 4.6(a) shows that the probability for the critical water depth (the minimum water depth per time step) being 2.8 m or lower for all discharges is 1.88%. Thus the simulations suggest that the OLR-criterion is fulfilled far more often than the desired 95% of the time. The probability for discharges higher than 818 m^3/s is of course lower with 0.2%.

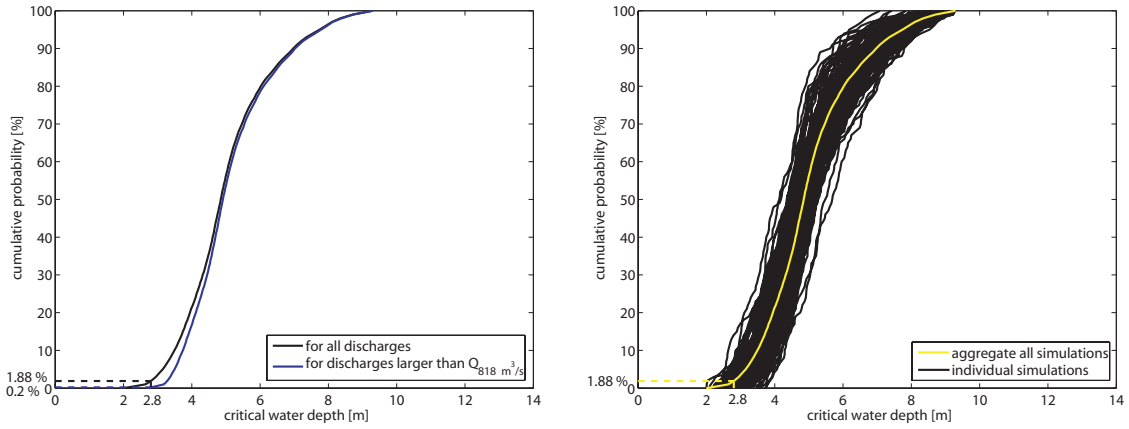

(a) All discharges and discharges>OLA

(b) All simulations individually

Figure 4.6: Cumulative probability curves of the critical water depth, without correction

Figure 4.6(b) shows the cumulative probability curves for all simulations individually; every line represents one single simulation. The chance to not fulfill the OLR-criterion for each single simulation varies between 0% and approx. 16%. This high bandwidth again gives valuable insight into the involved uncertainties. In case of a deterministic analysis only one of those curves would have been computed, with one value for the chance of not fulfilling the navigation requirements. The 100 conducted simulations state that this value actually can vary in an interval of approx. 16%, due to the included uncertainty in the discharge time series.

4.2 Results with transverse slope correction after Talmon

The SOBEK model is working with symmetrical cross-sections and does not consider any secondary flow effects. Especially the secondary flow in river bends has a great effect on the bed level of the river thus on the navigability (see Section 2.4.2). For this reason a correction factor following Talmon et al. [49] is applied to adjust the water depth in bends. The correction was developed by Van Vuren&Barneveld [59].

Transverse slope correction after Talmon et al. Talmon et al. developed a formula for the lateral bed slope in bends depending on the bend radius and the water depth. The lateral slope is calculated as follows:

$$\tan i_b = A f(\Theta) \frac{h}{r} \tag{4.1}$$

with:

$$A = \frac{2\epsilon}{\kappa^2}\left(1 - \frac{\sqrt{g}}{\kappa C}\right)$$

$$f(\Theta) = 9\left(\frac{D_{50}}{h}\right)^{0.3}\sqrt{\Theta}$$

in which:
$\tan i_b$ is the lateral bed slope, h is the water depth, r is the bend radius, ϵ is a calibration factor (≈ 1), κ is the Von Karman coefficient (≈ 0.4), g is the gravitional acceleration, C is the Chézy roughness, D_{50} is the mean grain diameter and Θ is the Shields parameter.

With this formula the corrected water depth related to the bend radius in the Midden-Waal is calculated for each spatial step [59]:

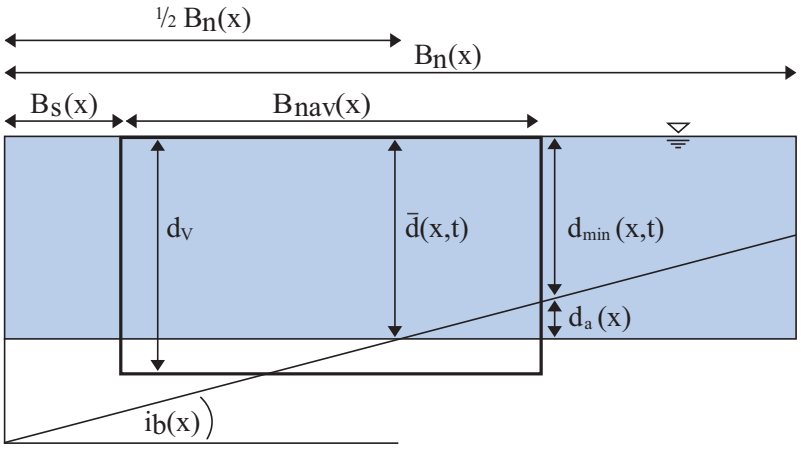

Figure 4.7: Correction of the water depth for the transversal slope effect, after Talmon

$$d_{min}(x,t) = \overline{d}(x,t) + d_a = \overline{d}(x,t) + \left(\frac{B_n(x)}{2} - B_s(x) - B_{nav}(x)\right) i_b(x) \tag{4.2}$$

in which:
$d_{min}(x,t)$ is the corrected water depth, $\overline{d}(x,t)$ is the water depth calculated by SOBEK, d_a is the correction for the water depth, $B_n(x)$ is the normal channel width (260 m for the Waal), $B_s(x)$ is the security distance from the banks (25 m), $B_{nav}(x)$ is the navigation channel width (150 m) and i_b is the above calculated transverse slope (see Figure 4.7).

The correction for the Midden-Waal was calculated using the characteristic discharge of 1,800 m^3/s. The bend radius and the resulting correction for the water depth are shown in Figure 4.8. For the narrow bend at Nijmegen (km 884-886) a bottom protection structure is placed in order to enhance the navigation profile. For this reason the correction for the lateral slope is set to be zero at km 886.

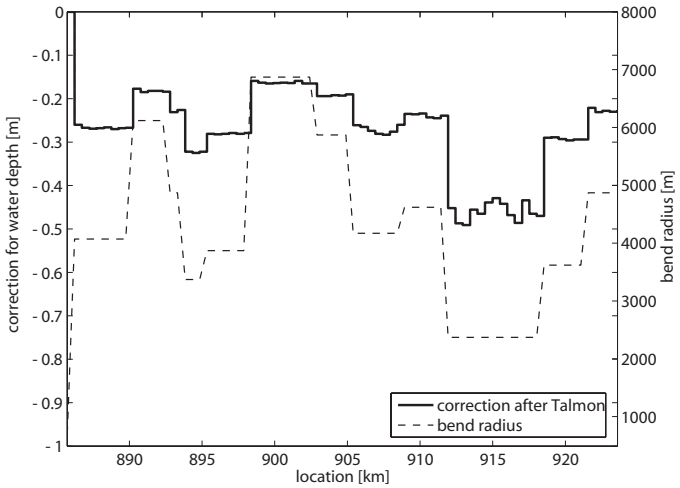

Figure 4.8: Resulting correction for the water depth in bends, after Talmon

1. Navigability for the complete Midden-Waal In Figure 4.9(a) the results for the same three simulations (number 20, 50 and 90) as in Figure 4.1(a) are shown. A decrease in the predicted percentage of navigability can be seen for all three simulations. Also the relation between the three simulation has changed. It seems that the correction has larger influence, in terms of a larger decrease of the navigable percentage, on simulation number 50 than on the other two. This can be best seen for a draught of 5.0 m. This means that the applied correction has a different influence on different simulations.

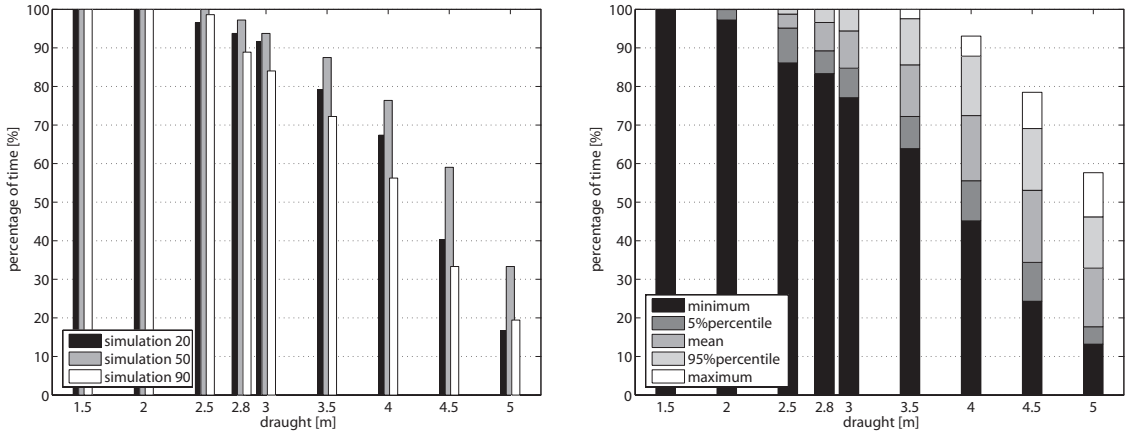

(a) Navigable percentage for three simulations

(b) Navigable percentage for all simulations

Figure 4.9: Navigable percentage for the complete Midden-Waal, Talmon correction

Figure 4.9(b) now shows the statistics of the navigability for all 100 simulations with the correction for the water depth in bends applied. It can be seen that the navigable percent-

age is reasonably lower than in Figure 4.1(b). For a draught of 3.5 m the river is navigable for 85% of the time in average. The minimum and maximum navigable percentage for this draught are 63% and 100%. With a probability of 90% the navigability at this draught lies between 72% and 98%. The size of the 90% confidence interval (as a measure of the uncertainty) increases from 22% to 26%, the minimum navigability has decreased from 71% to 63%. It can be concluded that the applied correction has especially a high effect on simulations that predict a low navigability. It causes an effect similar to the increasing uncertainty for a larger draught, as seen in Figure 4.3.

2. Navigability of each location In Figures 4.10 (a) to (h) the navigability as function of the river location is given. The percentage of the mean navigability decreases in comparison to Figure 4.3. The river is only navigable without limitation for ships up to a draught of 2.0 m. The size of the 90% confidence interval also slightly increases. Locations with a lower navigability can be found after the bend of Nijmegen (km 887-889), Ochten (km 907), Beneden-Leeuwen (km 908-910), Wamel (km 912), and Zennewijnen (km 917).

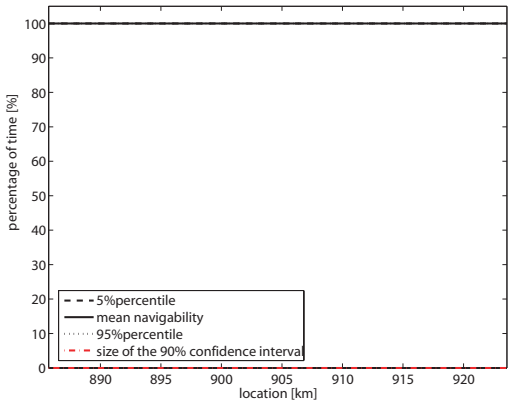

(a) Navigability for a draught of 1.5 m

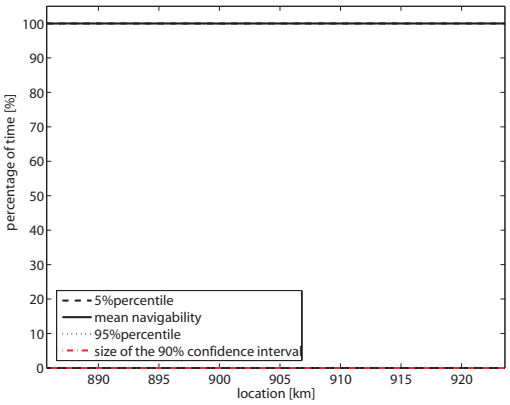

(b) Navigability for a draught of 2.0 m

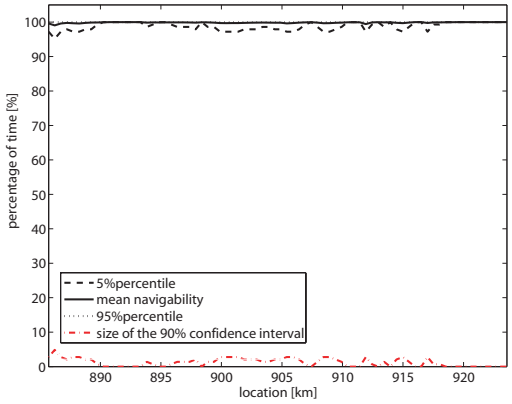

(c) Navigability for a draught of 2.5 m

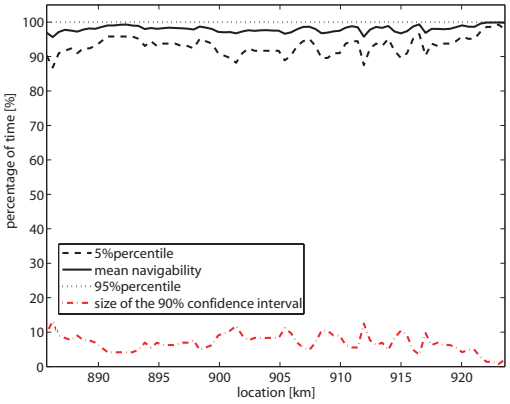

(d) Navigability for a draught of 3.0 m

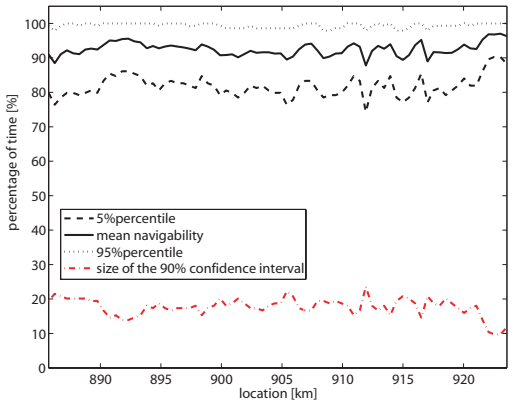

(e) Navigability for a draught of 3.5 m

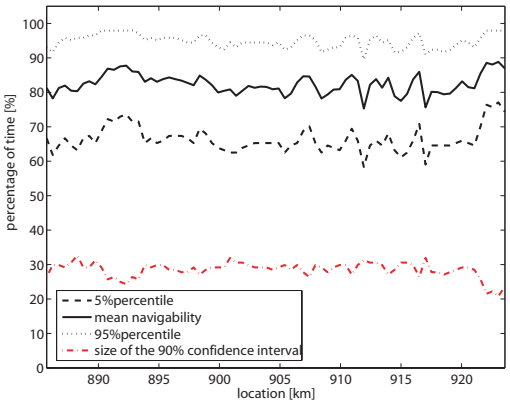

(f) Navigability for a draught of 4.0 m

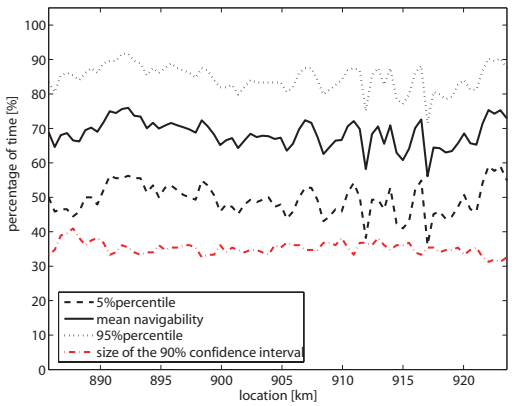

(g) Navigability for a draught of 4.5 m

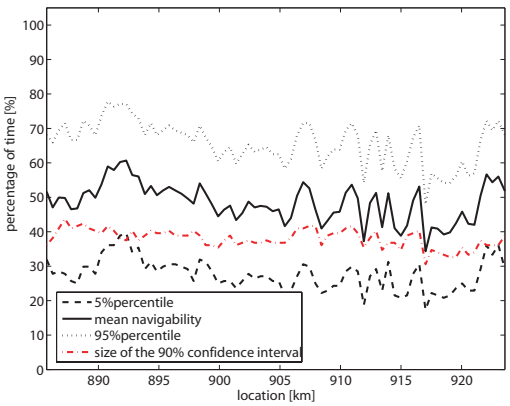

(h) Navigability for a draught of 5.0 m

Figure 4.10: Navigable percentage as function of the location, Talmon correction

3. Navigability as function of time Figure 4.11 shows the navigability of the river as a function of time during the four analysed years for a draught of 3.5 m. The river has similar to Figure 4.4 a lower navigability during the dry season. The percentages of the corrected values are lower than the original results, meaning less locations are navigable at a certain time step.

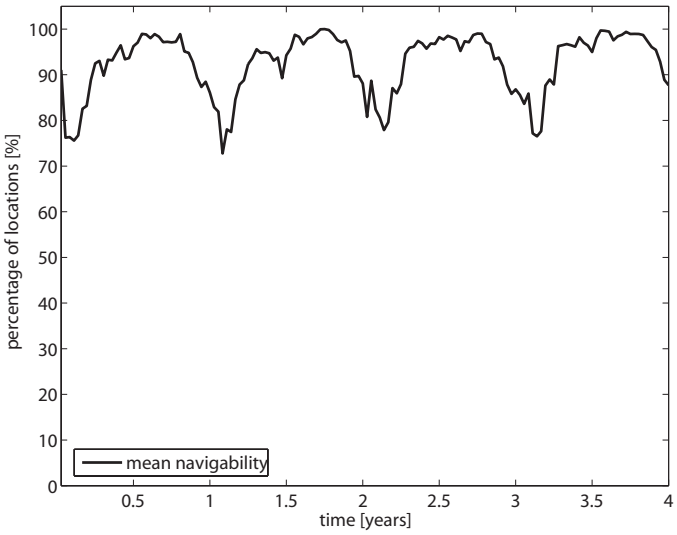

Figure 4.11: Navigable percentage as function of time, Talmon correction

4. Bottleneck location Figures 4.12 (a) and (b) show the percentage that a location forms a bottleneck in relation to the bend radius and the relative change in total flow width.

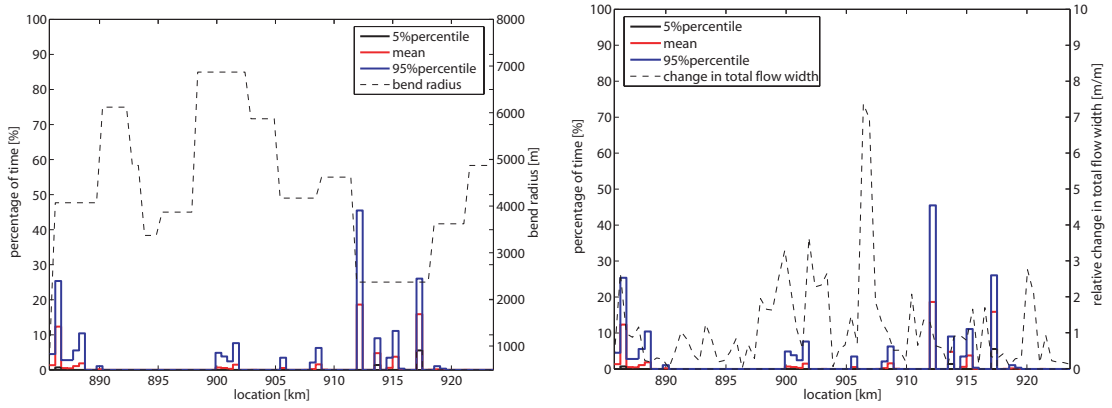

(a) Including the bend radius

(b) Including the relative change in total flow width

Figure 4.12: Percentage that a location forms a bottleneck, Talmon correction

A good agreement between the predicted statistics and the bend radius can be seen. This is of course only the case because a correction of the water depth related to the bend radius is applied. The lower the bend radius and thus the sharper the curve, the higher the correction factor deducted from the water depth. On the other hand, the former observed analogy between the relative change in total flow width cannot be found any more. The dominating restricting locations now are Zennewijnen (km 917) with an average of 21%,

Wamel (km 913) and the part after Nijmegen (km 887) with 18% and 13%, respectively. This means that a certain shifting has taken place. The locations on the beginning of the stretch have now less importance, the highest number of bottlenecks can be found in the reach from km 912 to km 918, where bends with lower radii are situated.

5. Fulfillment of the navigation requirements Figure 4.13(a) shows that the probability for a water depth of 2.8 m or lower for all discharges is 3.41%, the probability for discharges higher than OLA is lower with 0.59%. Thus the model predicts that the OLR-criterion is still fulfilled even if the percentages are much higher than in case without the transverse slope correction. Figure 4.13(b) shows the cumulative probability curves for all simulations individually, the chance to not fulfill the OLR-criterion here varies between 0% and approx. 20%. This means that the applied correction leads to an increase of this interval (16% for the case without correction).

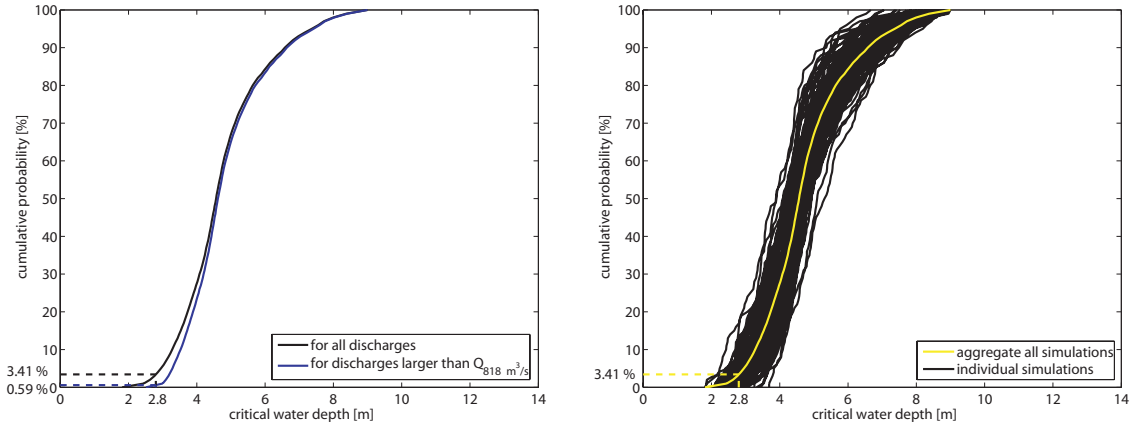

(a) All discharges and discharges>OLA (b) All simulations individually

Figure 4.13: Cumulative probability curves of the critical water depth, Talmon correction

4.3 Results with transverse slope correction after the Delft3D model

The parametrisation for the correction of the lateral bed slope following the approach of Talmon et al. includes several assumptions. It is only applicable for the equilibrium state of the river bed and it only treats the slope as a function of the water depth and the bend radius. Furthermore, in the previous section the correction is calculated using the characteristic discharge of 1,800 m^3/s resulting in a constant correction factor for each location, independent from the changing discharge regime. A second possibility to derive a analytical correction is shown in this section.

Transverse slope correction after the Delft3D model For the one-dimensional SOBEK model and the quasi-3D Delft3D model the same discharge time series are used. The Delft3D model gives the possibility to assess the cross-sectional bed profile evolution depending on the discharge time series. For a second parametrisation the transverse bed slopes computed with the Delft3D model for each time step are implemented as a correction factor in the analysis of the SOBEK results. The resulting correction is shown in Figure

4.14. The correction now depends on the discharge time series and therefore is space and time dependent. It is presented as minimum, mean and maximum correction for each location.

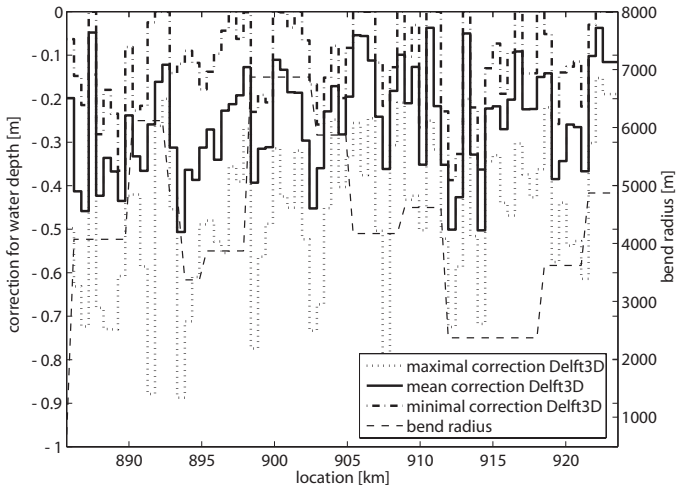

Figure 4.14: Resulting correction for the water depth in bends, after Delft3D

Figure 4.15 shows a comparison between the Talmon correction and the mean of the now used Delft3D correction.

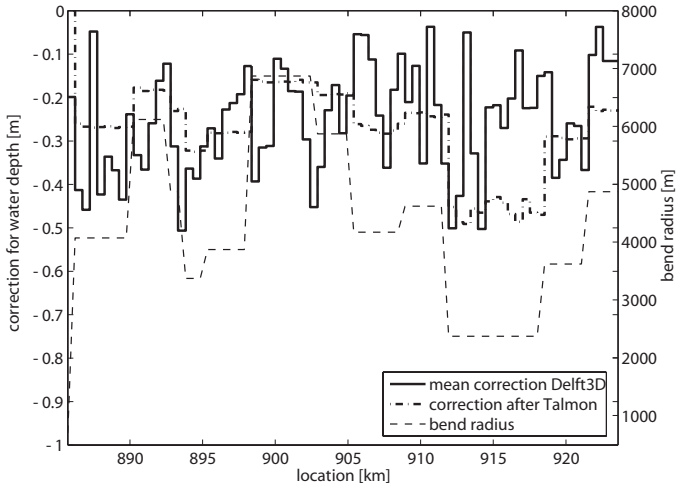

Figure 4.15: Comparison of the Talmon and Delft3D corrections for the slope effect

It can be seen that both correction factors stay in the same range, but nonetheless differ significantly for several locations. The reason for this is as follows: The bend radius in the Talmon correction is assigned using tables and maps. Thus, longer reaches of several kilometer length are assigned to have the same bend radius (see Table 1.1), used in for the calculation of the transverse slope in Eq. 4.1. In the Delft3D model the correction is included in the model topography, which has cross-sections every 100 m along the river. The Delft3D outcome for the transverse bed slope is then averaged over reaches of 500 m to match the SOBEK grid (using a moving average). Thus, the Delft3D correction uses a higher longitudinal resolution to calculate the transverse bed slope (500 m instead of several km) and gives a more precise outcome.

1. Navigability for the complete Midden-Waal Figure 4.16(a) shows the results for the same three simulations as in Figure 4.1(b) and 4.9(a). Again, a further slight decrease in comparison to the two previous results can be seen in all three simulations. The Delft3D correction seems, similar to the Talmon correction, to have a different effect on different simulations. This can be seen in the fact that the decrease in the navigability predicted by simulation 50 compared to Figure 4.1(b) is higher than for simulation 20 or 90.

Figure 4.16(b) now shows the statistics of the navigability for all 100 simulations with the correction from the Delft3D model applied. It can be seen that the navigable percentage is reasonably lower than in Figure 4.2 and also slightly lower than in Figure 4.9(b). For a draught of 3.5 m the river is now navigable for 82% of the time in average. The minimum and maximum navigable percentage for this draught are 60% and 97%. With a probability of 90% the navigability at this draught lies between 69% and 95%. The size of the confidence interval is with 26% equal to the Talmon correction, the minimum navigability has decreased sligthly from 63% to 60%. This suggests that both corrections increase the uncertainty in the same order. The mean navigability has decreased slightly more in the Delft3D case.

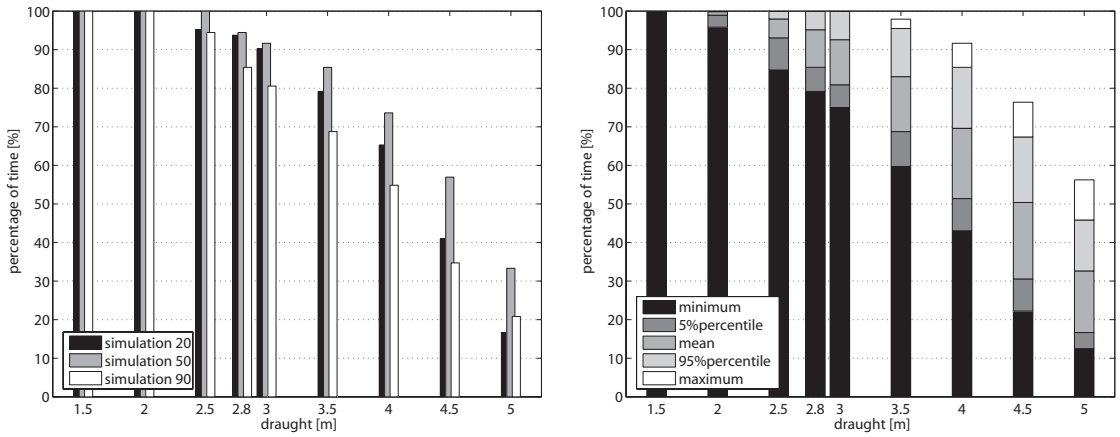

(a) Navigable percentage for three simulations

(b) Navigable percentage for all simulations

Figure 4.16: Navigable percentage for the complete Midden-Waal, Delft3D correction

2. Navigability of each location Figure 4.17 (a) to (h) shows the navigability for each location for different draughts. It can be seen that the size of the 90% confidence interval is in the same range as in the previous section. The predicted navigability in general now is slightly lower. Most important is the fact that the difference between the locations is more pronounced. Several distinct locations show higher navigability and several other distinct locations show a lower navigability than in Figure 4.10. This is due to the above mentioned higher longitudinal resolution and the time dependency of the Delft3D correction. Especially the better mean navigability at the locations km 914, km 916 and km 921 can clearly be seen. It seems that the correction after Talmon is overestimated for these locations. The locations that show to be constricting the navigability do not change. A restricted navigability still can be found at Ochten (km 907), Beneden-Leeuwen (km 908-910), Wamel (km 912) and Zennewijnen (km 917). Only the location Druten (km 903) has been added.

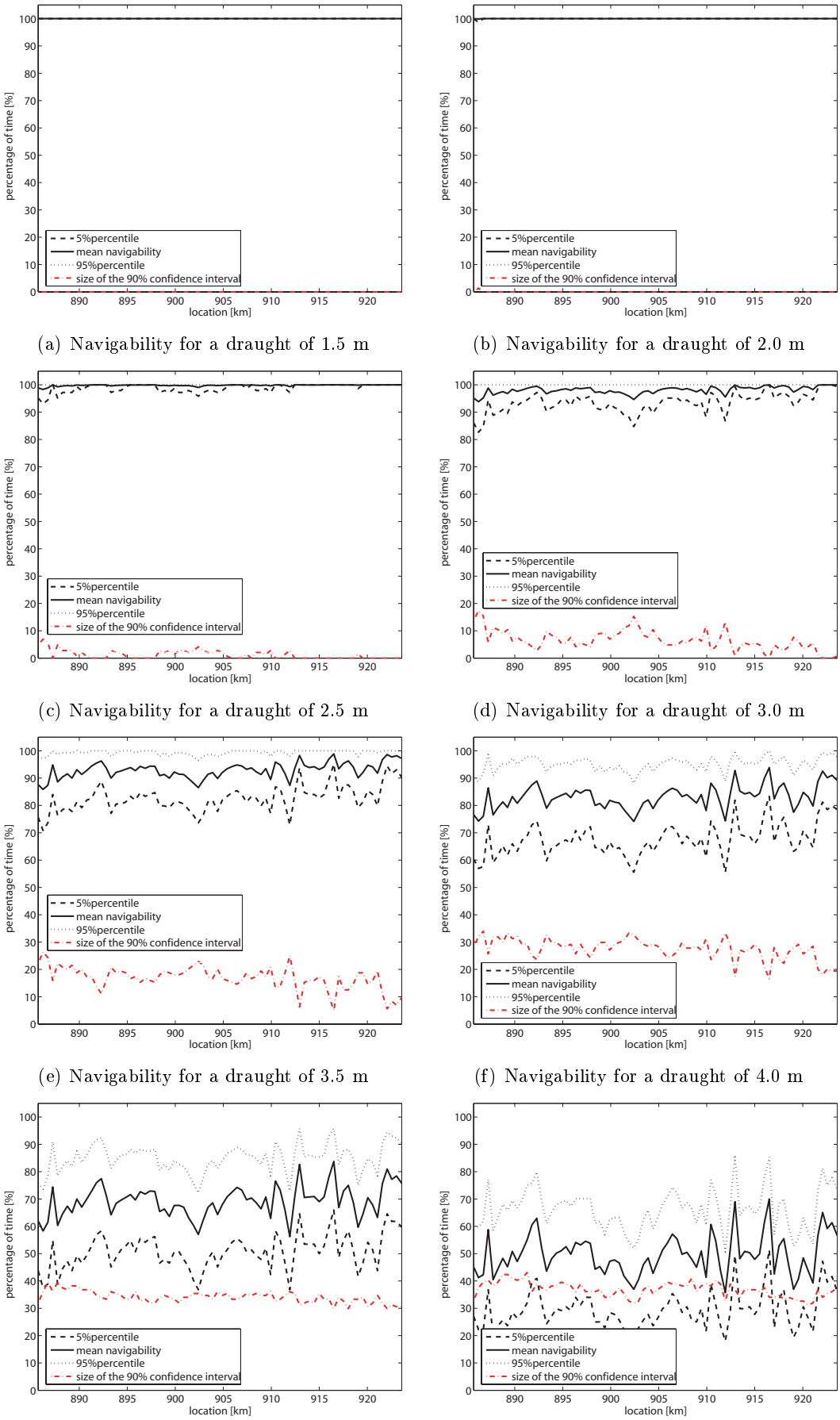

(a) Navigability for a draught of 1.5 m

(b) Navigability for a draught of 2.0 m

(c) Navigability for a draught of 2.5 m

(d) Navigability for a draught of 3.0 m

(e) Navigability for a draught of 3.5 m

(f) Navigability for a draught of 4.0 m

(g) Navigability for a draught of 4.5 m

(h) Navigability for a draught of 5.0 m

Figure 4.17: Navigable percentage as function of the location, Delft3D correction

3. Navigability as function of time Figure 4.18 gives insight into the time intervals over the four year simulation period where the river is navigable for ships of a draught of 3.5 m. The percentages of the corrected values are lower than the original SOBEK results in Figure 4.4, but very similar to the results with the Talmon correction (see Figure 4.11).

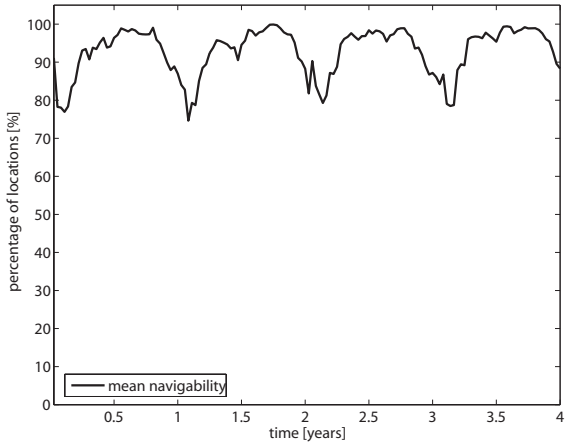

Figure 4.18: Navigable percentage as function of time, Delft3D correction

4. Bottleneck location Figures 4.19 (a) and (b) show the percentage that a location forms a bottleneck in relation to the bend radius and the relative change in total flow width. The bottleneck locations have changed considerably for the new correction. Now the dominating locations can be found after the bend of Nijmegen (km 887) with a mean of approx. 20%, Druten (km 903) with 12% and Wamel (km 913) with 10%. A relation of these locations to the bend radius like in the case of the Talmon correction, or a relation to the change in total flow width like in the original results cannot be identified.

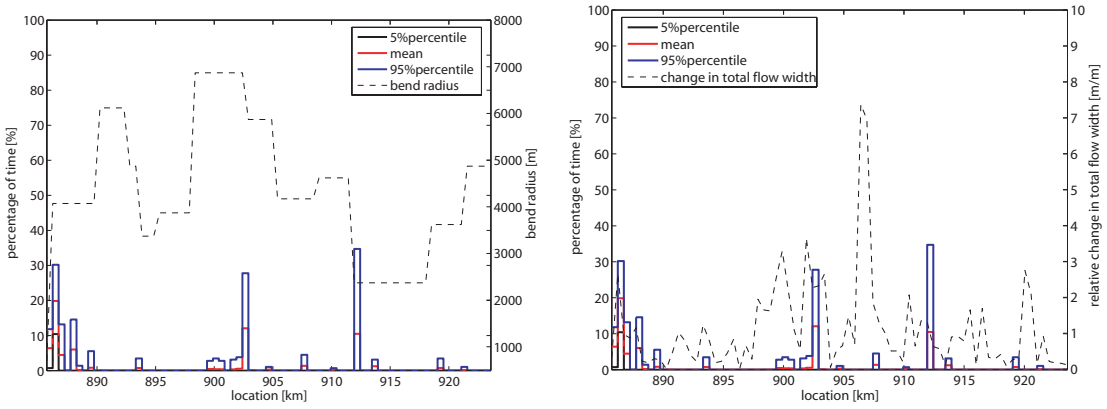

(a) Including the bend radius

(b) Including the relative change in total flow width

Figure 4.19: Percentage that a location forms a bottleneck, Delft3D correction

The reasons for this considerable change are the following: (1) the accumulation of bottlenecks at the beginning of the Midden-Waal could be due to boundary effects in the Delft3D model (as the boundary in the model is placed directly at km 886); (2) the Delft3D model has a higher longitudinal resolution and time dependency, thus the correction factor differs significantly from the Talmon correction. Finally, (3) the bottleneck criterion is a very

sensitive measure. Only the one location with the lowest water depth per time step is included, even if the difference between two locations is only in the order of several cm. Small changes in the data, like the different applied corrections, can lead to large differences in the results.

5. Fulfillment of the navigation requirements Figure 4.20(a) shows that the probability for a water depth of 2.8 m for all discharges is 4.81%, the probability for discharges higher than OLA is lower with 0.91%. Hence, the model predicts that the OLR-criterion is still fulfilled even if the percentages are much higher than in case without the transverse slope correction and slightly higher than in the case with the Talmon correction. Figure 4.20(b) shows the cumulative probability curves for all simulations indiviudally, the chance to not fulfill the OLR-criterion here varies between 0% and approx. 20%. This means that the applied Delft3D correction leads to the same band of uncertainty as the Talmon correction.

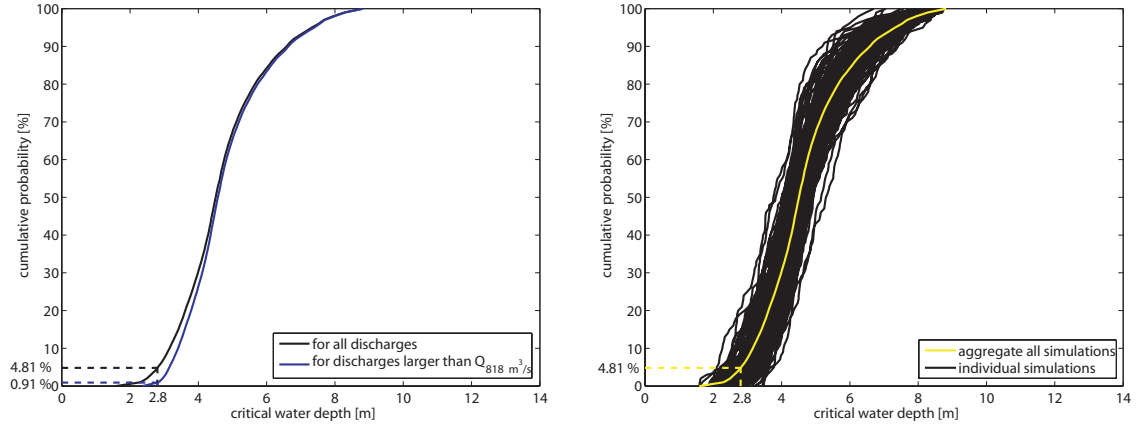

(a) All discharges and discharges>OLA (b) All simulations individual

Figure 4.20: Cumulative probability curves of the critical water depth, Delft3D correction

Conclusions of the model analysis From the previous three sections the first conclusions considering the results of the SOBEK model both for the navigability and the aspect of stochastic modelling with the help of a Monte Carlo Analysis can be made.

First, for the involved uncertainties, exemplary shown on the original model results from Section 4.1:

- A Monte Carlo Analysis can give valuable insight into involved uncertainties (Figure 4.1(a) as deterministic example in contrast to Figures 4.1(b) and 4.2).
- A Monte Carlo Analysis can point out locations with restricted navigability. The uncertainty is found to increase as a function of the draught (Figures 4.3 (a) to (h)).
- The size of the 90% confidence interval can be used as a measure of the involved uncertainty (Figures 4.2 and 4.3).

Second, for the influence of the different applied corrections:

1. **Navigability of the complete Midden-Waal** With the application of the Talmon correction the navigability decreases significantly. On the other hand, the involved uncertainty increases (Figure 4.9(b) in comparison to Figure 4.2). This effect is similar to the increasing uncertainty with a higher draught. With the Delft3D correction the navigability decreases even somewhat further (Figure 4.16(b)). The uncertainty stays in the same range than in the case with the Talmon correction.

   Both of the corrections seem to have a different influence on different single simulations (e.g. the stronger decrease in navigability in simulation 20 in Figures 4.9(a) and 4.16(a) compared to Figure 4.1(b)).

2. **Navigability of each location** The Delft3D correction gives a more distinct view on locations that constrict the navigation than the two other approaches, due to the higher spatial resolution included in the correction (Figure 4.17 in comparison to Figures 4.3 and 4.10).

3. **Navigability as function of time** The time periods during which the river has a lower navigability is represented well for all three approaches. Only for the two applied corrections the percentage of locations that are not navigable is higher (see Figures 4.4, 4.11 and 4.18).

4. **Bottleneck location** The original results show an influence of the change in total flow width on the bottleneck location. With the application of the Talmon correction this influence gets lost, a correlation to the bend radius can be seen. With the Delft3D correction, neither of both effects can be observed.

   The bottleneck criterion shows to be a very sensitive criterion, even small changes in the data lead to large changes in this characteristic. The corrections for the water depth in bends show totally different outcomes for this criterion (see Figures 4.5, 4.12 and 4.19).

5. **Fulfillment of the navigation requirements** The percentage that the navigation requirements are not met increases in both cases of the applied corrections. Also the related uncertainty in terms of the variation of the single simulations increases (see Figures 4.13 and 4.20 in comparison to Figure 4.6).

4.4 Comparison with Least Measured Depth data

In this section the original results and the two results with the correction of the SOBEK model are compared to the measured values of the Least Measured Depth. The practice of measuring as well as an analysis of the LMD is shown in Section 3.3.1.
The comparison can only be made on the basis of two statistic characteristics:

1. The percentage that a location forms a bottleneck

2. The fulfillment of the navigation requirements

1. Bottleneck location First the percentage that a location forms a bottleneck (the restricting location for each time step) predicted by the SOBEK model is compared to the values resulting from the LMD measurements. Comparing the model results to the LMD is very complicated, due to the sampling method of the LMD. Only one LMD is measured daily on the complete Waal and Niederrhein (a 88 km long stretch). The data set used for the 37 kilometers of the Midden-Waal is thus not complete. For this reason it might be possible that several locations are missing in the data-set. Also, the percentages for the LMD shown in the graphs could be a lot higher. Nonetheless, the above shown graphs for the "bottleneck location" (see Figures 4.5, 4.12 and 4.19) are used for a comparison with the data. The comparison with the original SOBEK results is shown including the change in total flow width, while in the comparison of the two corrected results the bend radius is included.

- The original results of the SOBEK model show nearly no agreement with the values of the LMD (see Figure 4.21(a)). The only valuable outcome is that the original results show a certain pattern related to the change in total flow width with a lag of approx. 500 m to 1.0 km.

- The results with the transverse slope correction from the Talmon approach show a better agreement with the LMD data (see Figure 4.21(b)), even if there are large differences at the locations after Nijmegen (km 887-889) and around Wamel (km 913-915). The deviation at Nijmegen could result from the influence of the bed protection structure placed in the bend of Nijmegen (km 884-885). One example of a good fit is the location Zennewijnen (km 917), which is the location with the highest probability of a LMD; it's percentage is fairly well represented by the model results. Furthermore, the corrected results show a good agreement with the bend radius, while a relation to the change in total flow width cannot be seen anymore. The reason for the agreement at the location Zennewijnen is not completely clear. In reality LMD are frequently measured at this spot because an overlying effect of defect groynes and a bad alignment of the navigation channel in this area. The effect of defect groynes is not implemented in the model, while the alignment of the navigation channel could be reproduced by the model. The extent to which those effects contribute to the occurrence of a LMD cannot be estimated. One further influence on the model results in this area could be the fact that the Midden-Waal is divided into two parts for the matter of calibration. At km 913 the roughness of the model changes, thus an irregularity in the bed level evolution might lead to the high bottleneck percentage downstream of this location.

- The results with the Delft3D correction hardly show any agreement with the LMD data (see Figure 4.21(c)). This could be due the above mentioned boundary effects in Delft3D, the higher spatial resolution and the fact that the bottleneck criterion is very sensitive. For this case neither a relation to the change in total flow width nor to the bend radius can be seen.

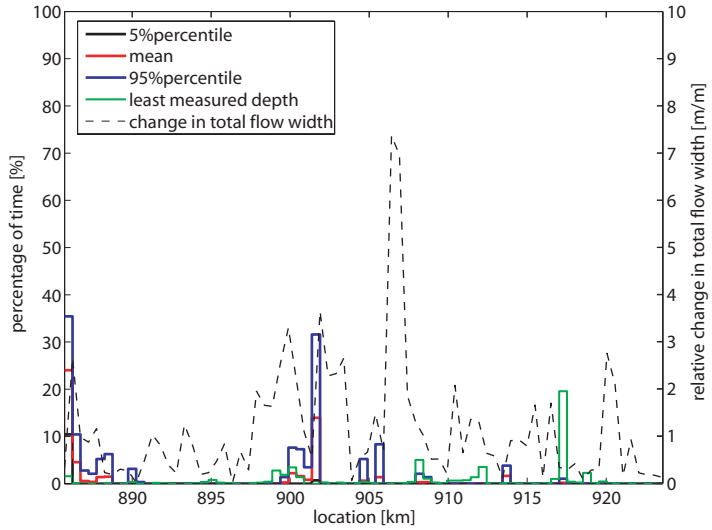

(a) SOBEK without correction

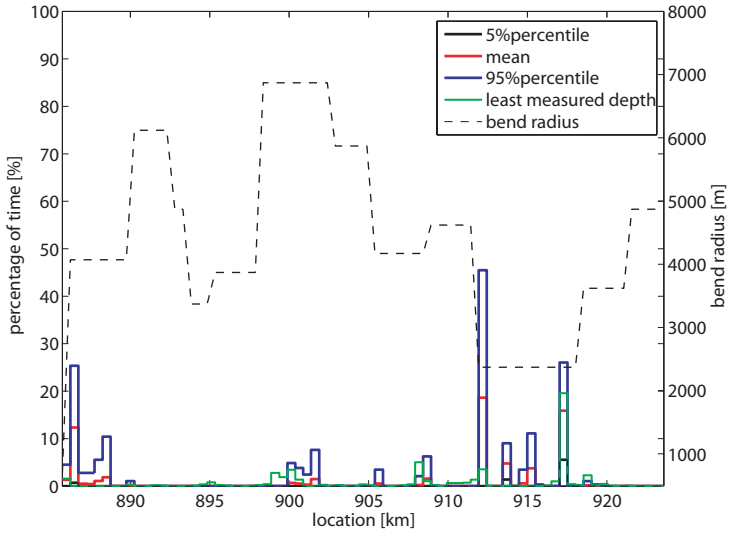

(b) SOBEK with Talmon correction

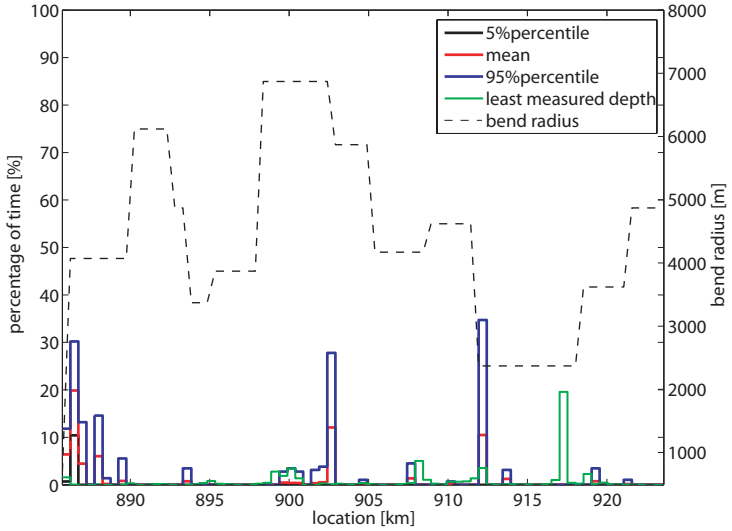

(c) SOBEK with Delft3D correction

Figure 4.21: Comparison of the bottleneck location, SOBEK&Data

2. Fulfillment of the navigation requirements Figure 4.22 shows a comparison between the cumulative probability curves of the critical water depth for all three cases of the SOBEK results. Also included in the graph is the probability of a water depth equal or smaller than 2.8 m (OLR-criterion) derived from the LMD data. This figure can be used to examine the extent that the probability of meeting the channel requirements predicted by the model matches the measured LMD data.

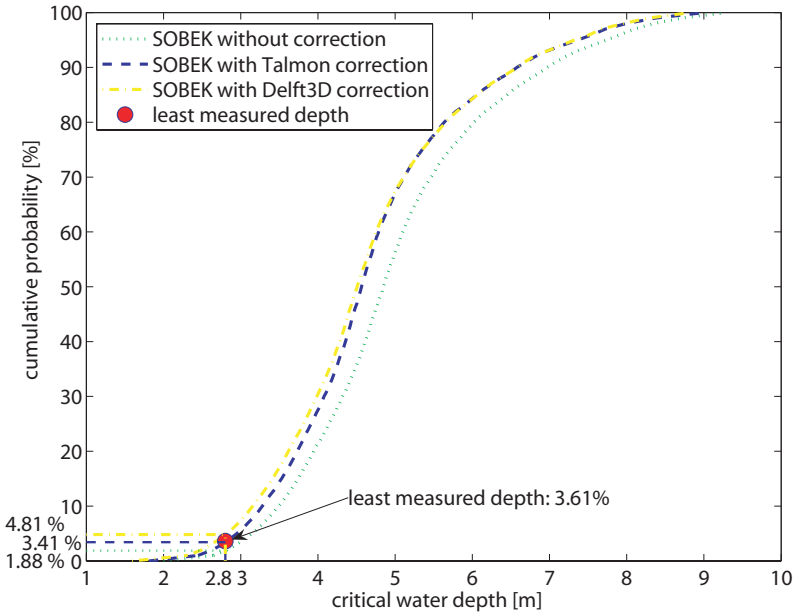

Figure 4.22: Comparison of the cumulative probability curves, SOBEK&Data

Figure 4.22 shows that both of the the corrected results show a fair agreement with the LMD values. They predict the occurrence of the OLR-depth with approx 4.8% (Delft3D correction) and 3.4% (Talmon correction). In reality a water depth of 2.8 m or lower occurs for 3.6% of the time. Again it has to be mentioned that in reality this percentage could be higher, due to the non-completeness of the LMD data-set. The model values without transverse slope correction differ significantly and predict an OLR-depth for less than 1.9% of the time.

Conclusions of the data comparison The LMD data makes a comparison with the model results complicated because:

- Only one LMD location is measured every day, which means that only the one minimum location for the complete Niederrhein and Waal is noted. In reality several locations can restrict the navigability at the same time, but only one of those will appear in the LMD data. Thus, the above estimated percentages for each location should be a lot higher.
- Because only the LMD data for a part of the Waal is used, the data-set is not complete. Instead of bottleneck locations that occur in the Midden-Waal, locations outside of the stretch could have been defined as LMD location and so the locations in the Midden-Waal might not have been considered.
- The measurement of the LMD is influenced by the placement of buoys to sustain a deeper but narrower navigation channel. This is the case in nine reaches on the

Midden-Waal, and not included in the SOBEK model. This distorts the meaning of the Least Measured Depth (see Section 3.3.2).

- The occurrence of LMDs is influenced by different morphologic phenomena like pool/ point bar formation and groyne flames. Those effects are not included in the SOBEK model. It was also found that the navigation traffic on the Waal has influence on the morphology in flattening the top of the dunes [69]. Finally, the river undergoes continuous dredging operations, which are carried out to enhance the navigation profile of the river. This of course has large influence on the data of LMD.

Therefore, from the comparison of the model with the data it can be concluded:

1. **Bottleneck location** The degree to which the results of the SOBEK model represent the measured values of the LMD is not satisfying. The original model results show now agreement with the data (Figure 4.21(a)). By applying a correction for the transverse slope effect in bends after Talmon, the model results get closer to the measured values (Figure 4.21(b)), but with the Delft3D correction again the results drift further away (Figure 4.21(c)). The bottleneck criterion is found to be too sensitive to be used for a comparison with the model results. Only one location, even if the difference in water depth is just one centimeter, is defined as bottleneck location per time step. It has to be questioned if the models perform with that kind of accuracy. The three totally different outcomes for rather small changes in the model results (shown in Figure 4.21) suggest that the models should not be used with this kind of criterion. In addition, effects like pool/ point bars, groyne flames, the influence of navigation traffic of morphology and dredging are not included in the models, but are supposed to have large influence on the LMDs.

   The SOBEK model can give a good impression of the navigability of the Midden-Waal, especially the two applied corrections for the transverse slope effect seem to give reliable results. Anyway, the models should not be used to point out "the one critical location" with the accuracy demanded by the bottleneck criterion.

2. **Fulfillment of the navigation requirements** The fulfillment of the navigation requirements can be estimated rather good with both of the applied corrections, while the original results show no agreement (see Figure 4.22). This again stresses the point that in general the results of the SOBEK model, especially with the applied correction for the water depth in bends, can be used to get an impression of the navigability of the river, as long as it is not used to point out this characteristic with a too high standard of accuracy like in the bottleneck criterion.

It is now necessary to investigate the influence of two-dimensional morphological effects with a multi-dimensional model to find out whether the one-dimensional SOBEK model is sufficient to investigate the navigability of the river in terms of the five used characteristics or if two-dimensional effects that have not been included yet have a dominating influence on the results. It also has to be examined whether the two-dimensional model can be better used for a comparison with the LMD data in means of the bottleneck criterion.

Chapter 5

Results of the two-dimensional model

The outcome of the Delft3D model is given on a computational grid consisting of 370 cells along the river axis (with a cell size of 90-110 m) and 70 cells perpendicular to the river axis (with a cell size of 22-27 m; 12 cells constitute the main channel). Computations are conducted for 100 simulations with a duration of five years; the water and bed level is saved every ten days. Due to initial effects only the years 2-4 are used for the analysis. The discretisation of the discharge hydrograph used in the Delft3D model makes a post-processing of the water level results necessary.

In this chapter the same five characteristics as in the Chapter 4 are used to get an impression of the navigability of the river and so answer the questions of the river manager:

1. The navigable percentage of time of the complete Midden-Waal
2. The navigable percentage of time of each location along the river
3. The navigable percentage of locations along the river as a function of time
4. The percentage that a location forms the bottleneck location
5. The probability that the navigation requirements (OLR-criterion) are not given

In contrast to the SOBEK model, the two-dimensional approach now gives the possibility to assess the navigability of the river on the basis of two parameters: the water depth and the related width of the channel. As the cross-sectional profile evolution is included in the model (by a parameterised curvature-induced secondary flow, see Section 3.1.3.2), a correction of the water depth in bends is no longer necessary.

The model outcome is analysed in three different ways: (1) by defining a 150 m wide navigation channel and then analysing the water depth in this channel; (2) by a cross-sectional averaged approach; (3) by a "fixed-bed" approach, to get insight into the influence of the uncertainty in the discharge on the uncertainty in the navigability.
The analysis of the Delft3D results is therefore divided into five parts:

1. A necessary post-processing for the water levels is explained
2. An analysis with a defined, 150 m wide navigation channel is shown
3. The model is analysed in a cross-sectional averaged mode
4. The results of a "fixed-bed" approach are discussed
5. The results of 2. and 3. are compared to the LMD and buoy placement data

5.1 Post-processing of the model output

In order to save computation time (which is highly dependent on the time the flow module needs to converge) one important step is made in the simulations with Delft3D (see Section 3.1.3.2): The discharge hydrograph is discretised using steps of 500 m^3/s, resulting in a range of 16 discharge stages, varying from 500 up to 8,000 m^3/s. An example of the five year discharge hydrograph for simulation number 3 is shown in Figure 5.1(a).

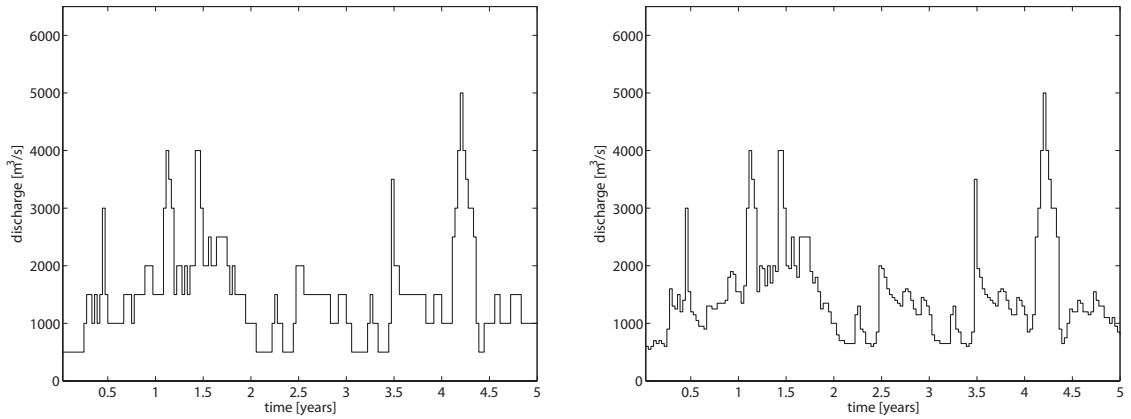

(a) Discharge time series discretized in steps of 500 m^3/s

(b) New discharge time series discretized in steps of 50 m^3/s from 500 m^3/s to 2,000 m^3/s

Figure 5.1: Original and newly discretized discharge time series for one simulation

This has large influence on the water levels computed by the model and the resulting water depth that is used for the analysis. Figure 5.2(a) shows the cumulative probability curve of the cross-sectional averaged water depth, calculated with the original bed and water level outputs from the Delft3D model. The cumulative probability curve of the water depth is observed to be a stair-curve, reflecting the 500 m^3/s steps that are used in the discharge time series. This constitutes a problem, because the information about the distribution of the very important low water depth between 2 m and 4 m (caused by discharges between 500 m^3/s and 1,000 m^3/s) is missing.

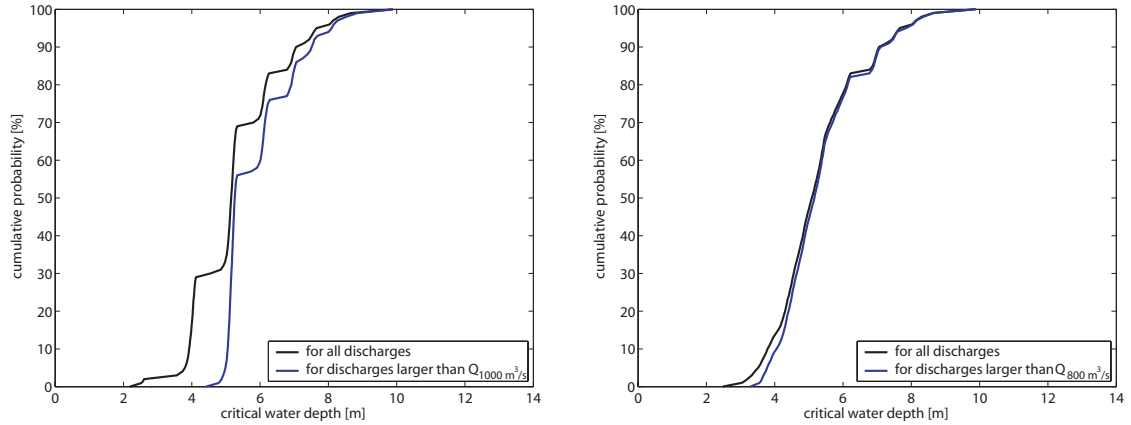

(a) Cumulative probability curve with the original water levels

(b) Cumulative probability curve with the interpolated water levels

Figure 5.2: Cumulative prob. curves of the original water depth and after interpolation

For this reason, a post-processing of the model results is necessary. The discharge hydrograph shown in Figure 5.1(a) is discretized once again, this time with steps of 50 m^3/s from 500 to 2,000 m^3/s (Figure 5.1(b)). This range includes water depth up to approx. 6 m. Above 2,000 m^3/s the original steps of 500 m^3/s are kept unchanged, because the water depth above 6 m is not important for the upcoming analysis of the navigability.

Linear interpolation is used to interpolate the computed water levels in steps of 50 m^3/s. The interpolated water levels are then placed at the according positions given by the new discharge hydrograph. This is done for each location along the river, each time step and each of the 100 simulations individually. The water depth is calculated with this new set of water level data and the bed level data computed by the Delft3D model. The cumulative probability curve of the interpolated water depth is shown in Figure 5.2(b). The low and moderate water depths up to 6 m are now well represented, above a water depth of 6 m the influence of the coarser discretized hydrograph can still be seen.

A linear interpolation is appropriate to use, as can be seen on hand of the stage-discharge relationship in Figure 5.3. In this figure the original water level, a third order polynomial fitting and the interpolated water levels are shown in relation to the discharge for the cross-section at km 889. It proves that the interpolated water levels show a good fitting to the third order fitting of the original water levels.

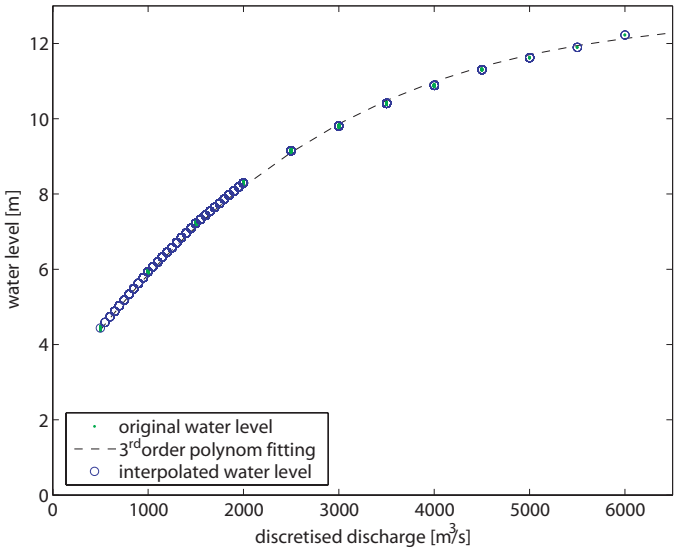

Figure 5.3: Stage-discharge relationship, original and interpolated water levels, km 889

5.2 Results for a channel width of 150 m

For the first analysis a channel with a width of 150 m is defined, see Figure 5.4(a). The navigability of this channel is then analysed for ships with draughts varying from 1.5 to 5.0 m. This approach gives the possibility to assess the OLR-criterion in two dimensions, with a channel width of 150 m and a water depth of 2.8 m.

Furthermore, this method gives the possibility to represent the behaviour of the navigation channel in reality: Due to the cross-sectional bed evolution and the formation of a pool and a point bar in bends, the navigation channel will always shift to the outer bend where the water depth is higher (see Figure 5.4(b)).

With the help of this definition of the navigation channel the same five characteristics as in the previous chapter are used to analyse the navigability of the Midden-Waal.

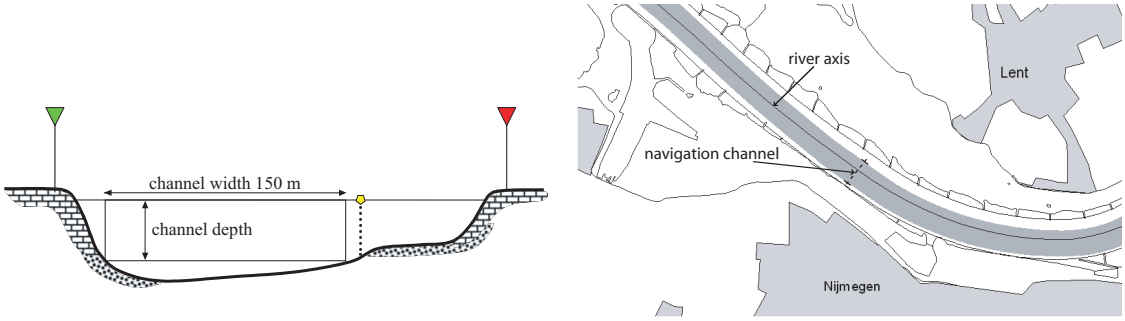

(a) Definition of a 150 m wide navigation channel

(b) Shifting navigation channel in a right bend, after Siegfried [44]

Figure 5.4: Two-dimensional analysis of the navigability

1. Navigability of the complete Midden-Waal Figure 5.5(a) shows the navigable percentages for the three arbitrary chosen simulations 20, 50 and 90. Figure 5.5(b) presents the statistics of all 100 simulations for the navigability of the complete Midden-Waal. The mean of the simulations predict that the river is navigable for 88% of the time for ships with a draugth of 3.5 m. The minimum lies at 63%, the maximum at 100%. The size of the 90% confidence interval is 24%.

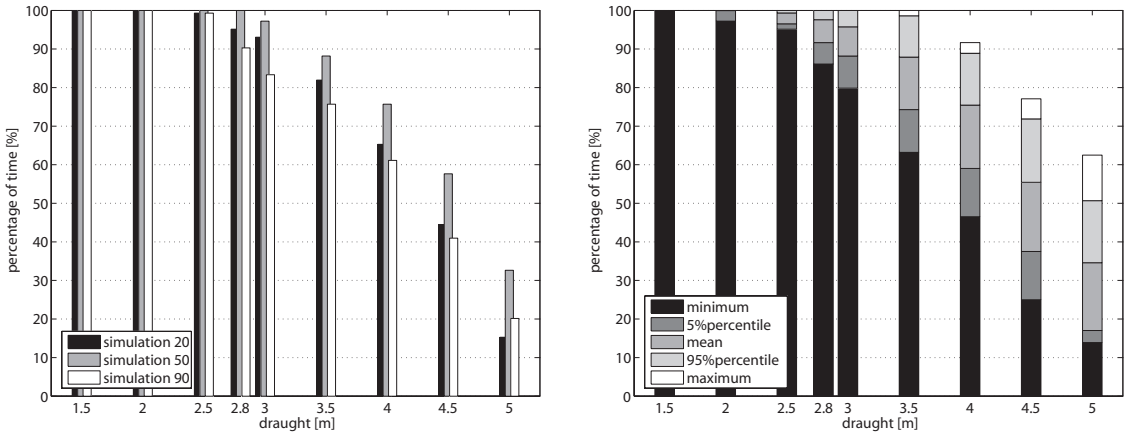

(a) Navigable percentage for three simulations

(b) Navigable percentage for all simulations

Figure 5.5: Navigable percentage for the complete Midden-Waal, channel width 150 m

2. Navigability of each location Figures 5.6 (a) to (h) show the navigable percentage of time of each location along the stretch for draughts from 1.5 to 5.0 m. It proves that the river is navigable for ships up to a draught of 2.5 m without constrictions. From this point on, the navigable percentage decreases as a function of draught. The size of the 90% confidence interval as a measure of the involved uncertainty increases. Locations that have a lower navigability are Ochten (km 906), Beneden-Leeuwen (km 908), Wamel (km 914) and Zennewijnen (km 917). Those locations are also characterized by a sligthly larger of the 90% confidence interval.

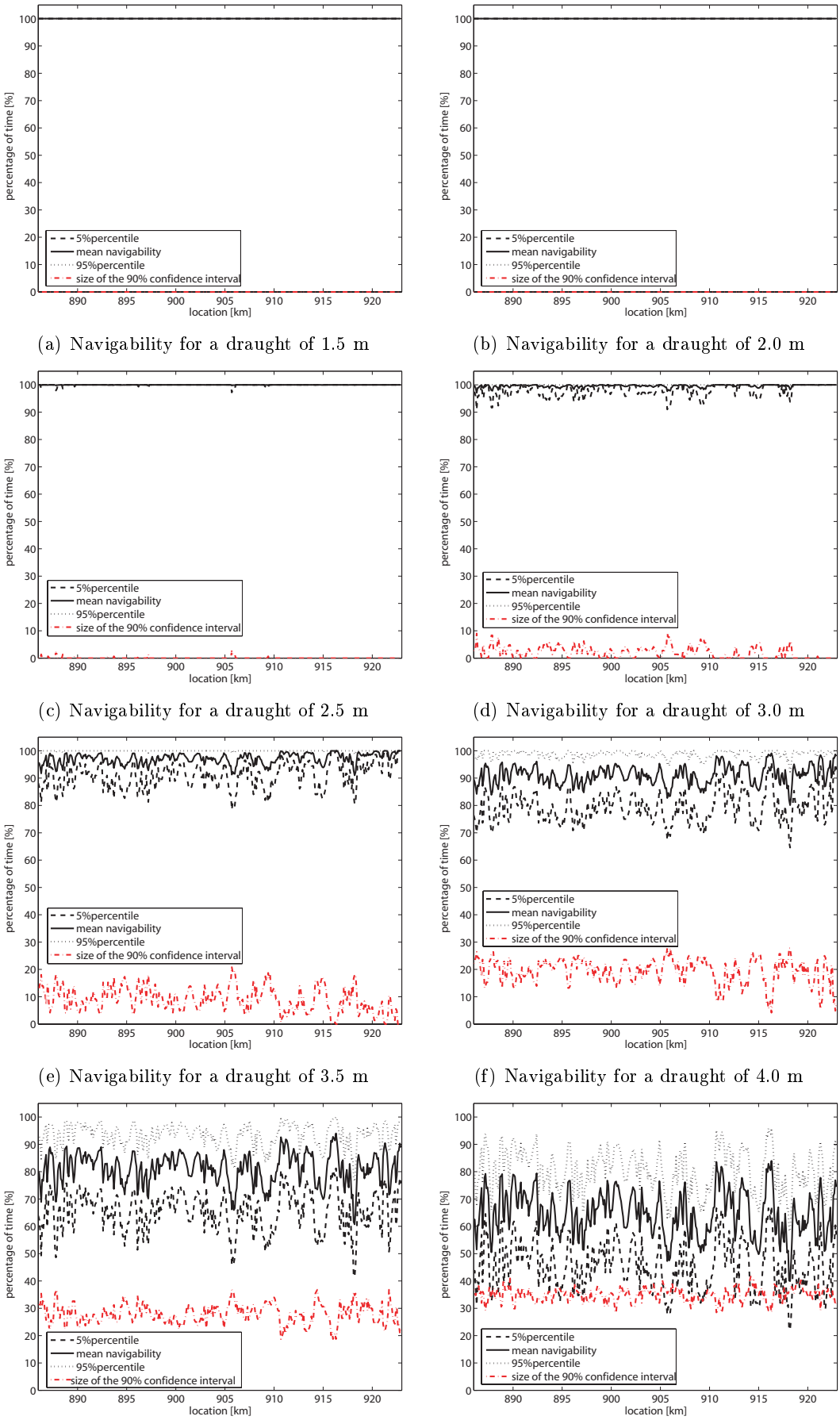

(a) Navigability for a draught of 1.5 m

(b) Navigability for a draught of 2.0 m

(c) Navigability for a draught of 2.5 m

(d) Navigability for a draught of 3.0 m

(e) Navigability for a draught of 3.5 m

(f) Navigability for a draught of 4.0 m

(g) Navigability for a draught of 4.5 m

(h) Navigability for a draught of 5.0 m

Figure 5.6: Navigable percentage as function of the location, channel width 150 m

Another way of presenting the navigable percentage of each location is shown in Figures 5.7(a) to (d). The 95$^{\text{th}}$ percentile, mean, 5$^{\text{th}}$ percentile and the standard deviation of the navigability (the percentage of time that this location is navigable) are plotted two-dimensionally, showing the curved river channel as well as the alternating floodplains.

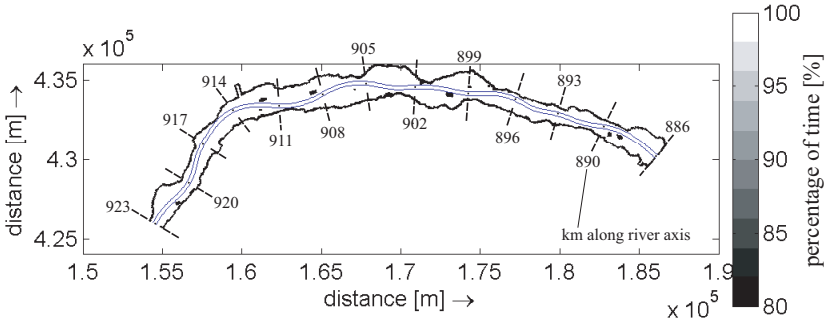

(a) 95$^{\text{th}}$ percentile of the navigability

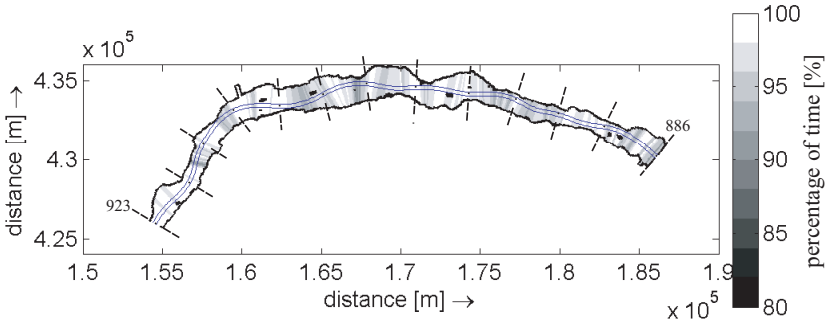

(b) Mean navigability

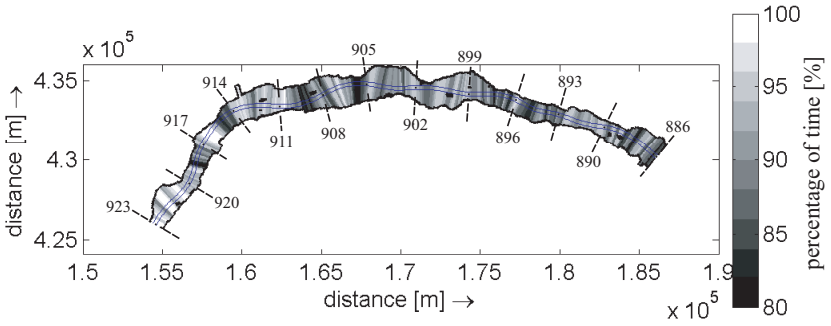

(c) 5$^{\text{th}}$ percentile of the navigability

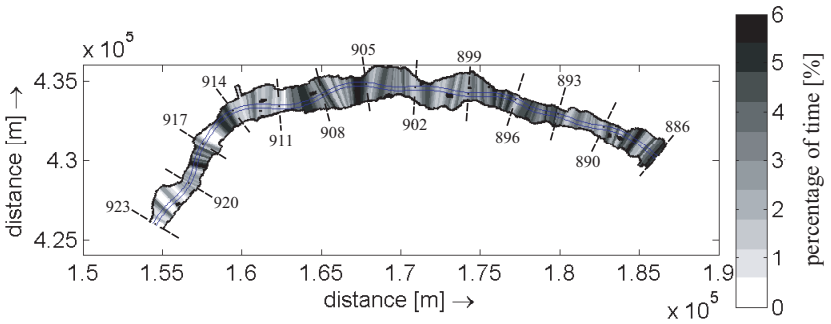

(d) Standard deviation of the navigability

Figure 5.7: Navigable perctg. as fct. of the location, width 150 m&draught 3.5 m, 2D

The standard deviation in this case can give an impression of the involved uncertainty, because the 90% confidence interval which was used so far is related to the standard deviation in its interval boundaries: $[\mu - 1.645\sigma; \mu + 1.645\sigma]$. From Figure 5.7(c) can be concluded that locations with a lower navigability can be found where a bend coincides with a narrowing of the total flow width. Figure 5.7(d) shows that at the same locations the standard deviation, meaning the related uncertainties, are high.

3. Navigability as function of time Figure 5.8 shows the percentage of locations along the river that are navigable for a certain time step. It can be seen that during the low flow periods the navigability is restricted.

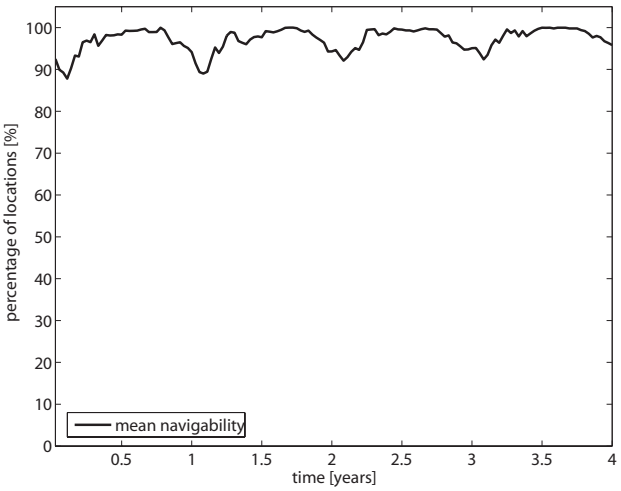

Figure 5.8: Navigable percentage as function of time, channel width 150 m

Another view on the space and time dependency of the navigability is shown in Figure 5.9, with the percentage of simulations that predict a location to be navigable at a certain time. Dark shaded areas indicate points where navigation is restricted, white areas the opposite. Continuous horizontal dark lines show time periods with a lower navigability, while vertical dark lines point out locations with very frequent restriction for navigation.

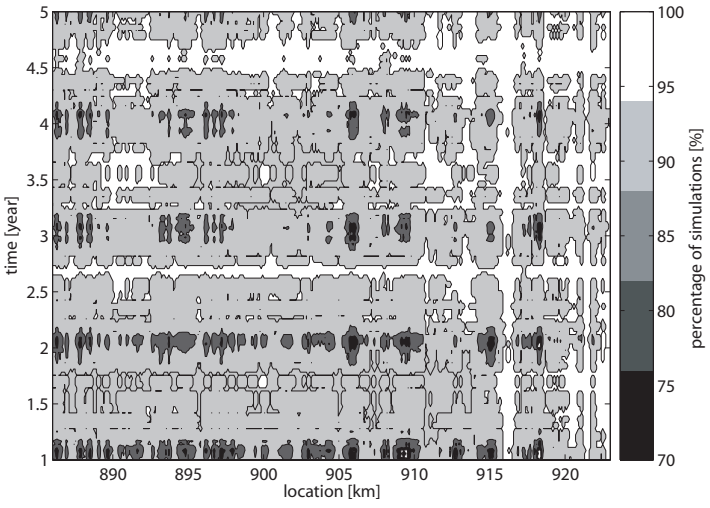

Figure 5.9: Navigability for a draught of 3.5 m, time&space dependent

4. Bottleneck location In this analysis the bottleneck location is defined as the location with the minimum water depth inside of a 150 m wide navigation channel at each time step. The results are shown in Figure 5.10(a), including the bend radius and Figure 5.10(b), including the relative change in total flow width. In contrast to the SOBEK model, the boundary of the Delft3D Waal model is placed directly at km 886. The travel speed of a bed disturbance in the Waal is approx. 1.5 km/year. Hence, the first 7.5 km (up to km 893.5) are left out of the analysis due to the possible influence of boundary effects.

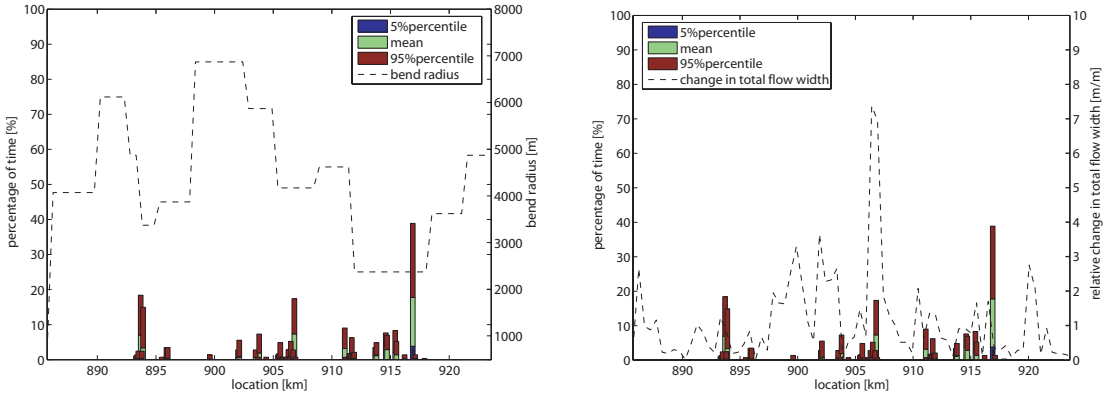

(a) Including the bend radius

(b) Including the relative change in total flow width

Figure 5.10: Percentage that a location forms a bottleneck, channel width 150 m

The location Zennewijnen (km 917) can be seen to be the dominating one with an average of approx. 20%, followed by the reaches around Winssen (km 893), Ochten (km 905) and Wamel (km 915) with less than 10% each. The model results give an indication of a relation of the bottleneck percentage to the bend radius; this is in agreement with the results of Figure 5.7. A relation of the change in total flow width cannot be observed. The bends seem to have a higher influence on the navigability than the alternating floodplains.

5. Fulfillment of the navigation requirements Figure 5.11 shows the cumulative probability curve for the critical water depth (the minimum water depth per time step).

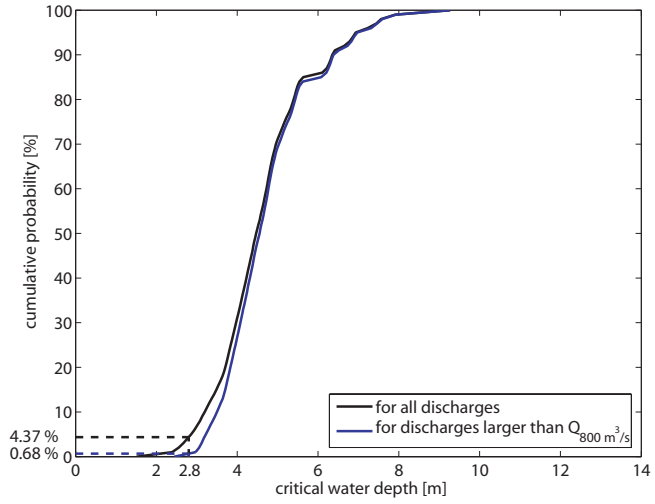

Figure 5.11: Cumulative probability curves of the crit. water depth, channel width 150 m

For this analysis the graph shows the presence of a water depth of 2.8 m for a 150 m wide navigation channel. Thus, it is possible to assess the fulfillment of the OLR-criterion in both dimensions, depth and width. It can be seen that the channel requirements are not met for 4.37% of the time. For discharges higher than the set treshold value, the requirements are not fulfilled for 0.68% of the time.

5.3 Results for a cross-sectional averaged analysis

For the second analysis of the Delft3D model, the water depth is averaged over each cross-section. This leads to an impression of the navigability similar to the one-dimensional SOBEK model. For this part only one parameter is left to estimate the navigability of the river: the cross-sectional averaged water depth. Therefore, the five characteristics describing the navigability of the river are analysed for draughts from 1.5 m to 5.0 m.

1. Navigability of the complete Midden-Waal Figure 5.12(a) shows the navigability of the complete stretch for three simulations number 20, 50 and 90. The percentages predicted by the cross-sectional averaged approach are slightly higher than the in the previous section with the defined 150 m wide channel. Especially simulation number 50 seems to increase significantly.

The statistics of all 100 simulations are presented in Figure 5.12(b). For a draught of 3.5 m the stretch is navigable for 88% of the time in average. The minimum is situated at 65%, the maximum at 100%. The size of the 90% confidence interval is 24%. The statistics are thus similar to the previous section (see Figure 5.5).

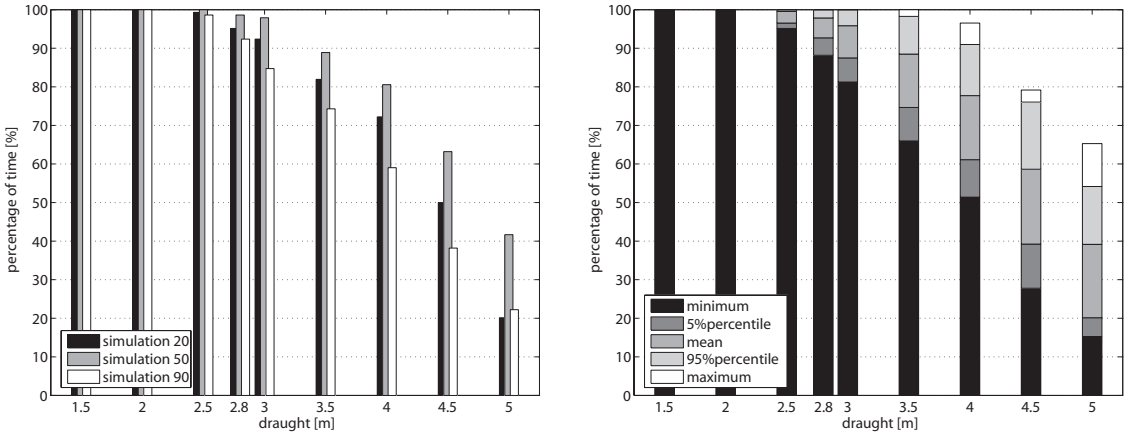

(a) Navigable percentage for three simulations

(b) Navigable percentage for all simulations

Figure 5.12: Navigable percentage for the complete Midden-Waal, cross-sect. averaged

2. Navigability of each location The navigability of each location along the river is presented in Figures 5.13 (a) to (h). The complete stretch is navigable for ships with a draught of 2.5 m without constrictions. The size of the 90% confidence interval stays in the same range as in Figure 5.6, while the locations that are predicted to restrict the navigability have changed, with Ochten seeming to be the most critical one. Also the locations Wamel (km 913) and Zennewijnen (km 917) seem to cause frequent problems for navigation traffic.

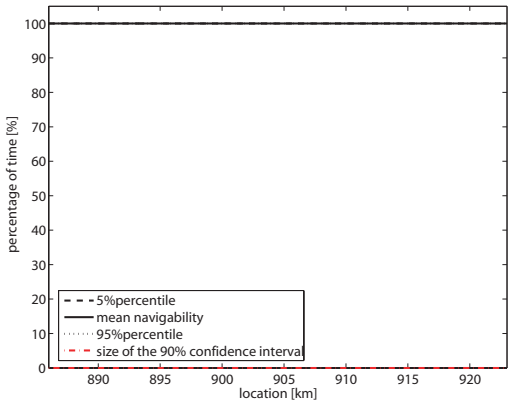

(a) Navigability for a draught of 1.5 m

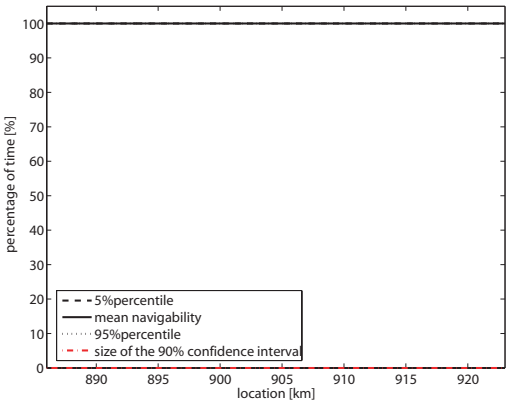

(b) Navigability for a draught of 2.0 m

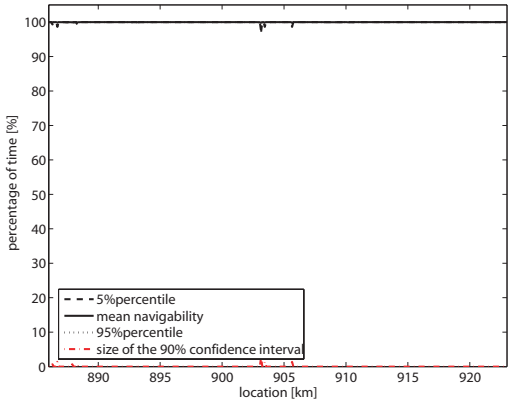

(c) Navigability for a draught of 2.5 m

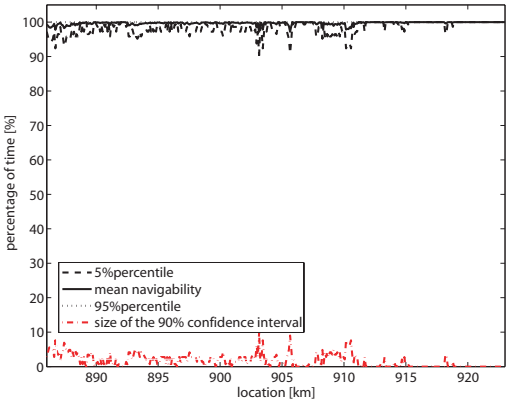

(d) Navigability for a draught of 3.0 m

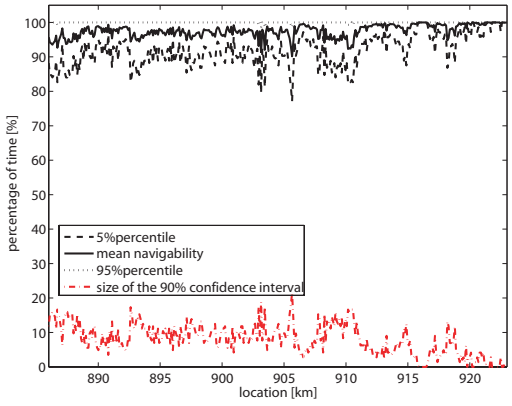

(e) Navigability for a draught of 3.5 m

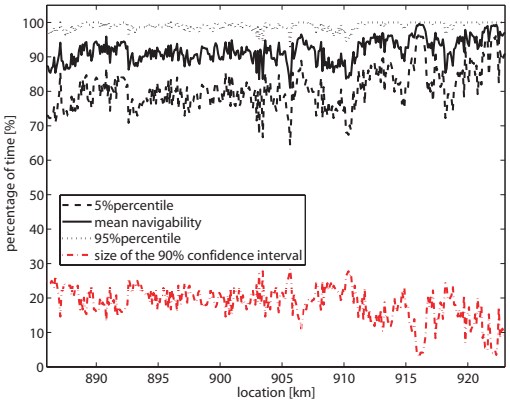

(f) Navigability for a draught of 4.0 m

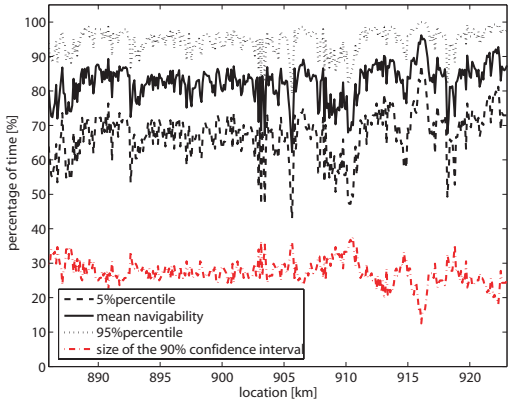

(g) Navigability for a draught of 4.5 m

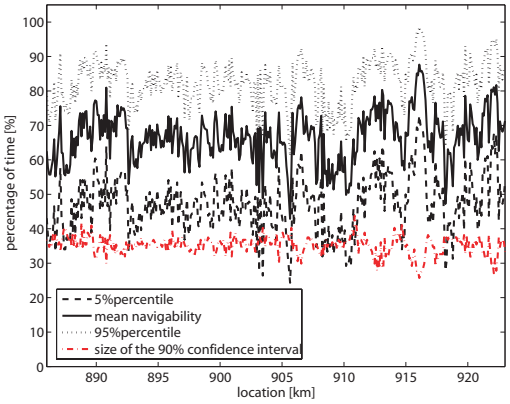

(h) Navigability for a draught of 5.0 m

Figure 5.13: Navigable percentage as function of the location, cross-sectional averaged

3. Navigability as function of time Figure 5.14 shows the navigability of the river as a function of time during the four analysed years. The periods of time where the river is not navigable as well as the percentage of locations that form restrictions look almost exactly like in the first case (Figure 5.8).

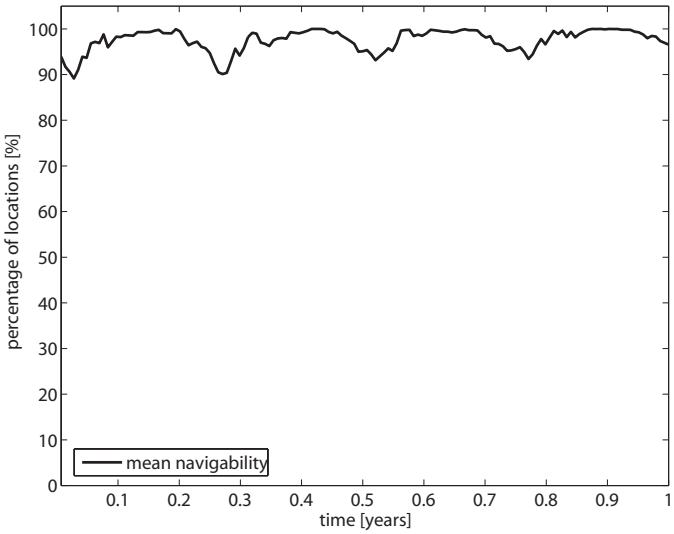

Figure 5.14: Navigable percentage as function of time, cross-sectional averaged

4. Bottleneck location Figures 5.15(a) and 5.15(b) show the percentages that a location forms the restricting location on the stretch for one time step. Again, the 7.5 km long reach from km 886 to km 893.5 was left out of consideration due to the possible boundary effects. The bottleneck locations changed considerably in comparison to the Figures 5.10(a) and 5.10(b). The dominating bottleneck location can now be found at Ochten (km 906) with an average of 24%, followed by Druten (km 903) and the area around Beneden-Leeuwen (km 908-910). A relation to the important morphological features bend radius and change in total flow width cannot be found.

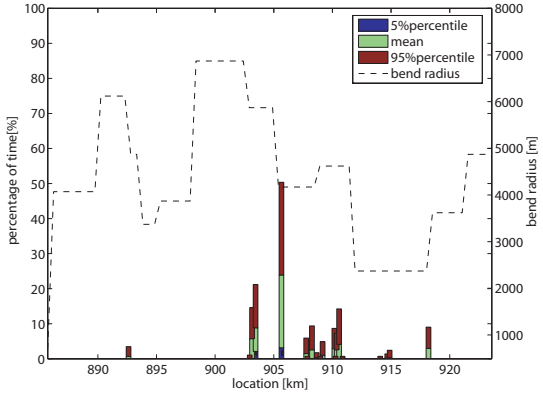

(a) Including the bend radius

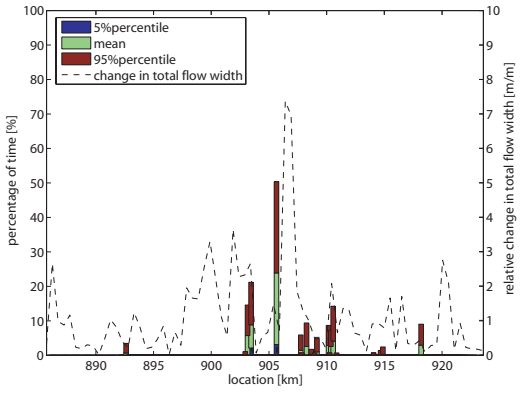

(b) Including the relative change in total flow width

Figure 5.15: Percentage that a location forms a bottleneck, cross-sectional averaged

5. Fulfillment of the navigation requirements From Figure 5.16 it can be seen that the probability of a water depth of 2.8 m or lower is 2.16%. For discharges higher than 800 m^3/s, the water depth stays always higher than this threshold. Thus the OLR-criterion of a water depth of 2.8 m is fulfilled. This method predicts a better navigability than the above shown approach with a channel width of 150 m (Figure 5.11).

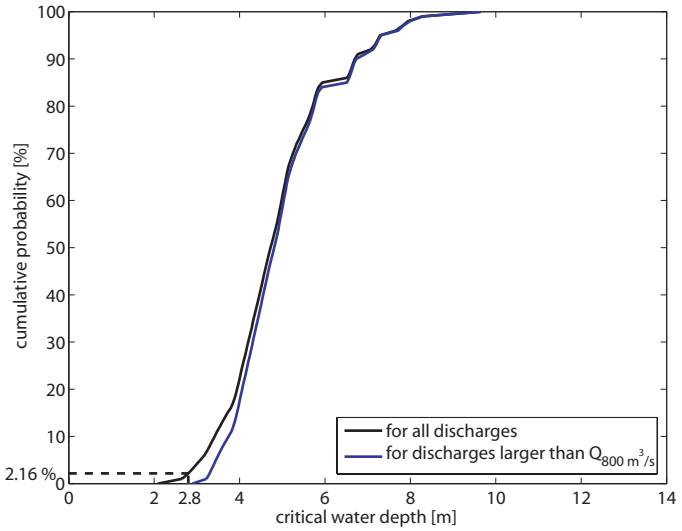

Figure 5.16: Cumulative probability curves of the critical water depth, cr.-sect. averaged

5.4 Results for a fixed-bed analysis

As the third analysis of the Delft3D model, a "fixed bed" approach is carried out. This approach is especially of interest for the modeller, as the influence of the morphology and the influence of the discharge on the navigability can now be assessed separately, and the results of the former analysis can be newly interpreted.

In the preparation of the Delft3D model, 16 discharge stages from 500 up to 8,000 m^3/s (see Section 3.1.3.2) are computed and used as starting points for the hydraulic module for beach time step. This discharge stages and the related water levels are now used in combination with the initial bed level of the Delft3D model. In that way, the water depth of a "fixed bed" model is calculated.

The water levels belonging to the 16 discharge stages are beforehand, similar to Section 5.1, interpolated in steps of 50 m^3/s from 500 to 2,000 m^3/s. After this step, they are placed at the according positions of the discharge time series used for the modelling process. Finally, the water depth is calculated in deducting the "fixed" initial bed level from the varying water level.

This approach with 16 discharge stages and one initial bed level does of course not correspond to reality, and thus is not used for an analysis of the navigability in absolute values. Rather than that, this approach can be seen as a view on how the variation in discharge influences the variation in navigability. The analysis is done similar to Section 5.2 for draughts between 1.5 and 5.0 m inside a 150 m wide navigation channel.

It is now important to have a look on how the five characteristics used so far in the analysis of the SOBEK and Delft3D models react if only a variation of the discharge is included. This should reveal for which analysis the variation of the discharge is the decisive factor and for which of the analysis the development of the river bed morphology is eminent.

1. Navigability of the complete Midden-Waal Figure 5.17(a) shows the navigability of the complete stretch for the three simulations 20, 50 and 90. It can be seen that in this analysis, like in the first approach (Figure 5.5(a)), the relation between the three simulations is the same. Hence, the discharge hydrograph seems to be responsible for this behaviour. The predicted navigability is slightly lower than in the first cases (Figures 5.5(a) and 5.12(a)).

The statistics of all 100 simulations in Figure 5.17(b) show only a small difference to the first two cases (Figures 5.5(b) and 5.12(b)). The mean navigability is predicted with 84%, minimum and maximum can be found at 57% and 99%, respectively. The size of the 90% confidence interval is estimated with 26%, thus matches the previous predicted 24% quite well. The mean navigability is somewhat lower.

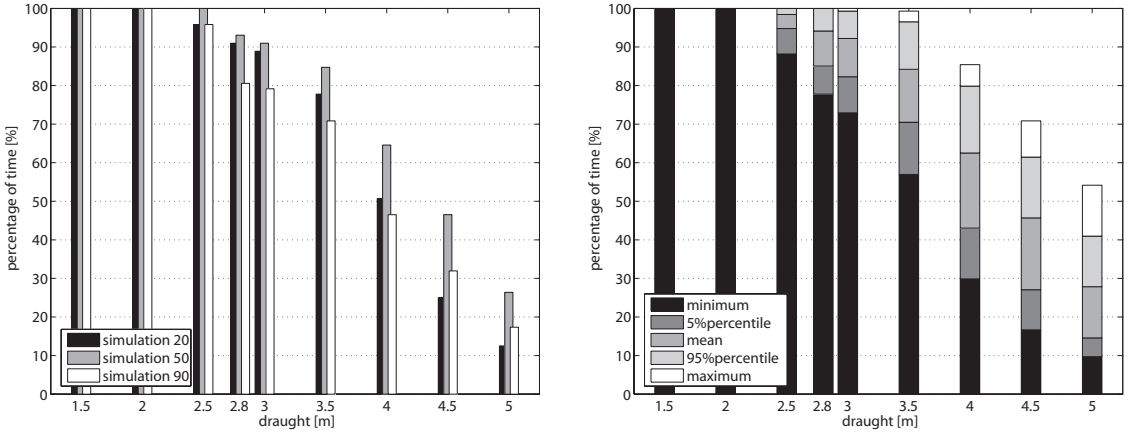

(a) Navigable percentage for three simulations

(b) Navigable percentage for all simulations

Figure 5.17: Navigable percentage for the complete Midden-Waal, fixed bed

2. Navigability of each location Figures 5.18 (a) to (h) show the navigability at each location for different draughts. The predicted mean navigability shows to be slightly lower than in Figures 5.6 and 5.13, the size of the 90% confidence interval is in the same order.

A major difference to the cases above is the fact that locations with constricted navigability cannot be identified. The graphs are characterized by large, rapid variations from location to location. A distinctive pattern seen in the previous cases has not developed. This is due to the missing influence of the development of the bed morphology.

The uncertainty in the discharge seems to be responsible for the degree of uncertainty in the navigability. This can be sustained by the matching size of the 90% confidence interval. Yet the development of the river morphology combined with the uncertainty in the discharge series seems to be decisive for the formation of destinctive locations that form problems for navigation.

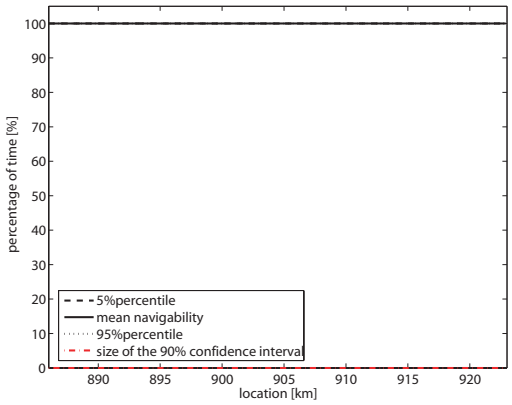

(a) Navigability for a draught of 1.5 m

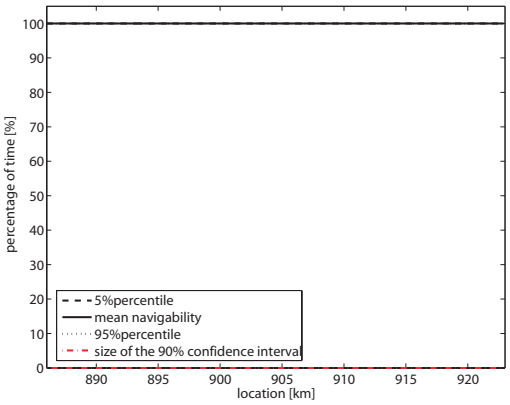

(b) Navigability for a draught of 2.0 m

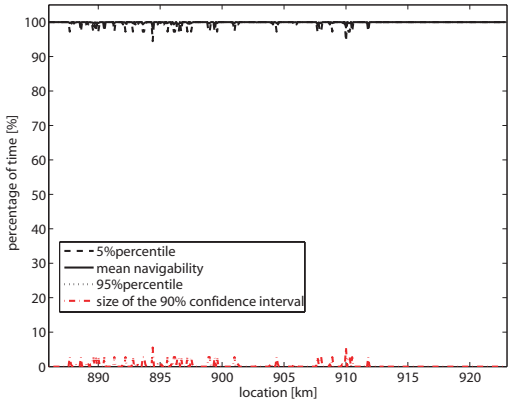

(c) Navigability for a draught of 2.5 m

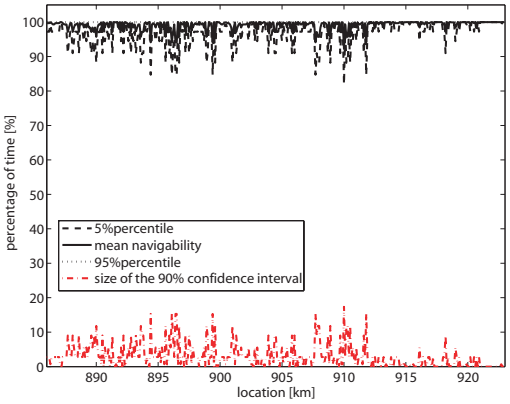

(d) Navigability for a draught of 3.0 m

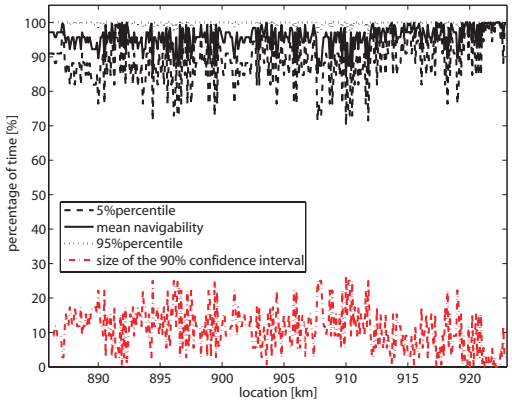

(e) Navigability for a draught of 3.5 m

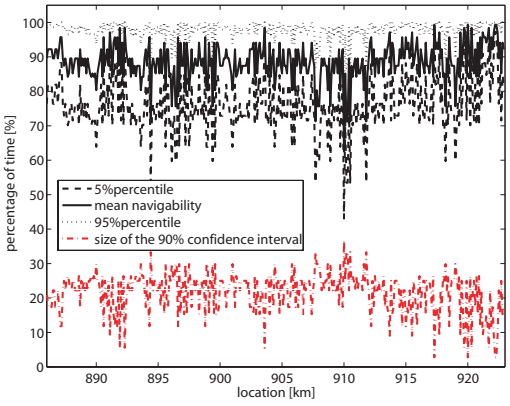

(f) Navigability for a draught of 4.0 m

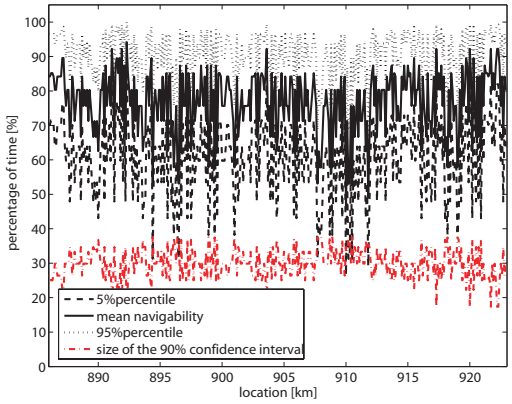

(g) Navigability for a draught of 4.5 m

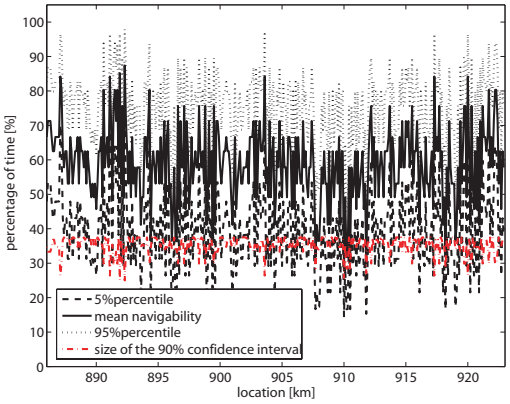

(h) Navigability for a draught of 5.0 m

Figure 5.18: Navigable percentage as function of the location, fixed bed

3. Navigability as function of time The percentage of navigable locations shown in Figure 5.19 reveals the same periods of time with restricted navigability as Figures 5.8 and 5.14. The navigable percentage is slightly lower than in the previous cases. The discharge is responsible for the time-periods during which the navigability of the river is lower.

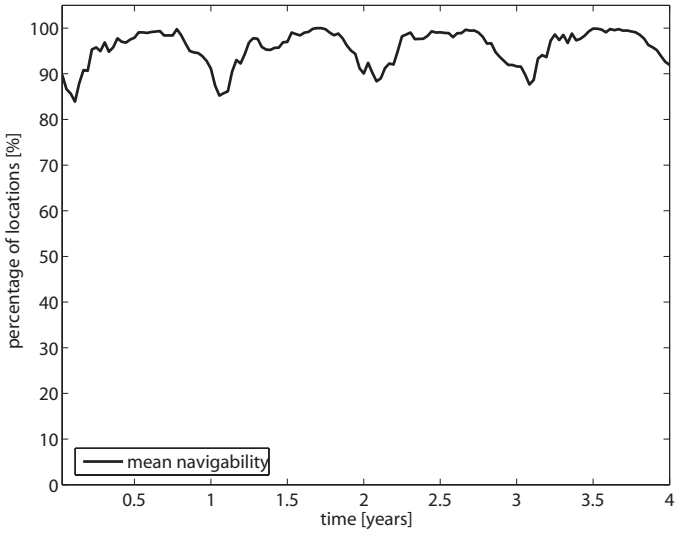

Figure 5.19: Navigable percentage as function of time, fixed bed

4. Bottleneck location The bottleneck percentage presented in Figure 5.20(a) and 5.20(b) differs significantly from the former shown patterns in the Figures 5.10 and 5.15. Only two locations, km 894 and km 907 prove to be the dominating bottleneck locations with a mean percentage of 38% and 30%. This supports the impression that the development of the bed morphology is important for the development of realistic locations that are critical for navigation. A relation to the bend radius and the change in total flow width cannot be seen.

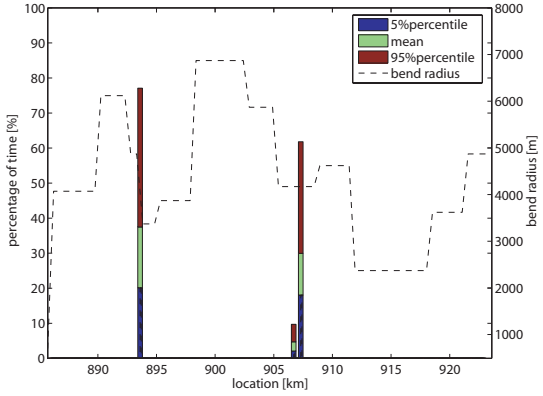

(a) Including the bend radius

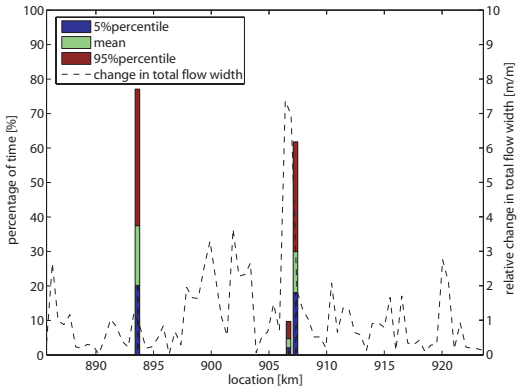

(b) Including the relative change in total flow width

Figure 5.20: Percentage that a location forms a bottleneck, fixed bed

5. Fulfillment of the navigation requirements The cumulative probability curve in Figure 5.21 shows to be a stair-curve. This is due to the not included variation in river bed

morphology. The discretized discharge hydrograph is reflected in the stepwise increasing distribution of the water depth. The percentages that the navigation requirements are not met are 5.4% for all discharges and 1.2% for discharges larger than 800 m^3/s (OLR-criterion). Thus, the missing variation in the bed morphology suggests a small decrease of the navigability.

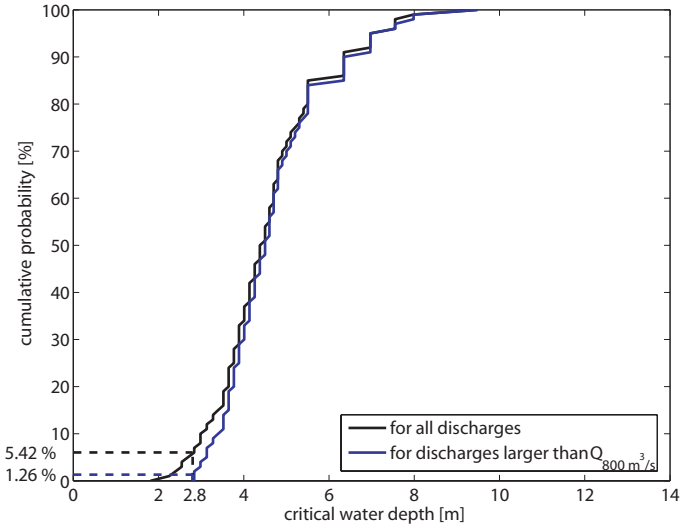

Figure 5.21: Cumulative probability curves of the critical water depth, fixed bed

Conclusions of the model analysis To finish the analysis of the Delft3D model, a short overview of the findings of the three different approaches is given:

1. **Navigability of the complete Midden-Waal** The navigability predicted by the 150 m approach and the width-averaged method are similar. Both methods show the same relation of the three chosen simulations (Figures 5.5(a) and 5.12(a)). The navigable percentage as well as the uncertainty are in the same range (Figures 5.5(b) and 5.12(b)). The navigability of the fixed bed approach is slightly lower (Figure 5.17(b)) and the relation between the three single simulations is different (Figure 5.17(a)). The discharge seems to be mostly responsible for the involved uncertainty.

2. **Navigability of each location** The uncertainty for the first two approaches is predicted equally, only the locations with restricted navigability changed (Figures 5.6 and 5.13). The uncertainty in the fixed bed approach is slightly lower. The discharge shows to be important for the degree of uncertainty. Due to the missing influence of the morphology no specific critical locations develop, the graph is characterized by large and fast oscillations (Figure 5.18). The river morphology proves to be decisive for the formation of critical locations. The two-dimensional plot of the navigability sustains this statement; locations where a curve and a constriction of the flow width coincide are characterised by a lowered navigability and a increased uncertainty.

3. **Navigability as function of time** All three graphs show a similar pattern, only the navigable percentage in the fixed approach is slightly lower (Figures 5.8, 5.14 and 5.19). The discharge is the dominating influence on this characteristic.

4. **Bottleneck location** The approach with the 150 m wide channel shows a relation to the bend radius (Figure 5.10(a)). A significant change in the bottleneck locations can be seen in Figure 5.15. No relation to bend radius or floodplain width is found. The fixed bed method shows only two bottleneck locations (Figure 5.20) and thus demonstrates the importance of the morphology for this criterion.

5. **Fulfillment of the navigation requirements** The first method shows a higher probability of not fulfilling the navigation channel requirements than the width-averaged approach (Figures 5.11 and 5.16). This can be explained by the fact that the OLR-criterion in the first approach is fulfilled in both dimensions. The fixed-bed analysis shows slightly higher percentages for not fulfilling the requirements (Figure 5.21). The discharge can be made responsible for the degree of fulfillment of the criterion.

5.5 Comparison with the data of depth and width

Three criteria are available to compare the outcome of the Delft3D results with the data. The model results from Section 5.2 (channel width of 150 m) and Section 5.3 (cross-sectional averaged) are compared (1) to the bottleneck percentage and (2) to the fulfillment of the channel requirements derived from the LMD data. Finally, (3) the standard deviation of the shipping width from Section 3.3.2 is compared to the locations where frequently buoys are placed to enhance the navigation profile of the river.

1. Bottleneck location Figure 5.22(a) shows the comparison between the bottleneck percentage from the Delft3D-150 m channel approach and the LMD data. For a large part of the Midden-Waal the model results do not match the data (km 893 to km 910). For the downstream part from km 910 to km 923, the model outcome and the data suggest an agreement.

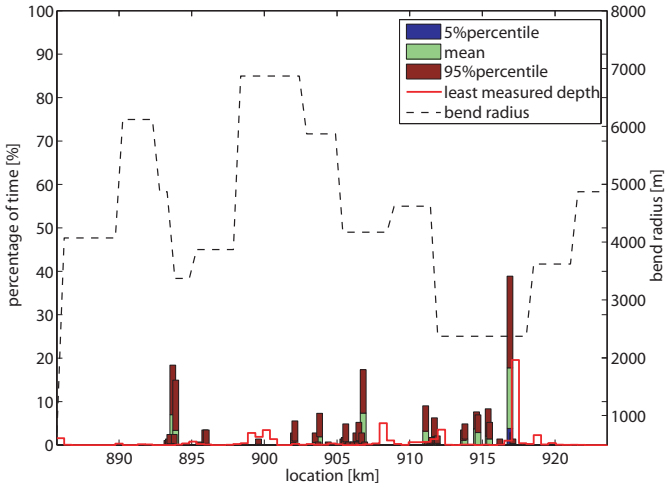

(a) Delft3D with a channel width of 150 m

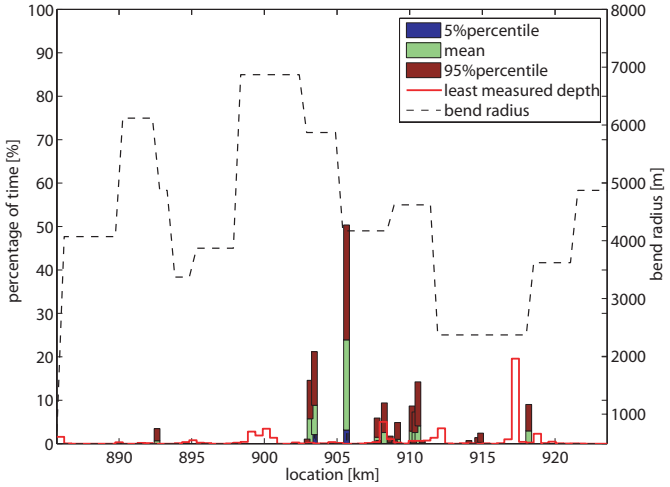

(b) Delft3D cross-sectional averaged

Figure 5.22: Comparison of the bottleneck location, Delft3D&Data

Figure 5.22(b) shows the Delft3D-width averaged approach and the LMD data. No agreement between the model results and the data can be seen.

An important factor that has to be considered is the influence of the placement of buoys on the occurrence of a LMD. Buoys are placed on nine reaches along the Midden-Waal in order to maintain a deeper navigation channel. An appearance of a LMD is thus suppressed.

Figure 5.23 shows the bottleneck percentage of the Delft3D-150 m approach with the LMD, this time the reaches with frequent buoy placement are indicated by dashed rectangles.

Several reaches where the buoy placement could have suppressed the occurrence LMD and thus lead to a mismatch of model results and data can be delineated: km 893-995, km 904-905 and km 910-912. The extend to which the buoy-placement prevents the definition of a LMD location cannot be estimated. Therefore, the shown graph is just an indication that the fitting between model and data could be better.

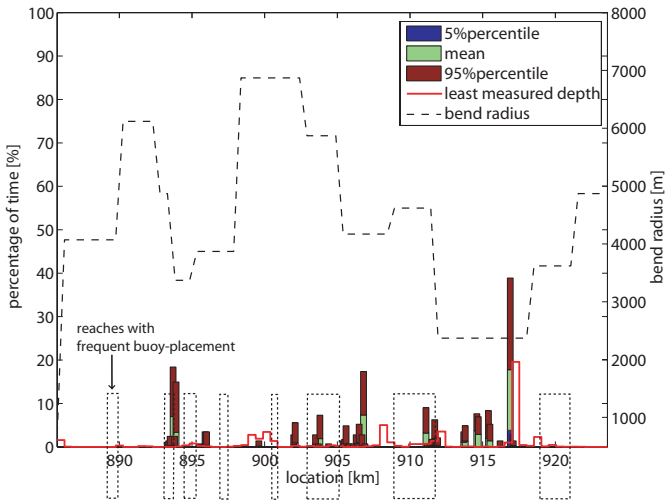

Figure 5.23: Comparison of the bottleneck location incl. buoy placement, Delft3D&Data

2. Fulfillment of the navigation requirements Figure 5.24 shows the cumulative probability curves for the Delft3D model with the 150 m wide navigation channel and the width-averaged approach as well as the probability of a water depth of 2.8 m or lower derived from the LMD data.

Both model curves show a similar shape, the navigability predicted by the width-averaged method is slightly higher. The LMD data shows water depths lower or equal to 2.8 m with 3.61% while the models predict the same characteristic with a probability of 4.37% and 2.16%. It is important to note that the Delft3D model with a defined channel width is representing the fulfillment of both the width and the depth criterion, this might be the explanation for the higher percentage of not fulfilling the requirements. Nonetheless, model results and data are in the same order, thus the model reproduces the fulfillment of the navigation requirements well in both approaches.

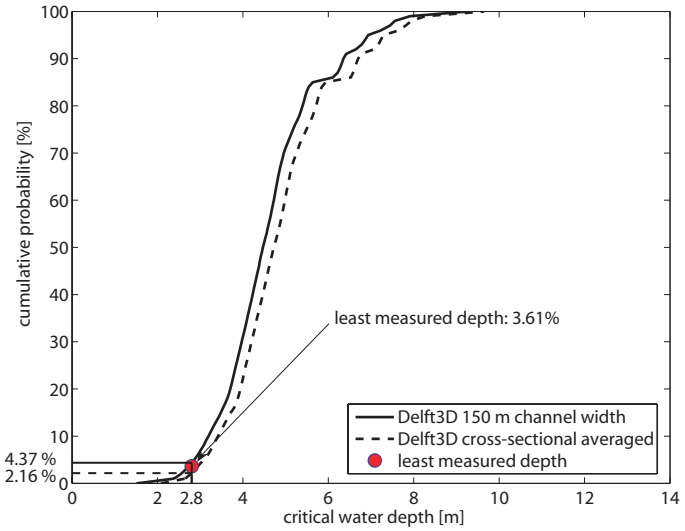

Figure 5.24: Comparison of the cumulative probability curves, Delft3D&Data

3. Shipping width The channel width derived from the data of the placement of the buoys in the Midden-Waal (see Section 3.3.2) can only be used to get an impression of reaches with frequent restrictions in channel width. The data of the buoy placement is plotted as dashed rectangles and gives insight into the reaches where the shipping width is frequently lower than 200 m. The depth of the channel delineated by the buoys is 3.5 m. This is compared to the standard deviation of the shipping width for a draught of 3.5 m from the Delft3D model.

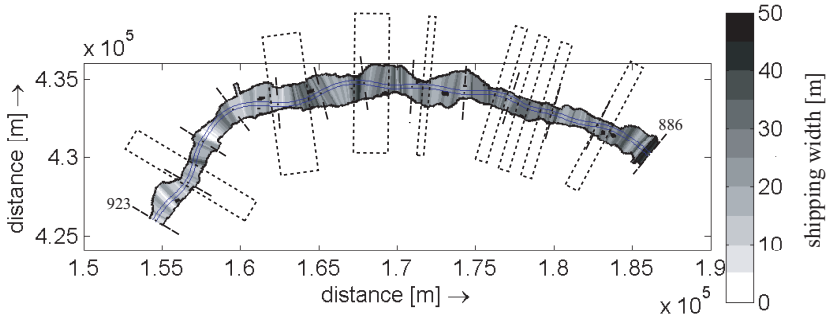

Figure 5.25: Comparison buoy data and standard deviation of the shipping width

A high standard deviation is found in the upstream part (km 886-887). This could be due to boundary effects. It can be seen that several of the reaches with frequent buoy placement also show a high standard deviation of the shipping width. Thus, locations that are predicted by the model to have a high variability of the shipping width should also form problematic locations in reality, otherwise buoys would not be placed there.

Conclusions of the data comparison For the comparison of the Delft3D results with the LMD data the same restrictions listed in Section 4.4 apply.
The following conclusions can be drawn from the comparison:

1. **Bottleneck location** The agreement between the model results and the measured data of the bottleneck location is not satisfying. The approach with a 150 m wide navigation channel indicates an agreement with the data only for a part of the Midden-Waal (Figure 5.22(a)). Especially at the location Zennewijnen (km 917) a good match is found. In reality the high LMD percentage is due to defect groynes and a bad aligned navigation channel. The defect groynes are not included in the model. The model results could also be influenced by the change in roughness at km 913. The cross-sectional averaged analysis shows no agreement with the bottleneck locations from the LMD data (Figure 5.22(b)).

   The bottleneck criterion shows not to be suitable for comparison: The LMD dataset is related to problems (Section 4.4). Also the analysis of the models for the bottleneck-criterion shows to be very sensitive. The influence of the morphology seems to be very important for the development of locations that are critical for navigation. The formation of pool/ point bars in bends as well as alternating wide and narrow floodplains are included in the Delft3D model. This could explain the better fit with the bottleneck criterion than the SOBEK model. Still several morphologic features with influence on LMDs are not included (groyne-flames, navigation traffic, dredging).

2. **Fulfillment of the navigation requirements** A good agreement between the fulfillment of the navigation requirements by the LMD data and both model analysis can be observed (Figure 5.24). The 150 m wide channel approach shows a higher percentage of not fulfilling the navigation requirements. This could be due to the fact that for this method the criterion is fulfilled for both, depth and width, dimensions, while the cross-sectional approach and the LMD data only reflect the compliance of the water depth. The outcome of this comparison suggests that discharge is very much responsible for this characteristic.

3. **Shipping width** The buoy placement data can only be used to qualitatively indicate locations with restrictions in navigation channel width. An indication of a fit of this data with the standard deviation of the shipping width from the Delft3D model is found (Figure 5.25).

As a conclusion for this chapter it can be said that for the analysis of the navigability two different parameters and their cause have to be distinguished:

1. The location that is critical for navigation, respectively the locations that have a restricted navigability. The river bed morphology seems to be the decisive factor for these characteristics.

2. The navigability of the complete stretch and the degree of uncertainty in the navigability. These characteristics are largely influenced by the discharge time series.

Chapter 6

Comparison of Models and Data

In the this chapter the numerical models are compared to each other and, where possible, to the measured data. One of the main focuses is the decision how long the use of a one-dimensional model is appropriate and for which problems a more sophisticated, but more computational intensive two-dimensional model has to be used.
Thus, the outcome of this section should give answer to the following questions:

- Do both models predict the same navigability and the same locations with problems for navigation? If not, are morphological phenomena responsible for the differences?
- What is the influence of the uncertainty in the discharge in the two models?
- For which problems of the navigability is each of the models applicable?
- Do the models coincide with the data? If not, what kind of data would be necessary?

The two alternatives which give the best impression are chosen for comparison:

1. The SOBEK model with the Talmon correction (see Section 4.2)

   This approach seems to give a good picture of the navigability; a correlation to the bend radius as dominating morphologic feature for the bottleneck criterion can be observed; the correction for the transverse slope effect can be- in contrast to the correction following the Delft3D model- rather easily calculated and applied.

2. The Delft3D model with the 150 m wide navigation channel (see Section 5.2)

   This method proves to give a valuable two-dimensional insight into the navigability of the river; it gives the possibility to reproduce the shifting of the navigation channel in curves in reality; a relation to the bend radius combined with the change in total flow width can be seen.

The model results are compared to each other for three characteristics (Section 6.1):

1. The navigable percentage of time of the complete Midden-Waal
2. The navigable percentage of time of each location along the river
3. The navigable percentage of locations along the river as a function of time

Furthermore, for two criteria the models are compared to the LMD data (Section 6.2):

4. The percentage that a location forms the bottleneck location
5. The probability that the navigation requirements (OLR-criterion) are not given

6.1 Comparison of the SOBEK and Delft3D results

1. Navigability for the complete Midden-Waal The graphs for the navigability of the complete 37 km long stretch for one simulation (number 20) are shown in Figure 6.1(a) (for the SOBEK model) and Figure 6.1(b) (for the Delft3D model). The Delft3D simulation shows a somewhat higher navigability than the SOBEK result.

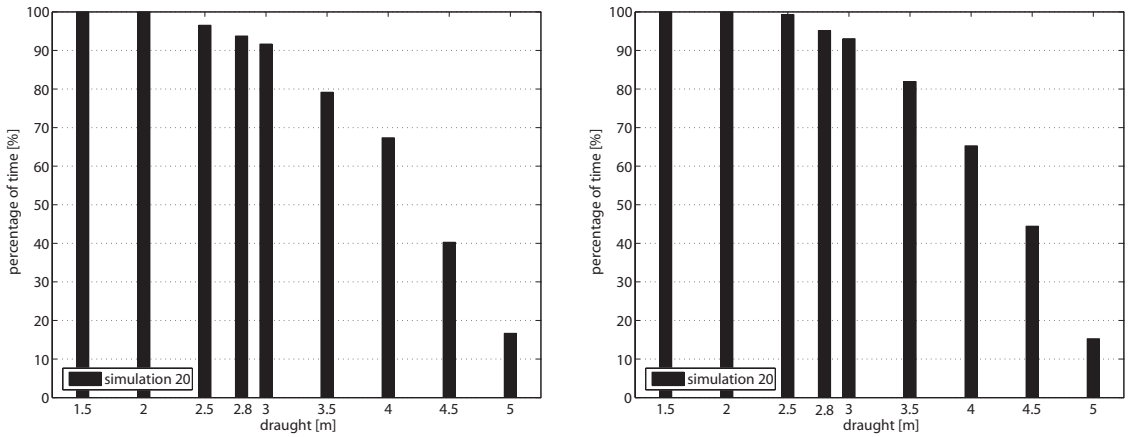

(a) Navigable percentage of the complete stretch, one simulation, SOBEK with Talmon correction

(b) Navigable percentage of the complete stretch, one simulation, Delft3D with 150 m channel width

Figure 6.1: Comparison navigable percentage, one simulation, SOBEK&Delft3D

The results for three different model runs (number 20, 50 and 90) is shown in Figures 6.2(a) and 6.2(b). It can be concluded that Delft3D predicts a slightly higher navigability for all three simulations. On the other hand, the three simulations show the same relation of the navigable percentage in both models.

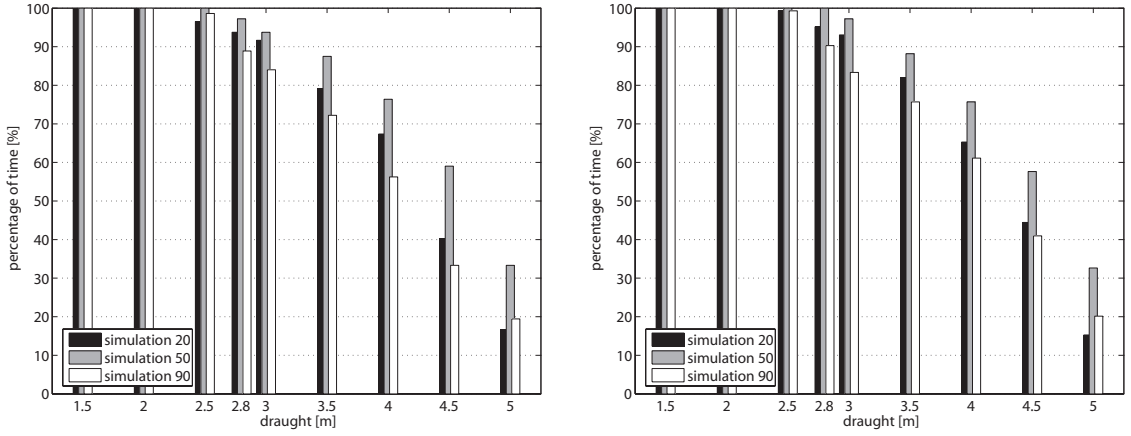

(a) Navigable percentage of the complete stretch, three simulations, SOBEK with Talmon correction

(b) Navigable percentage of the complete stretch, three simulations, Delft3D-150 m channel width

Figure 6.2: Comparison navigable percentage, three simulations, SOBEK&Delft3D

Figures 6.3(a) and 6.3(b) show the statistics of the navigability of the complete Midden-Waal for all 100 simulations.
It seems that the difference between those two results is only marginal. Both models predict the maximum and minimum navigability with 100% respectively 63% of the time

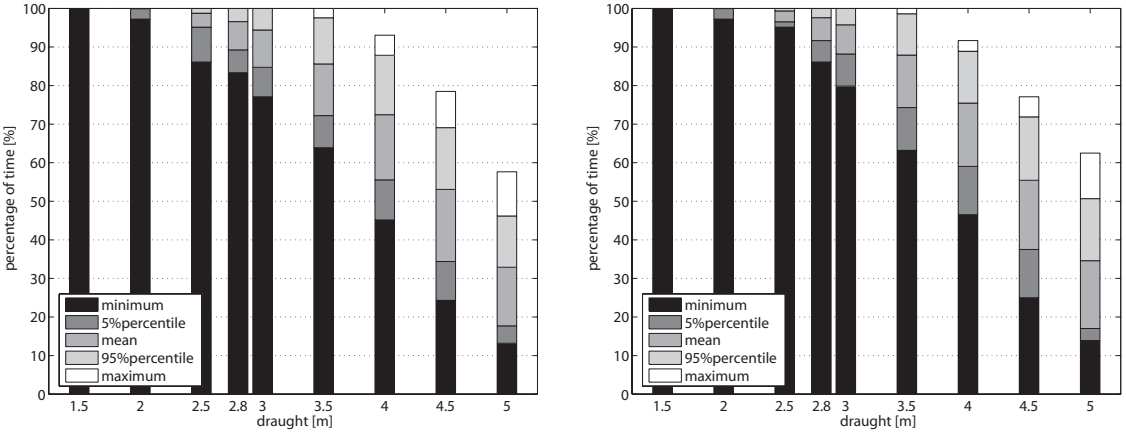

(a) Navigable percentage of the complete stretch, all simulations, SOBEK with Talmon correction

(b) Navigable percentage of the complete stretch, all simulations, Delft3D with 150 m channel width

Figure 6.3: Comparison navigable percentage, all simulations, SOBEK&Delft3D

for a draught of 3.5 m. For the same draught the mean navigability is 85% for the SOBEK model versus 88% for the Delft3D model. The uncertainty, expressed as the size of the 90% confidence interval, lies at 26% and 24%. Thus, the Delft3D model predicts a slightly better navigability with a somewhat lower uncertainty.

2. Navigability of each location The comparison between the navigable percentage of each location along the Midden-Waal is presented in Figures 6.4 (a) to (h). Three features can be deduced from these graphs:

(1) The navigability predicted by the two-dimensional model is significantly higher than the percentage of the one-dimensional model. This can be seen in the comparison of the mean navigability of both models. The definition of the 150 m wide navigation channel in the Delft3D model, which has the ability of shifting inside the river, could be one explanation for this. On the other hand, the water depth is predicted differently by both models. The water depth calculated with both models is compared in Figure 6.5. The graph includes the water depth on the left and right side as well as on the river axis for the Delft3D model. The variation of the water depth caused by the transverse slope effect in bends can clearly be seen. It turns out that the cross-sectional water depth of the Delft3D model is in the order of several decimeters higher than the SOBEK results.

(2) The curves for the mean navigability of both models follow the same pattern (Figure 6.4). This means that both models predict the same locations to be restricting for the navigation traffic. Thus, it can be concluded that the influence of the river morphology is predicted similar in both models. It has to be noted that the apparent higher variation in the graph for the Delft3D results is caused by cross-sections placed every 100 m, instead of the 500 m in the SOBEK model.

(3) Finally, it can be seen in Figure 6.4 that the size of the 90% confidence interval for both models stays in the same range. Therefore, it can be concluded that both models represent the involved uncertainty in the navigability in the same way.

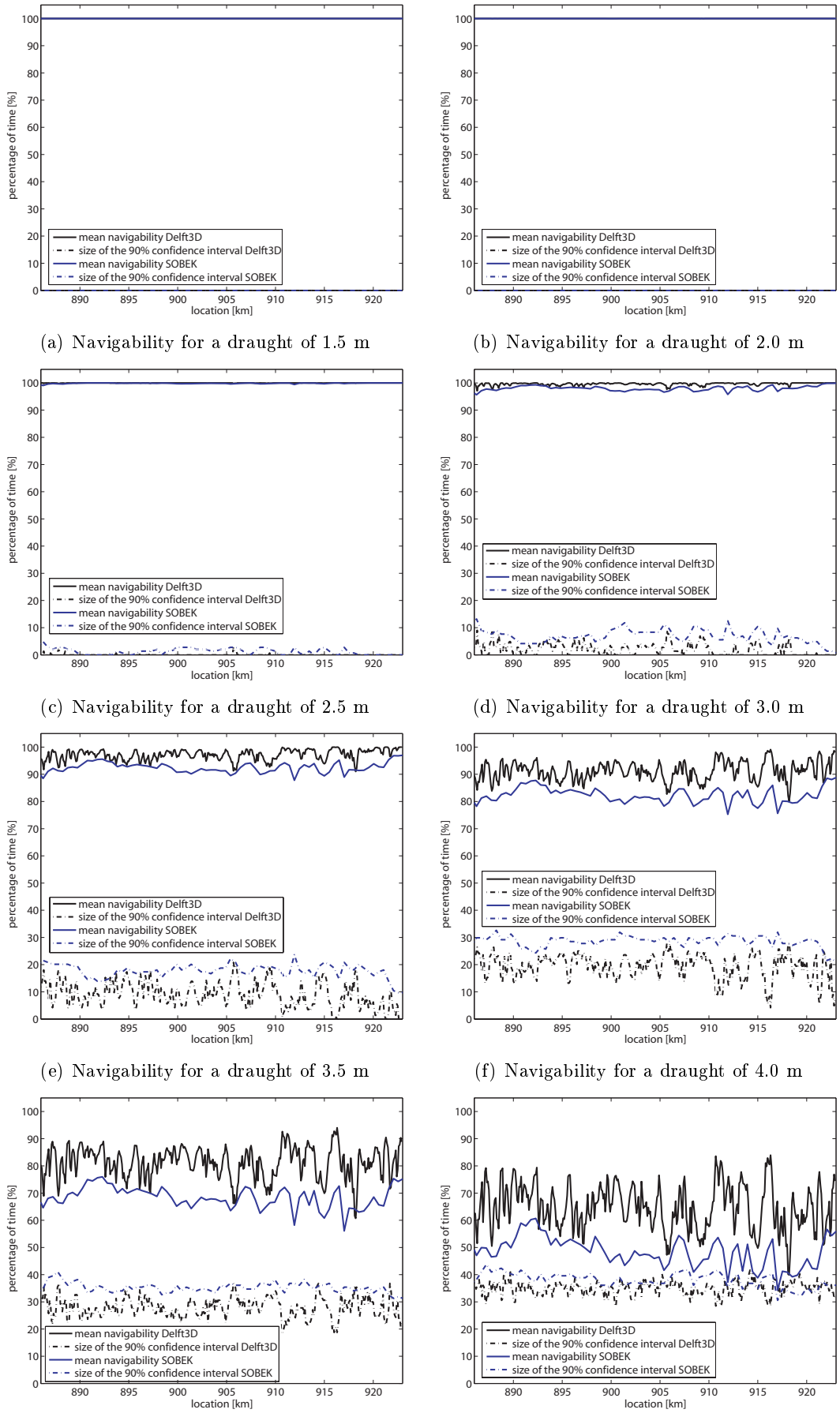

(a) Navigability for a draught of 1.5 m

(b) Navigability for a draught of 2.0 m

(c) Navigability for a draught of 2.5 m

(d) Navigability for a draught of 3.0 m

(e) Navigability for a draught of 3.5 m

(f) Navigability for a draught of 4.0 m

(g) Navigability for a draught of 4.5 m

(h) Navigability for a draught of 5.0 m

Figure 6.4: Comparison navigable percentage as fct. of the location, SOBEK&Delft3D

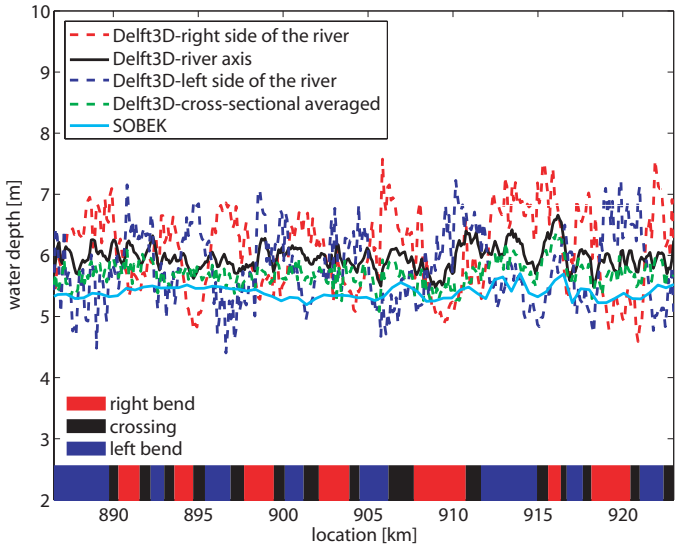

Figure 6.5: Comparison of the water depth, SOBEK&Delft3D

Additionally, the Figures 6.6 (a) to (h) show the mean navigability of each location along the river for the three individual simulations 20, 50 and 90 for different draughts.

The impression given by Figure 6.2 that these three simulations show the same relation to each other for both models can be sustained. The navigability predicted by the Delft3D model is higher. It can also be seen that all three curves for the navigability show the same pattern. Thus, the morphology is found to be important for the shape of this graph.

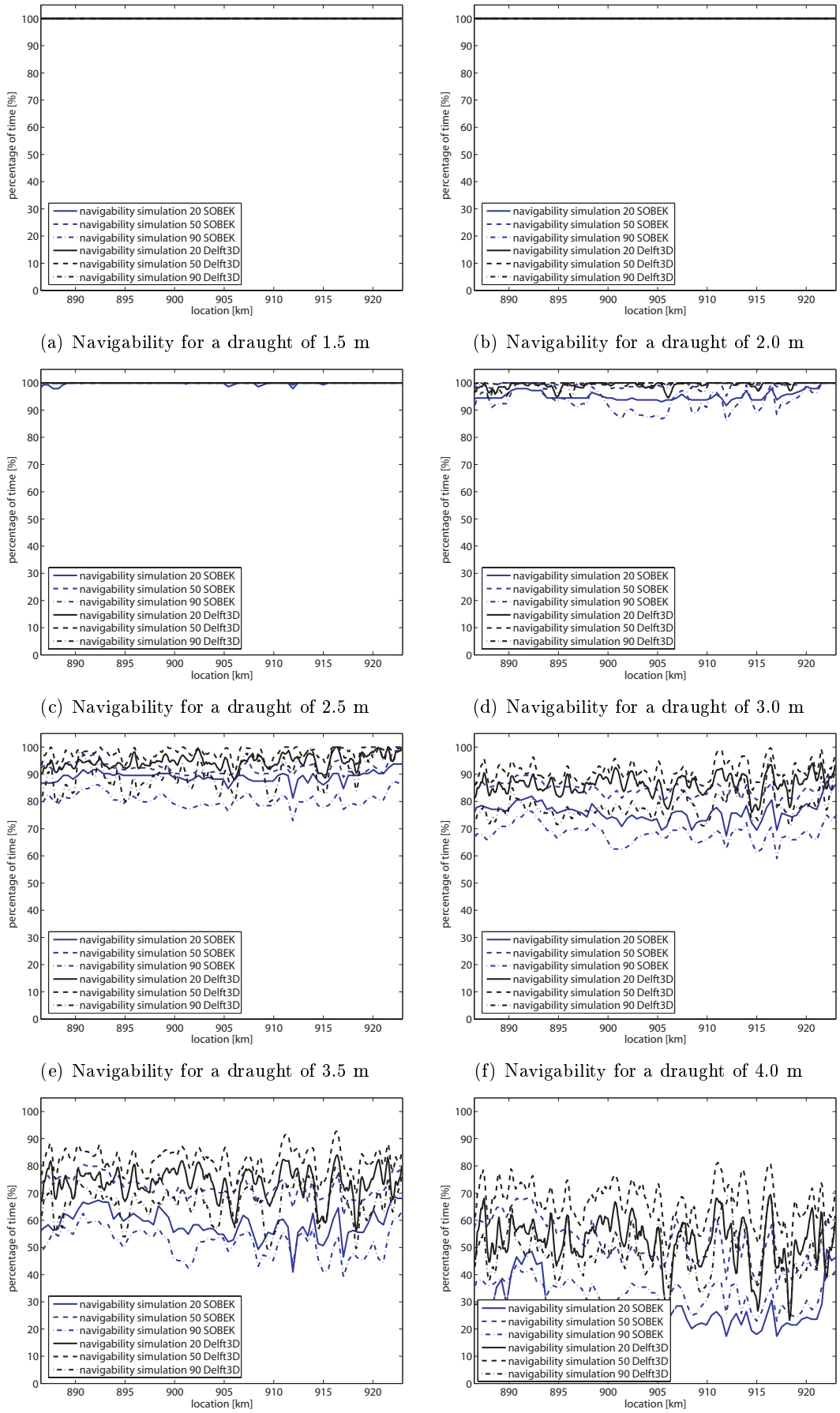

(a) Navigability for a draught of 1.5 m

(b) Navigability for a draught of 2.0 m

(c) Navigability for a draught of 2.5 m

(d) Navigability for a draught of 3.0 m

(e) Navigability for a draught of 3.5 m

(f) Navigability for a draught of 4.0 m

(g) Navigability for a draught of 4.5 m

(h) Navigability for a draught of 5.0 m

Figure 6.6: Comparison navigable percentage of three simulations, SOBEK&Delft3D

3. Navigability as function of time The navigable percentage of locations for each time step is nearly identical for both models (see Figure 6.7). Only the percentage for the Delft3D model is slightly lower.

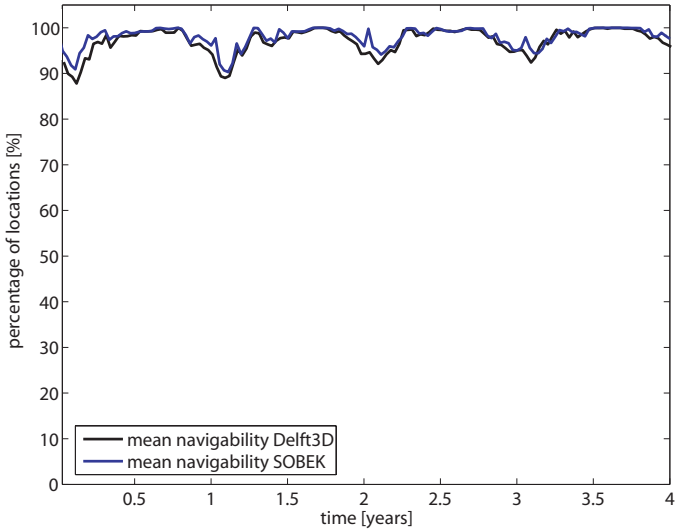

Figure 6.7: Comparison navigable percentage as a fct. of time, SOBEK&Delft3D

Conclusions of the model comparison From the comparison of the first three characteristics the conclusions for the similarities and differences of the models can be drawn:

1. **Navigability of the complete Midden-Waal** The navigability of the Midden-Waal predicted by the Delft3D model is slightly higher than by the SOBEK model (Figure 6.1). The three single simulations show the same relations (Figure 6.2) and the uncertainty stays in the same range (Figure 6.3). Hence, a severe difference caused by a dominating morphology cannot be seen. The uncertainty in the discharge seems to be responsible for the similar model results.

2. **Navigability of each location** The navigability of each location in the Delft3D model is higher than in SOBEK (Figure 6.4). This could be due to the different definitions of the analysis as well as the different prediction of the water depth (Figure 6.5). The pattern of the curves for the mean navigability show the same locations to be restricting the navigation traffic. This means that the SOBEK model with the Talmon correction for the transverse slope effect shows a similar effect on the morphology as the Delft3D model with the 150 m wide navigation channel. The Delft3D model shows a higher spatial resolution. Thus, the navigability can be predicted more accurate. These two findings are supported by the graphs for the three single simulations shown in Figure 6.6. The uncertainty in both models is in the same range. Again the uncertainty in discharge seems to be the cause for this.

3. **Navigability as function of time** The navigable percentage of locations related to the time (Figure 6.7) is nearly equal in both models. Again the discharge is supposed to be the dominating factor for this characteristic.

6.2 Comparison of the models with the Least Measured Depth data

For the last two characteristics, the data of the Least Measured Depth is included into the comparison.

1. Bottleneck location Figure 6.8 shows the comparison between the bottleneck percentage from the SOBEK-Talmon model, the Delft3D-150 m channel approach and the Least Measured Depth data. The first 7.5 km of the Delft3D model from km 886 to km 893.5 are not included because of possible boundary effects.

It can be seen that for a large part of the Waal the model results and the data do not match (up to km 910). In the downstream part from km 910 on, an indication for an agreement of the models with the data can be seen. The good fit for of both models and the data at km 917 again is astonishing. The high percentage of LMD in this area is apparently caused to a larger part by the bad alignment of the navigation channel, which is well reproduced by the models.

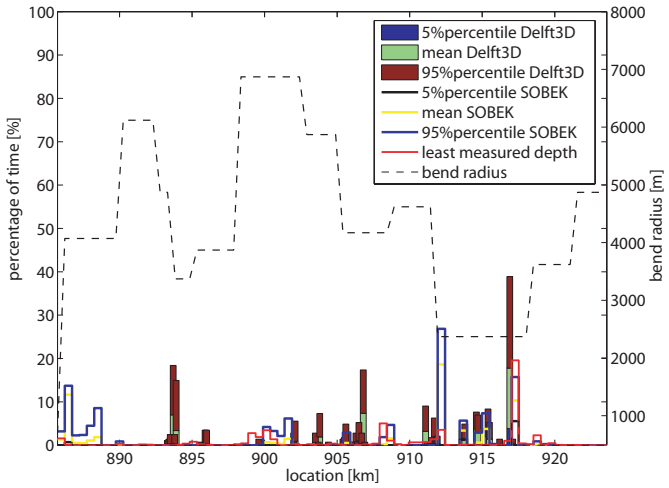

Figure 6.8: Comparison of the bottleneck location, SOBEK&Delft3D&Data

2. Fulfillment of the navigation requirements In Figure 6.9 the fulfillment of the navigation requirements is shown. The SOBEK results and the LMD data show the chance that a water depth of 2.8 m is not given with 3.4% and 3.6%. The Delft3D results show the fulfillment of a water depth of 2.8 m combined with a channel width of 150 m with 4.4%. It can be concluded that both models and data show a good fitting.

Furthermore, the course of both cumulative probability curves is nearly identical. Only for greater water depths the curves diverge, which is due to the still included coarse discharge discretization (in steps of 500 m^3/s for discharges above 2,000 m^3/s) in the Delft3D model.

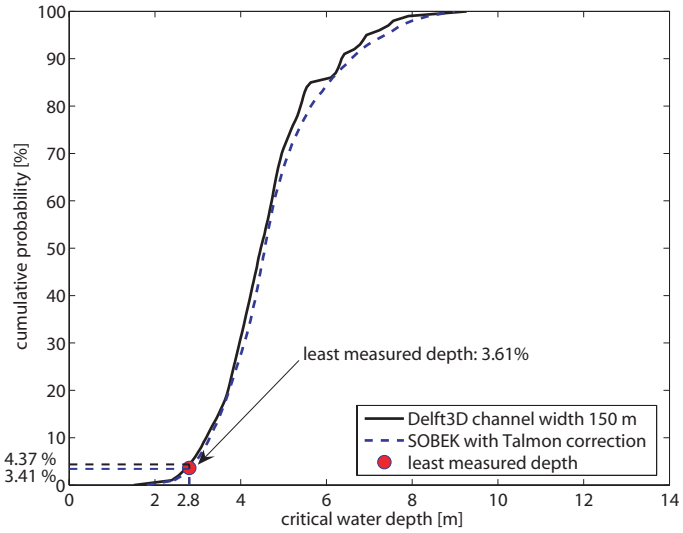

Figure 6.9: Comparison of the cumulative probability curves, SOBEK&Delft3D&Data

Conclusions of the data comparison

1. **Bottleneck location** For a large part of the Midden-Waal no agreement between the models and data can be found. For the downstream part from km 910 on, an indication of an agreement can be seen.
   Reasons for this behaviour could be:
   (1) km 886 until km 893.5 is left out of the analysis in the Delft3D model, due to possible boundary effects;
   (2) the bottleneck criterion is very sensitive, only the one location with the smallest water depth (even if the difference is just in the order of centimeters) is defined as bottleneck. The fact that only one location is reproduced well by the models points out that the models are only able to represent the correct location if a strong morphologic effect is causing the bottleneck.
   (3) the dataset of LMD is not complete, and influenced by the placement of buoys (see Section 3.3.1), dredging operations as well as the navigation traffic on the river.

   Further reasons for a disagreement between the models are:
   (4) Delft3D is used in a quasi-3D mode, different morphologic features are included in the model (e.g. the pool/ point bar formation in bends), that are not represented by the SOBEK model (see Table 3.2);
   (5) the Delft3D model uses a grid with a 100 m longitudinal resolution, SOBEK uses cross-sections every 500 m, thus morphological phenomena of different scales are predicted; for Delft3D this scale is in the order of several hundreds of meters, for SOBEK several kilometers.

   The evolution of the morphology can assumed to be the dominating factor for the formation of the bottleneck location. Thus, in combination with the very "hard definition" of the bottleneck criterion, it is not recommended to use this criterion for a data comparison. The measurement data for comparison is not sufficient, as discussed in Section 4.4. Especially the influence of effects like dredging, the navigation traffic and buoy placement (all not included in the models) on the occurrence of a Least Measured Depth cannot be estimated.

2. **Fulfillment of the navigation requirements** The cumulative probability curve of both models fit very well (see Figure 6.9). The fulfillment of the navigation requirements is predicted similar and also matches the data given by the LMD. For this criterion the exact location of a restriction of the navigability is not needed, only the percentage of time that one location along the river is not navigable, independent of its position is important. This can be predicted very well by the models.

Summing up, it can be stated that the SOBEK model with the correction for the transverse slope effect is applicable for a very wide range of assessments of the navigability. Especially the navigability of the complete stretch, the fulfillment of the navigation requirements and periods of time with restricted navigability can be reproduced very well. The similar patterns shown in the analysis of the navigability of each location along the river, indicate that the larger scale morphology is predicted similar to the Delft3D model.

The Delft3D model gives the opportunity to investigate the morphology and its effects on the navigability with a higher spatial resolution (100 m instead of 500 m) and in two dimensions, including the corresponding morphologic effects. This becomes important when locations that form restrictions for navigability should be identified. Even if the comparison with the LMD data is not completely satisfying, the Delft3D results give the impression to be more trustworthy. One large disadvantage of the two-dimensional model is the higher computational effort, thus it has to be carefully balanced to what extend it is necessary to use it instead of the SOBEK model.

For the future, two different approaches can be pursued to improve the comparison of the model results with the data:

Assuming that the data of Least Measured Depth is used in further comparisons: Then the effects that avoid the formation of a LMD have to be included in the models. For both models, the dredging and accompanied replacement of the dredged material has to be included. It also would be favorable if the models could predict morphologic effects like the formation of groyne flames.

Another possibility would be the establishment of a new data set. It could be recommended to leave the "hard definition" of the one bottleneck location per time step. Instead of this, a criterion similar to the "navigability of each location" (see Figure 6.4) should be used. In this kind of analysis the navigability of each location is assessed individually. Hence, a dominating effect of one single location like in the bottleneck criterion (which can be caused by just a difference of 1 cm in water depth) is avoided. A completely new data set would be needed for this comparison. It would be advised that for a single stretch of the river (e.g. the in this research used 37 km long Midden-Waal), the water depth and the related channel width is measured for several permanent locations along the river on a daily basis.

Chapter 7

Aspects of Stochastical Modelling

After answering the questions of the river manager concerning the navigability of the river, this chapter focuses on the interests of the modeller. It gives answers to the following questions:

- How many simulations are necessary to predict a statistical parameter of the model output with a certain degree of accuracy? (Section 7.1)
- What is the relation between the uncertainty and the duration, respectively the number of the conducted model runs? (Section 7.2)

So far, the results of 100 conducted simulations with a duration of 4 years are used for the analysis. It proves that MCA, especially when two-dimensional models are used, leads to an enormous computational effort. The information gained from this chapter should give advice to the modeller, in terms of reducing the effort for a Monte Carlo Simulation by minimizing the number of simulations and an efficient layout of the simulations in terms of time and number needed to describe a certain problem.

The one-dimensional SOBEK model is used to conduct 1,000 simulations with a duration of 10 years each, as a data basis for this chapter. For the upcoming analysis the original SOBEK model results are used (without a correction for the transverse-slope effect). This is appropriate, because only the statistic behaviour of certain characteristics of the distribution of the water depth is assessed, not the absolute values of the water depth. The corrections used in Section 4 have only little effect on the statistic variation of the water depth and thus the range of uncertainty.

7.1 Required sample size

In order to minimize the effort of a Monte Carlo Analysis, it is important to (1) define the desired degree of accuracy of the model results and then (2) estimate the minimum needed number of simulations to be carried out to reach this goal.

The model results from a MCA consist of independent random values from the distribution of the output. This means that the MCA results are not directly depending on the number of uncertain inputs. Thus, the accuracy of a certain parameter for a given output distribution depends on the sample size m, and not on the number of inputs. This means that in the case of additionally included uncertainties, there is usually no need to alter the number of simulations, as long as the added uncertainty does not considerably increase the variance of the model output [38].

Theory Morgan&Henrion [38] show a way to estimate the sample size needed to reach a certain degree of accuracy for the prediction of a statistical parameter of the model output. The accuracy in their approach is expressed as a fractile that needs to be estimated and maximum allowed deviation, represented by an interval of fractiles. In this research an adapted approach of the analysis done by Van der Klis [52], which was also based on the work of Morgan&Henrion, is used. The desired degree of accuracy is now expressed as a deviation from the estimated fractile in meters of water depth. With the help of this approach and the below shown example, the practical questions of the river manager concerning the navigability of the river can be combined with the interests of the modeller in the stochastic behaviour of the model results.
The estimation of the needed sample size m requires the following steps [38]:

1. The fractile p, the desired accuracy and the allowed deviation of the fractile have to be defined.

2. A rough estimate of the distribution parameters has to be given with the help of a Gaussian distribution that was set up with the mean and the standard deviation of a small sample size.

3. The fractiles corresponding to the boundaries of the interval of the maximum deviation defined in step 1 have to be estimated from the Gaussian distribution of step 2. The result is a fractile interval of the size $2\Delta p$, where: $\Delta p = \frac{(p_2 - p_1)}{2}$.

4. The required number of simulations can be estimated as follows:

$$m = p(1-p)\left(\frac{c_\alpha}{\Delta p}\right)^2 \tag{7.1}$$

   in which:
   c_α is the interval of the Gaussian distribution Φ that represents the desired level of accuracy ($P(-c_\alpha \leq \Phi \leq c_\alpha) = \alpha$).

Practical question The river manager is mainly interested in the chance that the navigation requirements (2.8 m in depth, 150 m in width, set in the OLR-criterion) are fulfilled. The OLR-criterion is related to a discharge, which in reality is exceeded for 95% of the time. Thus, the river manager is interested in estimating the low water depth, in this example the 5^{th} percentile of the cumulative probability of the critical water depth (the minimum water depth for the complete stretch per time step, see Figure 7.1) with a certain accuracy (e.g. 95%). The modelled 5^{th} percentile of the critical water depth should, with this accuracy of 95%, not vary more than ±5 cm.
The question thus can be formulated as follows:

> How many simulations need to be conducted, so that the 5^{th} percentile of the critical water depth lies with a 95% certainty in an interval of 10 cm?

The answer to this question is derived in detail with the results of the SOBEK model, first for simulations with a duration of four years (1)+(2), then for simulations with a duration of only one year (3). After that, the results for the same analysis for the Delft3D model are shortly presented to get insight into possible differences in the behaviour of both models (4).

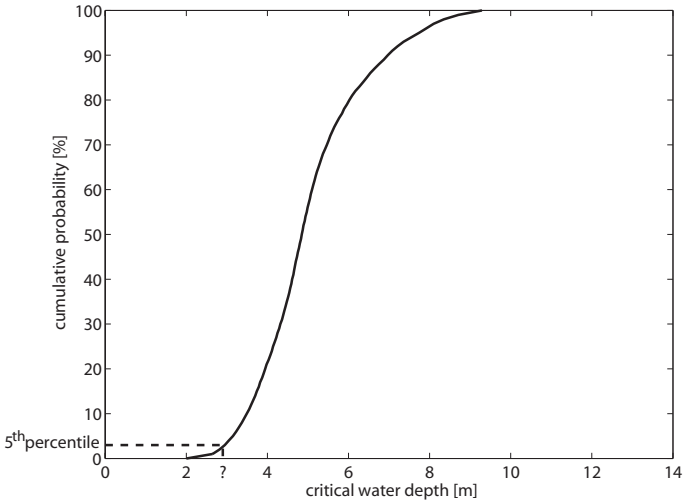

Figure 7.1: Parameter to be estimated: 5^{th} percentile of the critical water depth

1. Results of the SOBEK model, duration 4 years The probability distribution of the critical water depth is not known yet. Therefore, a Gaussian normal distribution is assumed. This shows to be appropriate for a first estimation: Figure 7.2(a) shows the probability density function of the critical water depth including the statistic parameters mean (5.04 m), standard deviation (1.33 m), skewness (0.71) and kurtosis (3.34). With the help of the skewness and the kurtosis of the probability density function the kind of distribution can be estimated (Figure 7.2(b)). The distribution of the critical water depth can be estimated to be close to a normal, beta or log normal distribution. For reasons of simplicity of the analysis a normal distribution is chosen.

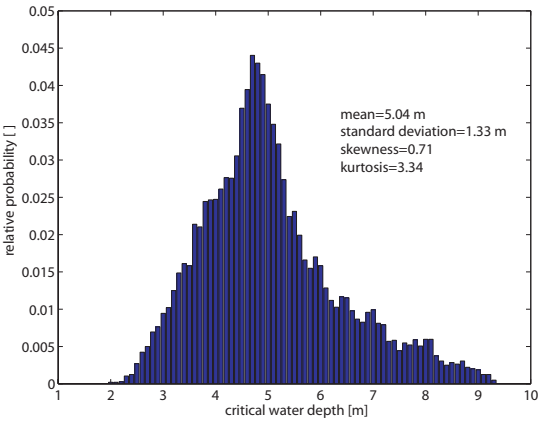

(a) Probability density function of the critical water depth, SOBEK, duration 4 years

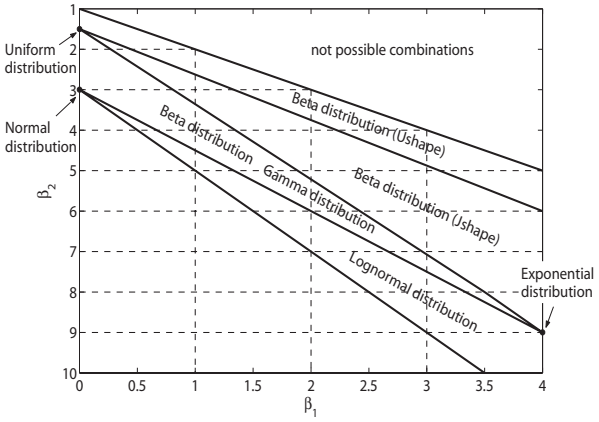

(b) Distribution classification graph, β_1 stands for the skewness, β_2 for the kurtosis, after Pearson [40]

Figure 7.2: Distribution function&kind of distribution of the critical water depth

For the estimation of the required sample size, the above shown four steps have to be executed:

1. The aim of this example is defined as predicting the estimate of the critical water depth, that is exceeded for 95% of the time with a precision of ±5 cm. Only a probability of 5% that this degree of precision is not reached is allowed. In other words: The 5^{th} percentile ($p = 0.05$) of the critical water depth should, with a confidence of 95% ($\alpha = 0.95$), lie in an estimated interval of maximum 10 cm.

2. 20 simulations are conducted to estimate the mean and standard deviation needed to set up the Gaussian distribution. The output of these 20 simulations leads to $\mu = 5.0$ m and $\sigma = 1.34$ m for the critical water depth. With the help of these parameters a cumulative probability curve assuming a Gaussian distribution is constructed (see Figure 7.3(a)).

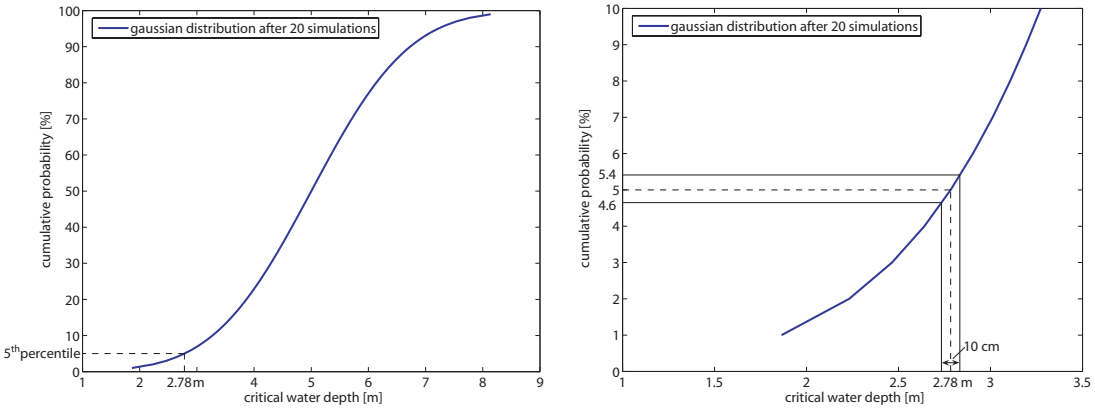

(a) 5^{th} percentile after 20 simulations (b) Interval of 10 cm around the 5^{th} percentile

Figure 7.3: Curve of the Gaussian distribution after 20 simulations, SOBEK, 4 years

3. With the assumption that the distribution is Gaussian, the 5^{th} percentile is estimated with 2.78 m (Figure 7.3(a)). The maximum desired interval would be [2.73m; 2.83m], which corresponds approximately with the 4.6^{th} and the 5.4^{th} fractiles (Figure 7.3(b)). The size of the interval, expressed in fractiles, calculates as:

$$\Delta p = \frac{(0.054 - 0.046)}{2} = 0.004$$

4. With the help of this information it is possible to estimate the necessary sample size:

$$m = p(1-p)\left(\frac{c_\alpha}{\Delta p}\right)^2 = 0.05(1-0.05)\left(\frac{1.96}{0.004}\right)^2 \approx 12,637$$

in which:
c_α is equal to 1.96 (taken from tables of the normal distribution, corresponding to a confidence of 0.95).

In this research, m is not equal to the number of simulations that need to be conducted. Every year of the model period consists of 36 ten day long periods, and so contributes 36 samples to the distribution. Hence, the above calculated number has

to be divided by a factor of $4 * 36 = 144$ to get the necessary number of simulations N:

$$N = 12,637/144 \approx 88$$

Apart from the 20 simulations already conducted, 68 more simulations are necessary to predict the 5^{th} percentile with the desired accuracy.

2. Check of the precision of the SOBEK results, duration 4 years After the above shown estimation it is important to check if the calculated required number of model runs N is large enough. This can be proved in two different ways:
(1) Figure 7.4 shows a plot of the development of the 5^{th} percentile of the critical water depth versus the number of simulations that are included into the analysis. The maximum allowed deviation is indicated as a 10 cm interval. It can be concluded that the estimated sample size of 88 simulations is large enough to predict this estimate with sufficient accuracy.

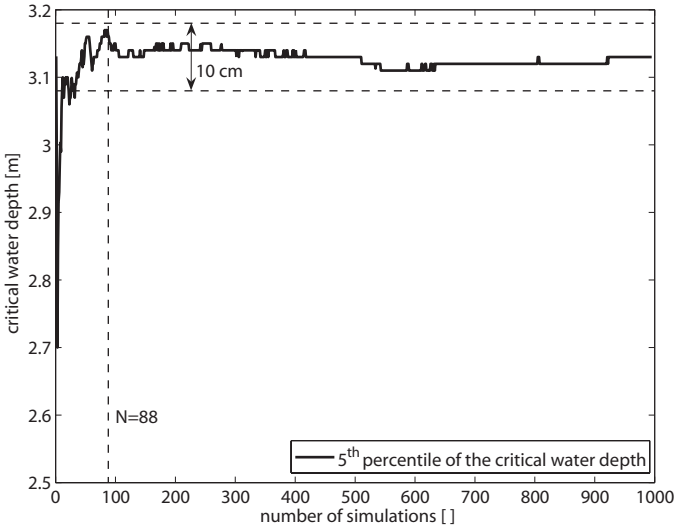

Figure 7.4: 5^{th} percentile versus number of simulations, SOBEK, 4 years

(2) A second way to prove the above used method is described by Morgan&Henrion [38], as a general method to estimate a confidence interval for the p^{th} fractile. This approach is independent of the kind of distribution of the model output, only the variation of the estimate (in this case the 5^{th} percentile) is assumed to be normal distributed. The confidence interval with a confidence α can be expressed by a pair of sample values x_k and x_i, which form the boundaries of the interval around the estimate in the ordered series of N simulations.
The index of x_k and x_i then read as follows:

$$k = \left\lceil Np + c\sqrt{Np(1-p)} \right\rceil \tag{7.2}$$

$$i = \left\lfloor Np - c\sqrt{Np(1-p)} \right\rfloor \tag{7.3}$$

in which:
c is the deviation enclosing probability α of the unit normal, $\lfloor x \rfloor$ means rounding x down and $\lceil x \rceil$ means rounding it up.

Figure 7.5 shows a plot of the difference between x_k and x_i versus the number of model runs. As soon as the difference between the boundaries that enclose the confidence interval around the estimated parameter is less than 10 cm, the desired accuracy of the estimate is fulfilled. It can be seen that the estimated number of 88 simulations is sufficient, even slightly overestimated for the desired analysis.

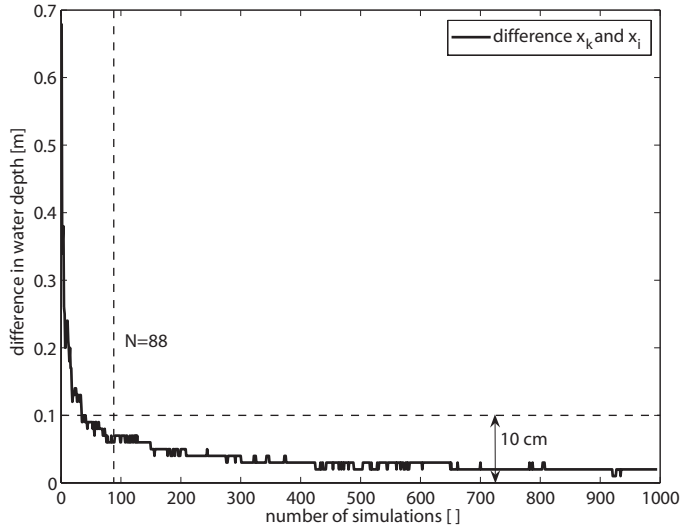

Figure 7.5: Size of the confidence interval around the 5$^{\text{th}}$ percentile, SOBEK, 4 years

3. Results & check of the precision of the SOBEK model, duration 1 year
With an increasing duration of the model runs, a higher number of samples is included per simulation (36 time steps per year). Therefore, the number of required simulations depends on their duration. In contrast to the above four year long simulations, only 36 time steps are included in a one year model period.

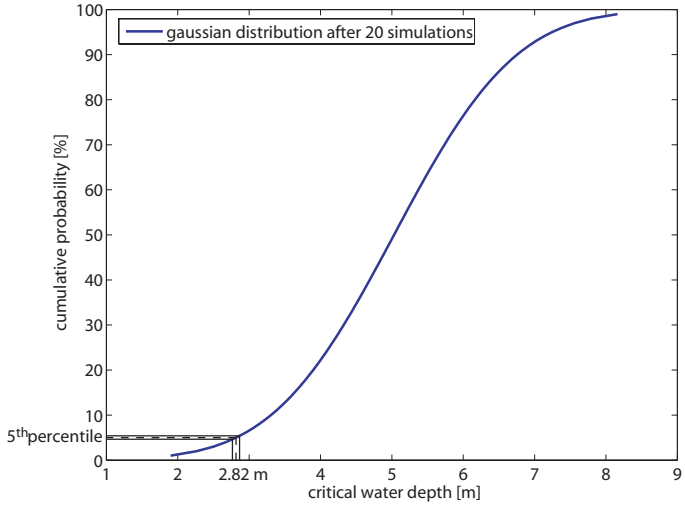

Figure 7.6: Curve of the Gaussian distribution after 20 simulations, SOBEK, 1 year

The estimation of the 5$^{\text{th}}$ percentile assuming a Gaussian distribution after 20 initial simulations is presented in Figure 7.6. The estimated 5$^{\text{th}}$ percentile after 20 simulations

increases only with 4 cm to 2.82 m. On the other hand, the with the help of Eq. 7.1 estimated required number of model runs is considerably higher with $N = 348$.
The two checks of this estimation, the plot of the 5^{th} percentile (Figure 7.7(a)) and the plot of the difference between x_k and x_i (Figure 7.7(b)), show that 348 seems to be a large enough number of simulations to fulfill the accuracy criterion.

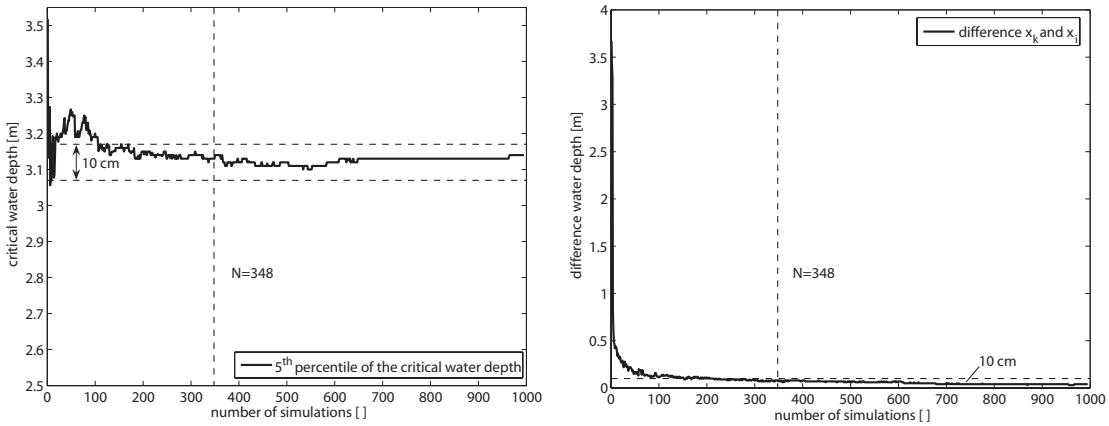

(a) 5^{th} percentile versus number of simulations, SOBEK, 1 year

(b) Size of the confidence interval around the 5^{th} percentile, SOBEK, 1 year

Figure 7.7: Check of the estimation for the SOBEK results, 1 year

4. Overview of the Delft3D results (1) For a duration of 4 years. The 5^{th} percentile estimated after 20 simulations with the Delft3D model is, with 2.58 m, significantly lower than the SOBEK estimate (Figure 7.8). The required minimum number of simulations calculated with Eq. 7.1 is also lower with 72 simulations.

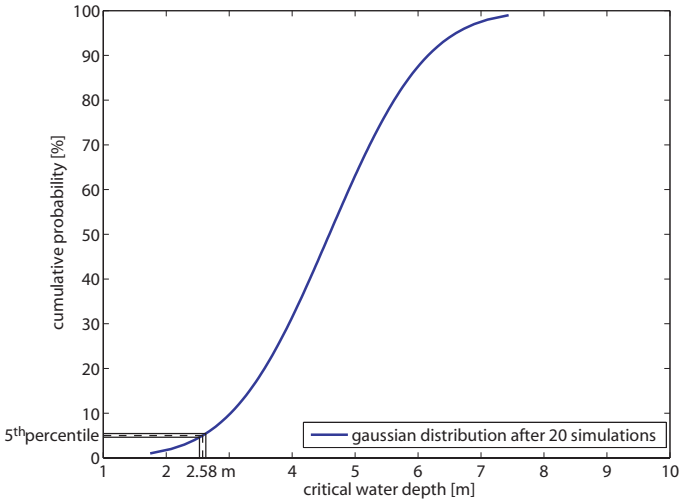

Figure 7.8: Curve of the Gaussian distribution after 20 simulations, Delft3D, 4 years

The prove that this estimated number of 72 model runs is sufficient is shown in Figures 7.9(a) and 7.9(b). The estimated sample size seems to be predicted well. Again the necessary number of simulations seems to be slightly overestimated.

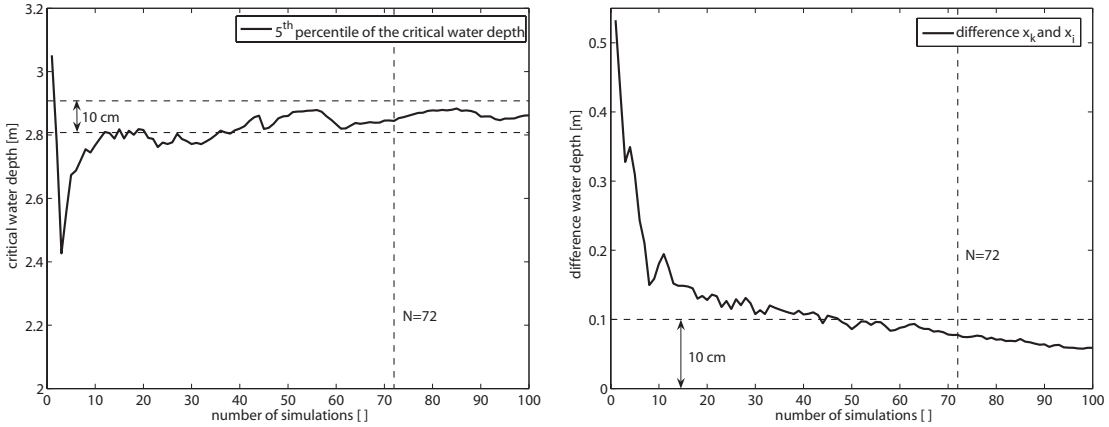

(a) 5^{th} percentile versus number of simulations, Delft3D, 4 years

(b) Size of the confidence interval around the 5^{th} percentile, Delft3D, 4 years

Figure 7.9: Check of the estimation for the Delft3D results, 4 years

(2) For a duration of 1 year. The estimated Gaussian distribution curve is shown in Figure 7.10. The estimate of the 5^{th} percentile after 20 simulations only increases slightly to 2.60 m. The required number of simulations increases significantly to 295.

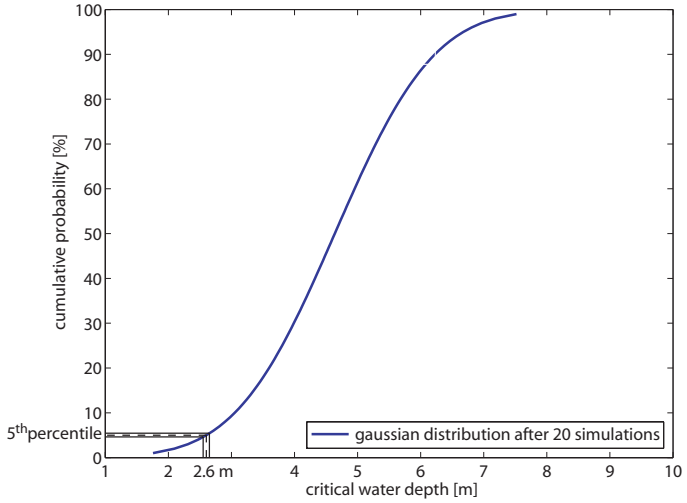

Figure 7.10: Curve of the Gaussian distribution after 20 simulations, Delft3D, 1 year

For the Delft3D model only a number of 100 simulations is available to prove the above calculated estimate of the sample size. Figures 7.11(a) and 7.11(b) show the plot of the 5^{th} percentile and the size of the 95% confidence interval, respectively. Only the first criterion, the plot of the percentile, shows that even for a number less than 100 simulations the goal for the accuracy is already reached. The size of the confidence interval shows to be close to the desired 10 cm, but is not reached yet after 100 simulations. Nonetheless, from the course of the curve, it can be assumed that after 295 simulations the difference between x_k and x_i will be less than 10 cm and the criterion fulfilled.

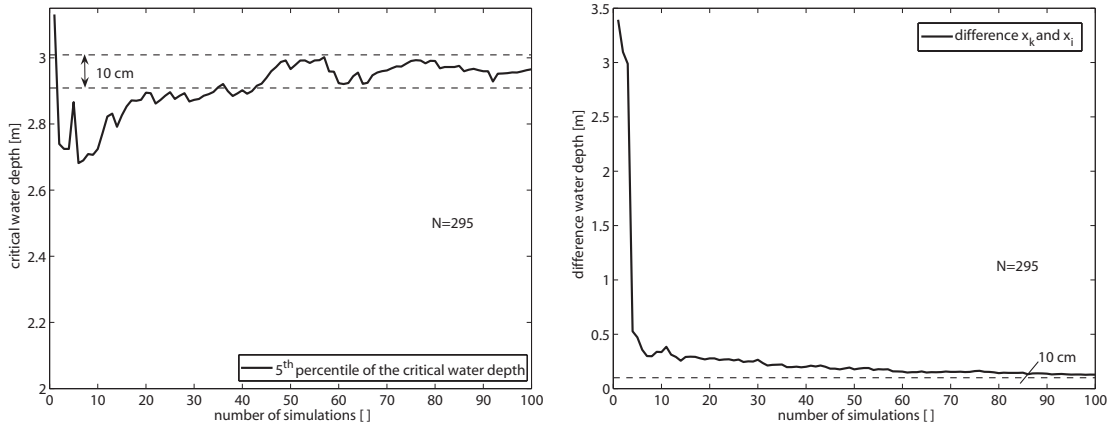

(a) 5^{th} percentile versus number of simulations, Delft3D, 1 year

(b) Size of the confidence interval around the 5^{th} percentile, Delft3D, 1 year

Figure 7.11: Check of the estimation for the Delft3D results, 1 year

Conclusions

1. The required sample size for the above posed question can be estimated very well. The effort in terms of the required number of model runs for a Monte Carlo Analysis can so be minimized. Note that the example only gives an estimate for the number of simulations needed to model the 5^{th} percentile of the critical water depth. The results for other questions can turn out to be different. Nonetheless can the above shown method be used to give a good estimate of the required model runs on hand of a small number starting simulations for other questions as well.

2. For both models the number of required simulations is in the same range (e.g. for a four year duration: 88 simulations, Delft3D: 72 simulations), thus the influence of the uncertainties on the variation of the estimated parameter of the output is similar.

3. For this example, the duration of the simulations has influence on the included samples per simulation. Therefore, for a shorter duration more model runs are necessary (e.g. SOBEK four year duration: 88 simulations, one year duration: 348 simulations). The number of required simulations is inverse proportional to the length of the simulations. On the other hand, with a finer time discretisation also less simulations are necessary. Note that this is only the case for this example. If e.g. the maximum erosion depth of the bed level during a certain model period is analysed, this time dependency is no longer true (see e.g. the example of Van der Klis [52]).

4. The required number of simulations seems to be slightly overestimated in all results. This might be due to the fact that the model outcome is assumed to be Gaussian distributed. In case of the assumption that the output is log normal distributed, the cumulative probability curve after 20 simulations would be steeper in the lower part. This results in a larger interval Δp, thus in an estimated lower number of necessary simulations needed to reach the desired accuracy.

5. In general it has to be carefully chosen which parameter wants to be estimated and which accuracy is demanded. It can be seen from Eq. 7.1 that the required sample size is proportional to the square of the degree of accuracy ($m \sim c_\alpha^2$) and inversely

proportional to the size of the interval of the allowed deviation ($m \sim \frac{1}{(\Delta p)^2}$). Thus, the demanded precision has to be carefully chosen. If the uncertainty in the model input is only very roughly known, it is questionable to demand a high precision of the output statistics [38].

7.2 Dependency of the uncertainty on the number&duration of the model runs

The in the previous section shown dependency of the output statistics to the number of model runs and their duration leads to the question what happens to the uncertainty in the navigability if those parameters are changed.

In the chapters 4 to 6, all analysis are carried out for 100 simulations with a duration of four years. Figure 7.12(a) shows the navigable percentage of time of the complete stretch for the SOBEK results without correction for the transverse slope effect (Section 4.1).

The same statistics are shown in Figure 7.12(b), now considering 100 simulations with a duration of only one year. It can be seen that, e.g. for a draught of 3.5 m, the mean navigability predicted by both figures is similar with nearly 90%. On the other hand, the size of the 90% confidence interval, which is used as a measure of the uncertainty, increases significantly from 19% in the four year case to 35% in the one year case. This indicates that the mean navigability predicted by simulations with different durations is similar, while the involved uncertainty (expressed by the size of the 90% confidence interval) is strongly dependent on this feature.

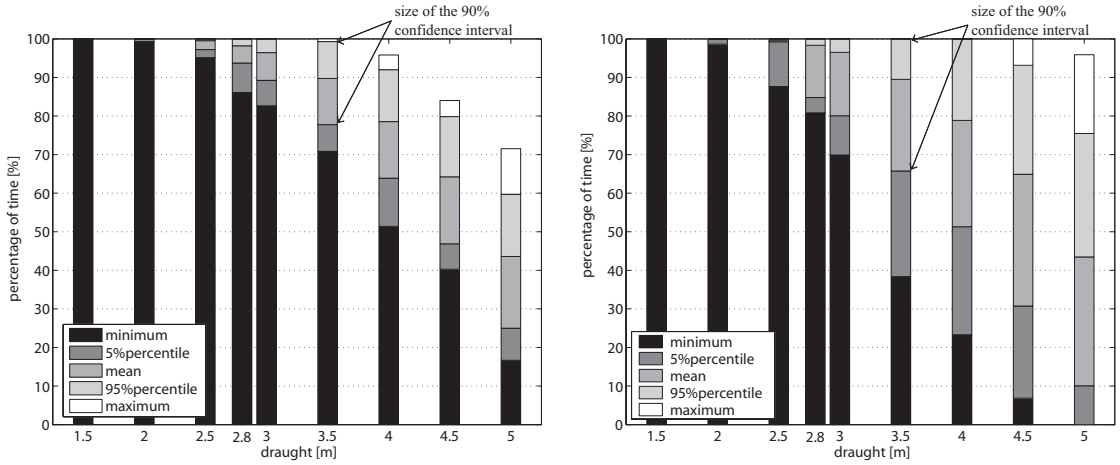

(a) 100 simulations with duration of four years

(b) 100 simulations with duration of one year

Figure 7.12: Navigability of the complete stretch for four years&one year, SOBEK

To investigate these findings, the above mentioned 1,000 simulations with a duration of the SOBEK model are used. With the help of this data, the behaviour of the mean navigabilty and the size of the 90% confidence interval of the navigability of the complete Midden-Waal is analysed for different combinations of the number of simulations and their time duration.

Again, the original results without a correction for the transverse slope are used, as the absolute value of the navigability is not important, but only the influence on the uncertainty is assessed. First the results of the SOBEK model (1)+(2) as well as an explanation for

the behaviour of the uncertainty is shown in detail (3)+(4), then a short overview over the Delft3D results are given to get insights into possible differences (5).

1. Size of the 90% confidence interval for the SOBEK model Figure 7.13 shows the development of the size of the 90% confidence interval versus the number of simulations and their duration.
The figure shows two important features:
(1) The size of the 90% confidence interval decreases significantly with an increasing duration of the simulations. For example for 1,000 simulations, the interval decreases from 37% for one year until 13% for a duration of ten years. The decrease seems to follow a logarithmic course.
(2) The size of the 90% confidence interval increases with the number of simulations. For a duration of ten years, the interval increases from 9% to a stable value of 13%. This increase seems to be restricted to the area from 5 to 50 simulations and to be irregular, as can be seen in the jumps of the graph in this reach.

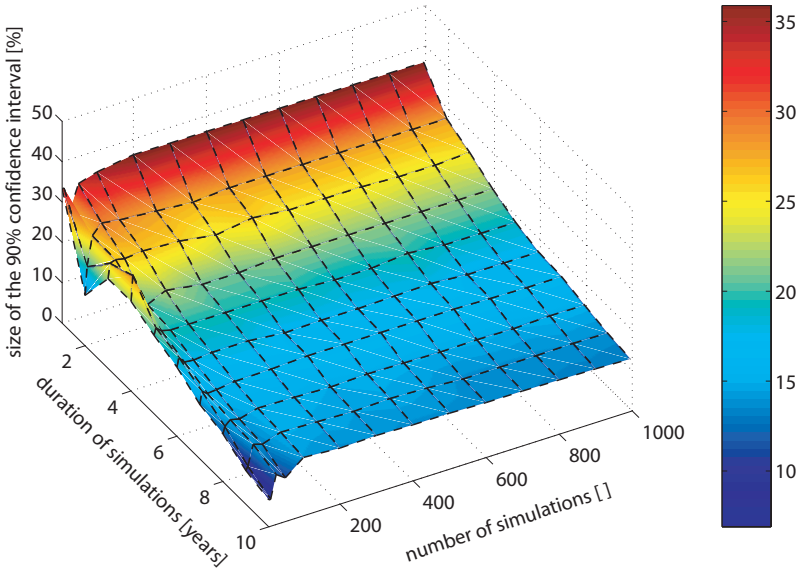

Figure 7.13: Development of the 90% confidence interval, SOBEK

Figures 7.14(a) and 7.14(b) show the trends of the mean size of the 90% confidence interval versus the duration of the simulations and the number of simulations, respectively. In the first case the mean over 1,000 simulations, in the second case the mean over the ten year model duration is shown.

It can be concluded that the decrease of the size of the 90% confidence interval will go on for an increasing duration of the simulations larger than ten years (Figure 7.14(a)). On the other hand, the increase for an increasing number of simulations seems to have ended for approximately 100 simulations. For a larger number of simulations, the size of the 90% confidence interval stays constant (Figure 7.14(b)).

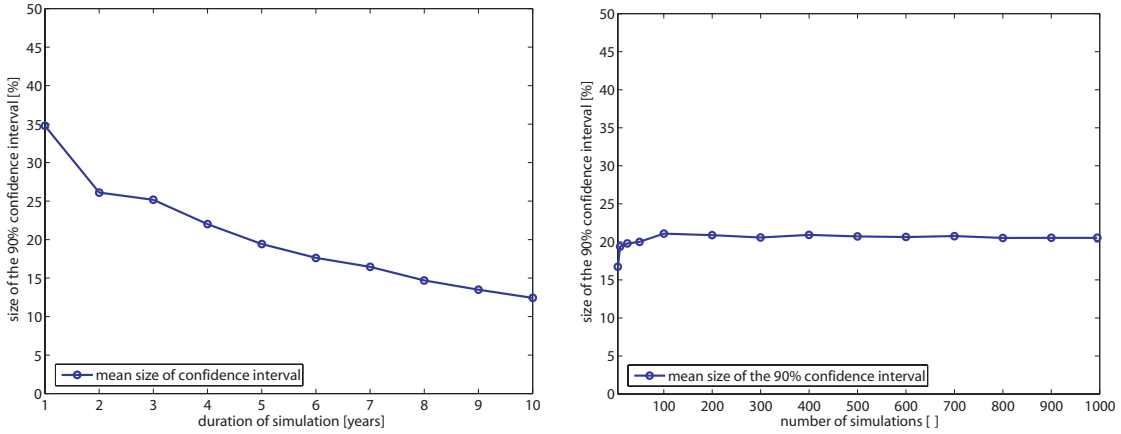

(a) Trend versus the duration of the simulations

(b) Trend versus the number of simulations

Figure 7.14: Trends in the 90% confidence interval, SOBEK

2. Mean navigability for the SOBEK model Figure 7.15 shows the development of the mean navigability of the complete stretch versus the number of simulations and their duration. The mean navigability shows to be nearly independent of the duration of the simulations. The graph shows an increasing navigability with an increasing number of simulations. After 100 simulations this value seems to be stable.

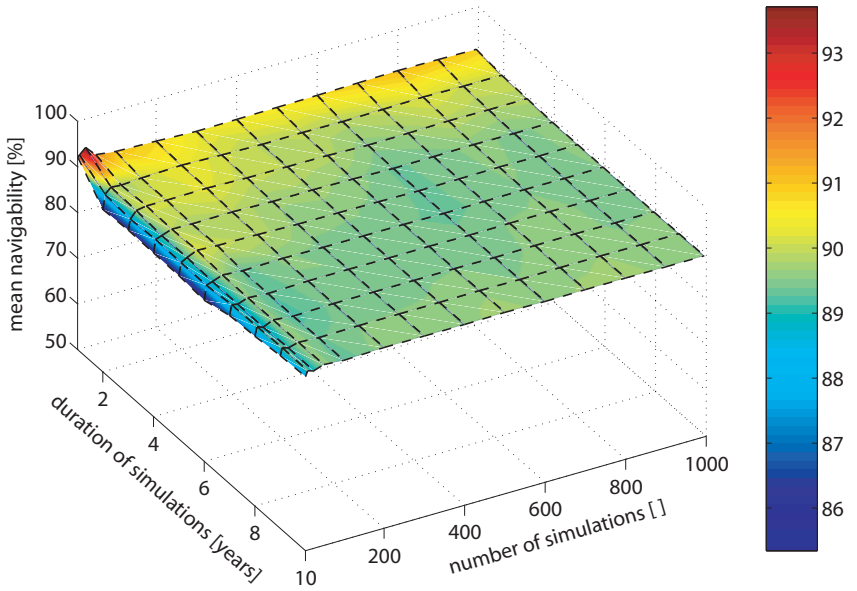

Figure 7.15: Development of the mean navigability, SOBEK

To find an explanation for these two behaviours, the distributions of the discharge as the uncertain input parameter and the distribution of the water depth as model output have to be analysed.

3. Distribution of the discharge The probability density function of the discharge (discretized in steps of 50 m^3/s from 500 m^3/s until 2,000 m^3/s, above this value in steps of 500 m^3/s) for three single simulations (number 20, 50 and 90), for a model period of one year and ten years are shown in Figures 7.16 (a) to (f).

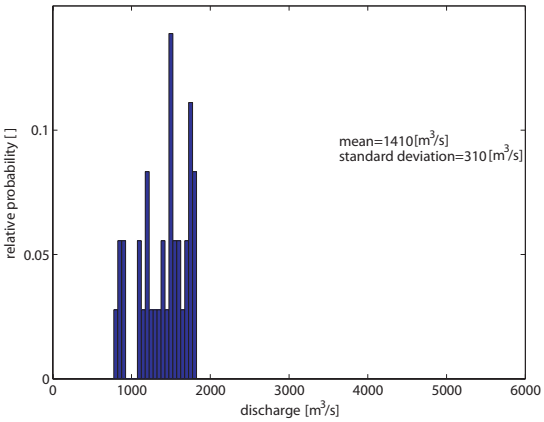

(a) Simulation 20, duration 1 year

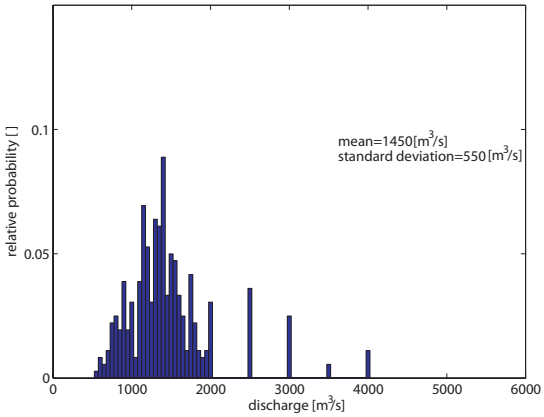

(b) Simulation 20, duration 10 years

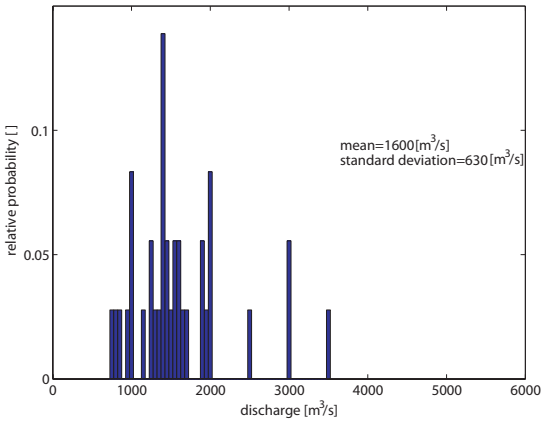

(c) Simulation 50, duration 1 year

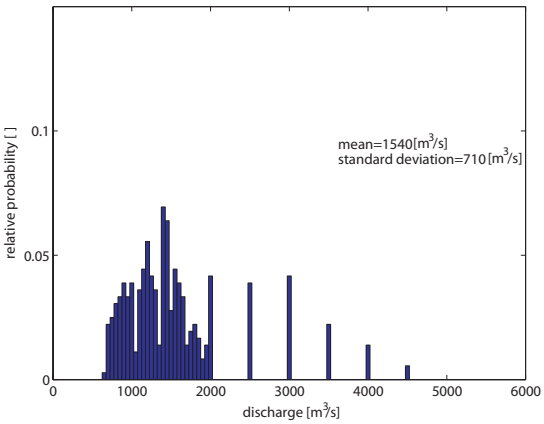

(d) Simulation 50, duration 10 years

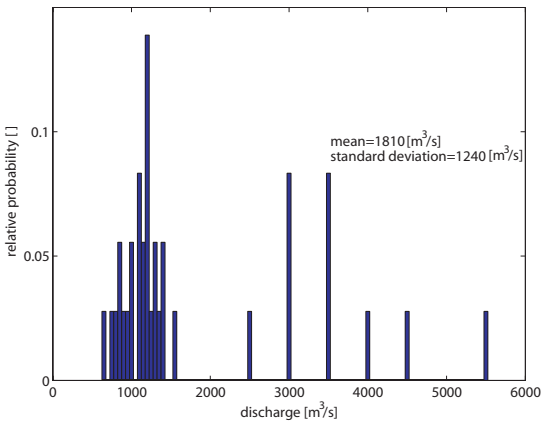

(e) Simulation 90, duration 1 year

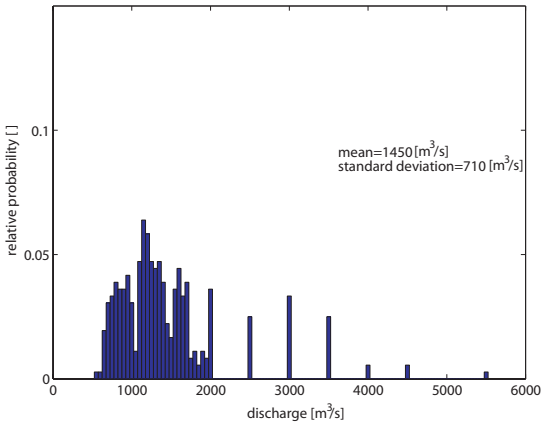

(f) Simulation 90, duration 10 years

Figure 7.16: Probability density functions of the discharge for different durations

The differences for the three simulations for a duration of one year can clearly be seen. The first year of simulation 20 shows to be very dry, simulation 50 shows a more balanced distribution of the discharge while simulation 90 shows a flood event as well as a significant dry period. This difference disappears for a longer model period. After ten years the three graphs look similar.

Two important parameters are the variation of the standard deviation and the mean of the discharge for the three simulations. For a duration of one year, the standard deviations differ with about 400% (Figures 7.16(a) and (e)). When the duration of the simulations is increased to 10 years, the difference in the three predicted standard deviations decreases significantly to approx. 30% (Figures 7.16(b) and (f)).

The mean values of the discharge varies only slightly, from approx. 25% for a duration of one year to approx. 10% for a period of 10 years.

4. Distribution of the water depth The probability density functions for the three single simulations 20, 50 and 90 are presented in Figures 7.17(a) to (f). The distribution of the water depths can be seen to reflect the distribution of the discharges.
The differences between the three distributions for an one year long model period can clearly be seen. Simulation 20 is dominated by a lower water depth, simulation 50 shows a balanced distribution of the water depth, while simulation 90 shows destinctive peaks at low and high water depths.

This difference can not be seen any more for a duration of ten years, the distribution curves now look very similar. Important to notice is that the mean values lie in the same order (between 5.0 m and 5.6 m, meaning a variation of approx. 10%), independent of the duration of the simulations, while the standard deviations vary by nearly 300% for the one year duration (Figures 7.17(a) and (e)). In the case of ten year long simulations the variation of the standard deviations is less than 20% (Figures 7.17(b) and (f)).

Thus, for a shorter time period the difference between single simulations in the predicted distribution of the water depth is large. This leads to a large spreading of the distribution of the 100 conducted simulations. The difference between the 5^{th} percentile and the 95^{th} percentile and so the size of the 90% confidence interval of the navigability is large.

Extreme distributions of the discharge in single simulations of one year duration have a large influence on the uncertainty of the 100 model runs. If more years are added to each model run, the difference between the single simulations gets smaller. The distribution curves tend to be more balanced. Thus, the distribution of the 100 simulations gets more balanced as well. The difference between the 5^{th} percentile and the 95^{th} percentile and so the uncertainty in the navigability decreases.

This behaviour reflects the fact that the discharge for a short time period, e.g. one year, in reality is more uncertain than the discharge of a longer period. The one year period can be dominated by a major drought or a flood event and thus show an extreme distribution of the discharge. A longer period will show a more evenly, balanced distributed of the discharge, as extreme years are compensated by the following "regular" discharge years. The answer to the question about the discharge distribution for the upcoming year, for example is: "It is uncertain." A major drought as well as regular discharge year or a high flood could happen. On the other hand, the discharge distribution for the coming 100 years can be statistically assessed with the help of discharge records from the past and possible new trends, e.g. for global warming. Thus for longer periods of time the uncertainty in the discharge decreases.

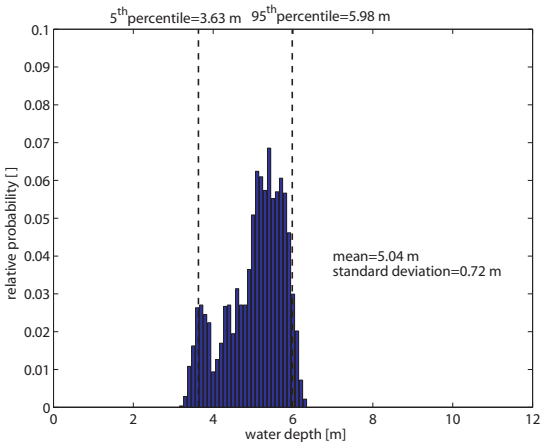

(a) Simulation 20, duration 1 year

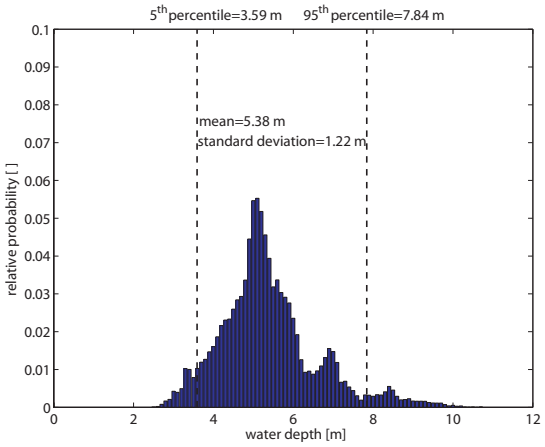

(b) Simulation 20, duration 10 years

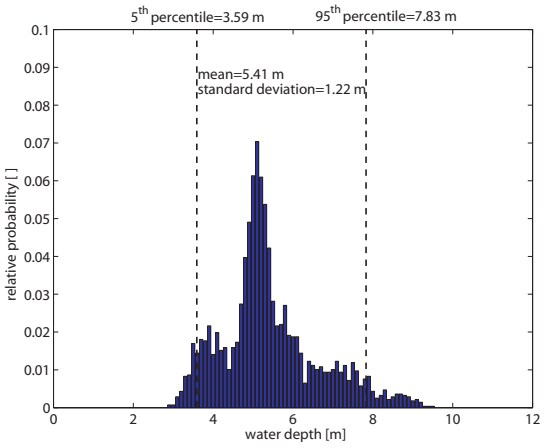

(c) Simulation 50, duration 1 year

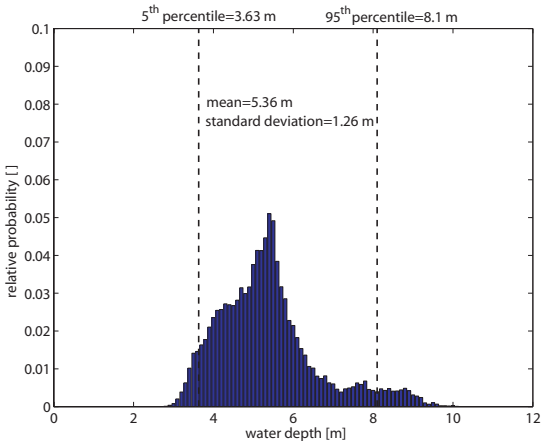

(d) Simulation 50, duration 10 years

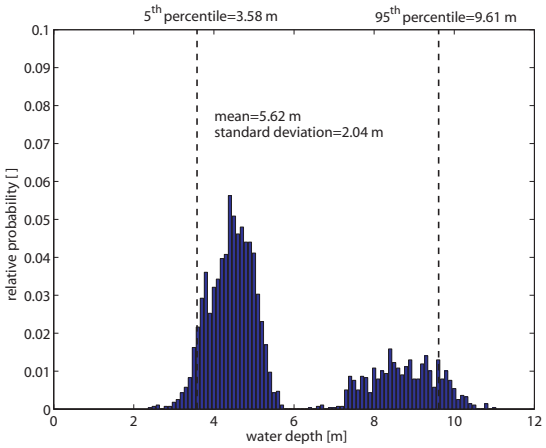

(e) Simulation 90, duration 1 year

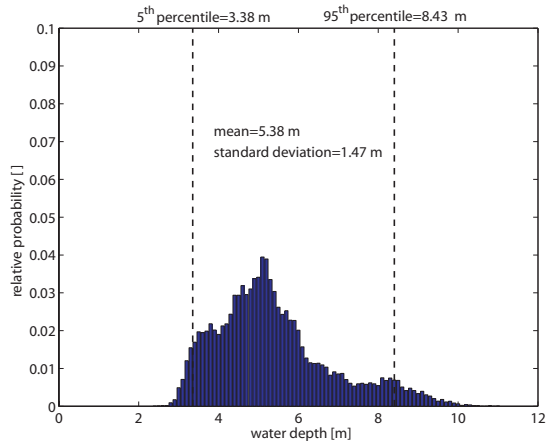

(f) Simulation 90, duration 10 years

Figure 7.17: Probability density fcts. of the water depth for different durations, SOBEK

5. Overview of the Delft3D model results In this paragraph the behaviour of the uncertainty and the mean navigability of the Delft3D model are shortly described. Due to the high computational effort no additional Delft3D simulations are conducted, only the results for 100 simulations with a duration of four years are shown.
(1) Size of the 90% confidence interval. The size of this interval shows similar behaviour as for the SOBEK results: it is decreasing with increasing time duration of the simulations and increasing with the number of simulations (Figure 7.18).

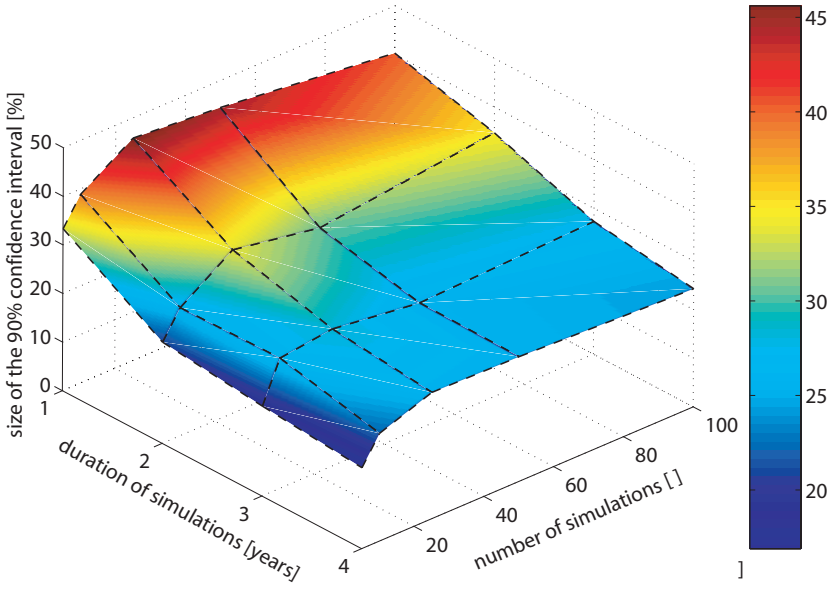

Figure 7.18: Development of the 90% confidence interval, Delft3D

Figures 7.19(a) and 7.19(b) show the trends of the size of the 90% confidence interval. The interval can be assumed to keep on decreasing for a duration longer than four years. After a number of 100 model runs the size of the confidence interval seems to stay constant.

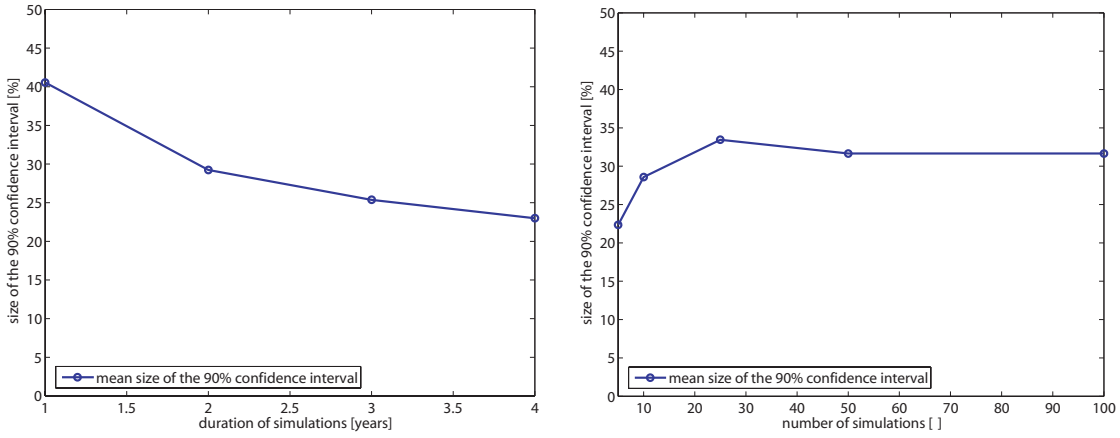

(a) Trend versus the duration of the simulations

(b) Trend versus the number of simulations

Figure 7.19: Trends in the 90% confidence interval, Delft3D

(2) Mean navigability. The mean navigability for the Delft3D model depending on the number and the duration of the simulations is shown in Figure 7.20. It proves that the mean navigability stays constant, independent of the duration of the simulations. Only a certain minimum number of simulations has to be included. In this case 100 simulations seem to be a good estimate.

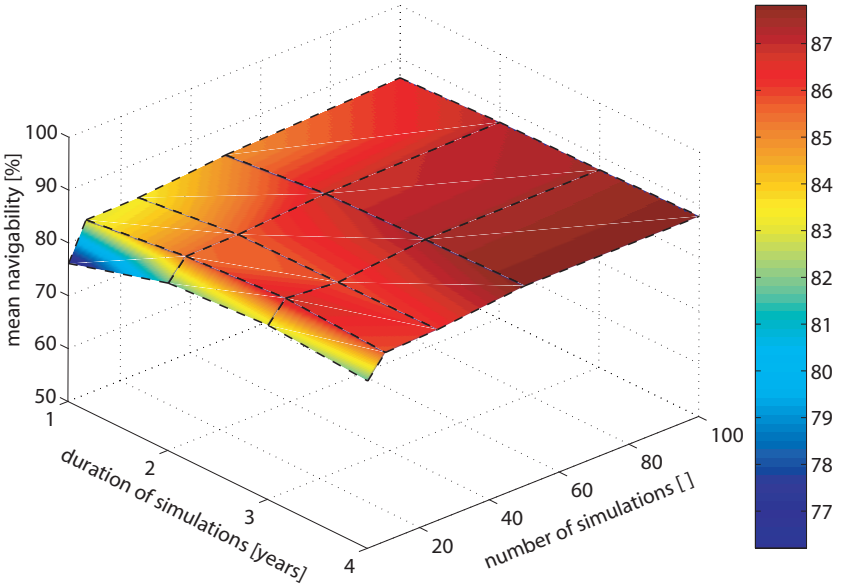

Figure 7.20: Development of the mean navigability, Delft3D

Conclusions

1. For a shorter time period, the uncertainty in the discharge is higher. This results in a higher uncertainty in the water depth and thus in the navigability of the river (Figures 7.13 and 7.18). The decrease of the 90% confidence interval is found to be logarithmic and seems to hold on even for a duration of the simulations longer than ten years (Figures 7.14(a) and 7.19(a)). The shorter the modelled time period, the more necessary is the use of Monte Carlo Analysis to take account of the high involved uncertainties.

2. The mean navigability shows to be independent of the duration of the simulations, only a certain sample size is necessary to get stable statistics. In the above shown example approx. 100 simulations seem to be sufficient (Figures 7.14(b) and 7.19(b)). This is in the same order as the estimated number of model runs from Section 7.1.

3. The reason for this behaviour can be found in the distributions of the discharge and the resulting water depth.

   From the above shown Figures 7.16(a),(c),(e) and 7.17(a),(c),(e) it can be seen that a variation of the standard deviation of the discharge of 400%, leads to variation of the standard deviation of the water depth of 300%. This variation of the standard deviation then influences the distribution of the 100 analysed simulations. A high variation in this parameter leads to a high uncertainty in the navigability. For a period of ten years, the variation of the standard deviation of the discharge has

decreased (see Figures 7.16(b),(d),(f)) and is lower than 30%. The variation of the standard deviation of the water depth has decreased as well and now lies at 20% (Figures 7.17(b),(d),(f)).

The mean discharge as well as the mean water depth and the resulting mean navigability stay in the same order, independent of the duration of the model runs (Figures 7.16(a) to (f) and 7.17(a) to (f)).

4. Both models show the same behaviour in terms that:

   (1) in both models the mean navigability stays constant over a varying duration;

   (2) for both models a minimum sample size of 100 simulations is needed to get a stable 90% confidence interval;

   (3) in both models the size of the confidence interval and thus the uncertainty in the navigability decreases with the duration of the simulations. Thus, the variation of the discharge has the same effect on both model results.

5. It can be concluded that for a very long duration of the simulations the distribution of the discharge of all simulations will be more or less similar. Thus, the distribution of the water depth and the resulting statistics of the conducted simulations will be similar as well. This will lead to a strong decrease of the uncertainty until a point, where the uncertainty in the navigability introduced by the uncertainty in the discharge is very small. Other uncertainties, like the uncertainties introduced by the model code will gain in importance compared to the uncertainty in the discharge.

   For this reason, for a longer time period a deterministic simulation to analyse the navigabilty of the river might be preferable instead of a Monte Carlo Analysis.

Chapter 8

Conclusions and Recommendations

This research uses stochastic modelling of river morphology to assess the navigability of a 37 km long stretch of the river Waal. The questions of the two groups of interest as well as further insights to be gained are shown in Section 1.2. Chapters 4 to 6 present the results of the two numerical models and a comparison with the measured data; several aspects of stochastical modelling are discussed in Chapter 7. This final chapter contains the conclusions and recommendations deduced from this thesis work. It is divided in two parts, in the first one the conclusions and recommendations for the river manager are shown, in the second part the same is done for the modeller.

8.1 Conclusions and recommendations concerning the model& data comparison

This section sums up the interests of the river manager on how to assess the navigability of the river with the help of the numerical models, as well as the comparison of the models with the measured data.

1. Capabilities and limitations of the models The one-dimensional SOBEK model is applicable for a very wide range of assessments of the navigability. Especially the navigability of the complete stretch, the fulfillment of the navigation requirements and periods of time with restricted navigability can be reproduced very well for the case of the applied correction for the transverse slope in bends following the approach of Talmon et al. [49]. These three features seem to be dominated by the uncertainty in the discharge. The two-dimensional morphological effects that are not included in SOBEK seem to be of minor importance. The similar patterns shown in the analysis of the navigability of each location along the river, indicate that the SOBEK model is able to predict the large-scale morphology (in the order of several kilometers) similar to the Delft3D model. Furthermore, the range of uncertainty of the navigability estimated by both models shows a high agreement. The uncertainty included in the discharge time series seems to have a similar effect on both model outputs.

The Delft3D model offers the opportunity to investigate the morphology and its effects on the navigability with a higher spatial resolution (100 m instead of 500 m) and in two dimensions, including the corresponding morphologic effects as well as the shifting behaviour of the navigation channel in curves. This becomes important when locations that form restrictions for the navigation traffic should be identified. Even if the comparison with the

Least Measured Depth data is not completely satisfying, the Delft3D results give the impression to be more trustworthy. One large disadvantage of the two-dimensional model is the higher computational effort, thus it has to be carefully balanced to what extent it is necessary to use it instead of the one-dimensional approach.

Both models do not give satisfying results for the comparison of the bottleneck location with the data of Least Measured Depth. Several reasons are responsible for this: (1) the bottleneck-criterion is very sensitive (only the one location with the smallest water depth, even if the difference is just one centimeter, is defined as bottleneck); (2) the dataset for the LMD is not complete; (3) the definition of LMDs is supposed to be influenced by different effects that are not included in the models (e.g. dredging, placement of buoys, navigation traffic, groyne flames).

In addition, the models show a bad agreement due to: (4) the different morphological effects that are included in the quasi-3D Delft3D model compared to the one-dimensional SOBEK model (transverse bed slope in bends, formation of shallow and deep parts in geometrical complex reaches); (5) the different computational grids used by both models (100 m for Delft3D, 500 m for SOBEK), which is responsible for the different scales on which morphologic changes can be predicted. Therefore, it is not recommendable to identify one single location as being limitative to navigation.

Possible improvements of the comparison are explained in the following section.

2. Possibilities and limitations of the data comparison Two different approaches can be followed for the future comparison of the model results with the data:

(1) The use of the Least Measured Depth data: In this case, the effects that avoid the occurrence of a LMD have to be included in the models. The placement of buoys has to be implemented into the analysis of the Least Measured Depth. For both models, the dredging and accompanied replacement of the dredged material has to be included in the modelling process. Eventually, it would be favorable if the models could predict morphologic effects like the formation of groyne flames and the correct evolution of ripples and dunes (so far bedforms are only included as a parameterisation).

(2) A second way could be to establish a new data set, independent of the bottleneck criterion. Instead, a criterion similar to the "navigability of each location" should be used. In this kind of analysis the navigability of each location is assessed individually. This prevents a dominating effect of one single location like the case of the bottleneck criterion and thus forms a criterion with a lower sensitivity. A completely new data set would be needed for this comparison. It would be advised that for a single stretch of the river (e.g. the in this research used 37 km long Midden-Waal), the water depth and the related channel width is measured and entered into a database for several permanent locations along the river on a daily basis. This would of course lead to a high effort in practice and thus has to be carefully considered. In this case the effect of dredging still has to be included into the models.

3. Model use in practice In this thesis the models are not used for predictions of changes in the navigability in the case of applied river measures. Nonetheless, one of the major applications of stochastic modelling of the navigability could be within the scope of the implementation of measures like floodplain lowering or summer dike removal considered in the Dutch "Room for the River" program. For this practical question it has

to be carefully considered which model to use, as resources are limited, and the spatial and temporal dimensions are significantly higher than the ones used in this research. For the application of large scale floodplain lowering or summer dike removal, it could be necessary to model a period of 20 or 30 years (in this research only five years are considered) and not only a short stretch of 37 km but for example the complete Waal, which is approx. 83 km long.

These circumstances more or less exclude the use of a two-dimensional model as the computational power is not available yet. On the other hand, it has to be argued if a two-dimensional model is really necessary. The one-dimensional SOBEK model shows good results for the navigability, especially with the applied parameterisation for the transverse slope in bends. Hence, one possibility could be to use a 1D model for large reaches of the model area, as well as to get first insights into the navigability of the complete stretch. For locations of special interest (e.g. bifurcation points) a two-dimensional model could be used. Besides the additional included morphological features, using a two-dimensional model for these locations has another important advantage: The implementation of features like groyne-extension or -shortening can be included directly two-dimensionally in the model, while for a one-dimensional model every effect has to be schematized first. With the help of this combined approach the desired insights could be gained with a still acceptable computational effort.

Finally, for a practical application, the in this research shown analysis of the navigability should not be used as "stand alone" analysis. The results of this work have to be combined with an analysis of the computed bed levels. That way, a very good picture of the state of the river and the resulting reactions of morphology and navigability to applied measures can be drawn. Especially the influence of the variation of the bed level on the variation in the water depth, and thus the formation of critical bottleneck locations for the navigation traffic would be of interest.

8.2 Conclusions and recommendations concerning stochastic modelling

In this section, the conclusions of the interests of the modeller concerning the behaviour of the uncertainty as well as different types of uncertainty which have not been assessed are discussed.

1. Minimum required sample size MCA turns out to be very computational extensive, which is due to the high number of simulations that need to be conducted. In this research a method is shown how to estimate the number of necessary simulations beforehand. The effort for stochastical modelling can thus be reduced. The method is also applicable for questions different than the one posed in this thesis. It can be used for both numerical models, and shows that the resulting numbers of required model runs are in the same order.

An interesting question in stochastic modelling, which still needs to be assessed in future research, is whether output samples could be gathered over time instead of separate simulations. For example, would one simulation with a duration of 100 years give the same statistics as 100 simulations with a duration of one year. In this case the computational effort could be reduced, because only one long-term simulation is necessary instead of a large number of short model runs [38].

2. Time dependency of the uncertainty The uncertainty expressed as the size of the 90% confidence interval is found to decrease with an increasing duration of the simulations, according to the decreasing uncertainty in the discharge. Both models show the same behaviour, which can be explained with the distribution functions of the discharge and the resulting distributions of the water depth. This finding leads to the conclusion that for a shorter time period the uncertainty in the discharge is high, thus the use of a Monte Carlo Analysis is recommended. On the other hand, for a very long duration of the simulations, a deterministic simulation might be more reasonable.

A question to investigate in upcoming research would be how this decrease in the uncertainty develops for time periods larger than the shown 10 years, thus from which point on it is no longer reasonable to use a MCA. This question is accompanied with the interest to examine how other involved uncertainties evolve with increasing time duration, e.g. whether a systematic error can accumulate and dominate over the in this research assessed uncertainty in the discharge. The following section gives a short overview of the uncertainties that are not examined in this work but still considered to be existent. The interpretation of model results for longer periods has to be handled with care. The SOBEK Rhine branches model for example was calibrated on a period of ten years. It is questionable if this model can be used for accurate predictions of 50 or 100 years in length.

For the practical application of a measure, the modelling period should be set as demanded by the problem, e.g. for floodplain lowering a duration of 20 or 30 years could be used. The output of the model then can easily be analysed for two different time spans, first for the entire 20 years, and a second time for a period of only one year. The uncertainty in the latter case will significantly increase. The outcome of those two analysis could be used as guidance for the river manager on a long- and a short-term basis: (1) the analysis of the complete model period shows where long-term influences and variabilities introduced by the implemented measures are high; (2) the short term analysis could give information about the influence of the measures during the first year and thus insight into locations which show a high variability. This could be used to identify locations that need special attention in the near future, like regular monitoring or dredging operations during the first year.

3. Importance of other uncertainties The discharge was found to be one of the most important parameters of uncertainty in the work of Van der Klis [52]. In her research it was seen that even the changes in bed level were dominated by the uncertainty in the discharge. Therefore, it was chosen to be the uncertain parameter to be assessed in this research. Yet, the discharge is not the only important uncertainty. Uncertainties in the hydraulic roughness and the grain size of the bed material for example could as well have large influence on the uncertainty of the navigability. The relative importance of these uncertainties is not investigated in this work and thus is an crucial subject of further research, which has to develop adequate descriptions of these uncertainties.

It can be expected that methodological uncertainty contributes to the uncertainty in the model results. This statement is founded on the sensitivity analysis done by Van der Klis [52]. The models seem to be very sensitive to the modelling choices. Hence, it cannot be excluded that a systematic error is included in the simulations, which leads to uncertainty in the model output.

Thus, the discharge is included and assessed as uncertain parameter in this research, but it should not be seen as the only source of uncertainty. Different other kinds of uncertainty could play a role, but are very difficult to quantify, if this is even possible.

4. Future model setup The discharge is found to be very important for the model output of this research. Yet, the discharge is only included in a very rough discretization. In the SOBEK model the discharge is taken to be invariant for periods of ten days. The same applies for the Delft3D model, here even a further step is necessary to save computational time: The discretization of the discharge in 16 stages from 500 m^3/s up to 8,000 m^3/s. This leads to large steps in the prediction of the distribution of the water depth and makes a post-processing inevitable. For future modelling, it should be considered to implement a finer discretization of the discharge, e.g. in steps of 100 m^3/s. This could be combined with a post-processing of the computed water levels, which then can be even interpolated to finer discretized values.

A decrease of the time increment could also be favorable if the computation power is available. One of the further important questions for navigation traffic is the chance that the river is navigable for a number of consecutive days. The discharge steps of 10 days are too large to give reasonable answer to this question.

This research shows that the influence of the uncertainty in the discharge on the uncertainty of the navigability is large. Monte Carlo Analysis proves to be a possibility to assess these uncertainties. One should be aware of uncertainties, and if sufficient resources are available, treat them. In this way, a better view of the possible states of rivers and influences of measures on the navigability can be established. Nonetheless, the dependency of the uncertainty on the time duration shows that stochastic modelling is not always reasonable. A deterministic modelling approach still has its justification for longer modelling periods.

The same conclusion accounts for the model choice. A two-dimensional model is not always necessary. For many of the relevant questions, a one-dimensional model can give sufficient insight with considerably lower effort.

Bibliography

[1] M. J. Baptist. *Modelling floodplain biogeomorphology.* Ph.D. dissertation, Delft University of Technology, The Netherlands, 2005.

[2] N.G Bhowmik, R. Xia, B.S. Mazunder, and T.W. Soong. Return flow in rivers due to navigation traffic. *Journal of Hydraulic Engineering*, pages 914–918, 1995.

[3] K. Blanckaert and H.J. De Vriend. Secondary flow in sharp open-channel bends. *Journal of Fluid Mechanics*, 498:353–380, 2004.

[4] A. Blom. *A vertical sorting model for rivers with non-uniform sediment and dunes.* Ph.D. dissertation, University of Twente, The Netherlands, 2003.

[5] H.J. De Vriend. A mathematical model of steady flow in curved shallow channels. *Journal of Hydraulic Research*, 15(1):37–54, 1977.

[6] H.J. De Vriend. Long-term morphodynamics of alluvial rivers and coasts. In G. Bianchi, editor, *Environmental Applications of Mechanics and Computer Science, CISM Courses and Lectures no. 409*, pages 1–19. Springer, 1999.

[7] H.J. De Vriend. Lecture Notes CT5311- River Dynamics, Section of Hydraulic Engineering, Delft University of Technology, The Netherlands, 2004.

[8] H.J. De Vriend. Onzekerheid in de Rivierwaterbouwkunde, Cursus Moderne Rivierkunde. Stichting Postacademisch Onderwijs in de Civiele Techniek en Bouwtechniek, Delft, The Netherlands (in Dutch), November 2004.

[9] M. De Vries. A morphological time-scale for rivers. In *Proceedings of the 16th Congress IAHR*, volume 2, paper B3, pages 17–23, Sao Paulo, 1975. DHL Publication. No. 147.

[10] M. De Vries. Use of models for river problems. Technical Report 51, UNESCO Publishing, 1993.

[11] M. De Wit. Hoe laag was het laagwater von 2003? *http://www.rijkswaterstaat.nl/*, (in Dutch), 2004.

[12] N. Douben. Knelpuntenanalyse Waal, Analyse van scheepvaartknelpunten op de Boven-Rijn en Waal, oplosingsrichtingen. Technical report, Ministerie van Verkeer en Waterstaat, Directoraat- Generaal Rijkswaterstaat, Notanr. 95.005, (in Dutch), 1995.

[13] B. Efron. *The Jackknife, the Bootstrap, and other resampling plans.* Society for Industrial and Applied Mathematics. Philadelphia publisher, 1982.

[14] ELWIS. ELektronisches Wasserstrassen- InformationsSystem. *http://www.elwis.de, (in German)*, 2004.

[15] Wikipedia Encyclopaedia. *http://de.wikipedia.org/*, (in German), 2005.

[16] F. Engelund and E. Hansen. *A monograph on Sediment transport in Alluvial Streams.* Teknisk Forlag, Copenhagen, 1967.

[17] EVD and NEDECO. Made in Holland/ Inland Waterway Transport. *Land + Water International*, (106), October 2004.

[18] R. Filarski and J.U. Brolsma. New opportunities for European Inland Navigation. *Bulletin of the Permanent International Association of Navigation Congress*, 63(66):110–122, 1989.

[19] G.H. Goldsteen and C.C. Glansdorp. The navigability of waterways. *The Hydrographic Journal*, (25):25– 33, 1998.

[20] J.M. Hammersly and D.C. Handscomb. *Monte Carlo Methods.* Methuen & Co Ltd., London, 1964.

[21] H. Havinga. Morphological effects of bend regulation measures in the Waal river. In *Proceedings of the 2nd IAHR Symposium on River, Coastal and Estuarine Morphodynamics*, pages 595– 604, Obihiro, Japan, 2001.

[22] M. Hirano. River bed degradation with armouring. *Transactions Japanese Society of Civil Engineering*, 3:194–195, 1971.

[23] WL|Delft Hydraulics. Delft3D-Flow: Simulation of multi-dimensional hydrodynamic flows and transport phenomena, including sediments; User Manual. Technical report - http://www.wldelft.nl/d3d/, 2003.

[24] WL|Delft Hydraulics. Delft3D-MOR: Simulation of long-term interaction of waves, currents, sediment transport and morphological development; User Manual. Technical report - http://www.wldelft.nl/d3d/, 2003.

[25] WL|Delft Hydraulics. SOBEK River Estuary; User Manual. Technical report - www.sobek.nl, 2002.

[26] P.Ph. Jansen, J. Bendegom, J. Van den Berg, M. De Vries, and A. Zanen. *Principles of River Engineering, The non-tidal alluvial river.* Delftse Uitgevers Maatschappij, Delft, 1979.

[27] P. Jesse and D.F. Kroekenstoel. *1-D Morfologisch Sobek Rijntakken model.* RIZA rapport 2001.040 (in Dutch), 2001.

[28] P. Y. Julien, G. J. Klaassen, M. Ten Heggeler, and A. W. E. Wilbers. Case Study: Bed resistance of the Rhine river during the 1998 flood. *Journal of Hydraulic Engineering*, 128(12):1042–1050, 2002.

[29] H. Kalweit, W. Buck, K. Felkel, H. Gerhard, K.-R. Nippes, B. Ploeger, W. Schmitz, and J. Van Malde. *Der Rhein unter der Einwirkung des Menschen: Ausbau, Schiffahrt, Wasserwirtschaft. KHR-Arbeitsgruppe "Anthropogene Einflüsse auf das Abflussregime", Bericht Nr. I-11.* (in German), 1993.

[30] M. G. Kleinhans. *Sorting out sand and gravel: sediment transport and deposition in sand-gravel rivers.* Ph.D. dissertation, Utrecht University, The Netherlands, 2002.

[31] D. Klopstra, H. J. Barneveld, J. M. Van Noortwijk, and E. H. Van Velzen. Analytical model for hydraulic roughness of submerged vegetation. In *27th Congress of the International Association for Hydraulic Research*, volume A, pages 775–780, San Francisco, 1997.

[32] D. W. Knight. Flow and sediment transport in two-stage channels. In *Proceedings of IAHR Symposium on River, Coastal and Estuarine Morphodynamics*, pages 1–20, Obihiro, Japan, 2001.

[33] K.-W. Koch. *Der Rhein: Verkehrsweg im Herzen Europas, Schienenwege und Schiffahrt.* Verlag für spezielle Verkehrsliteratur, (in German), 1985.

[34] E. Lattermann. *Wasserbau-Praxis, Band 1: Gewässerbau, Flussbau, Stauanlangen, Wasserkraftwerke.* Bauwerk-Verlag, Berlin, (in German), 1999.

[35] E. Meyer-Peter and R. Müller. Formulas for bed load transport. In *Proceedings of the 2nd Congress IAHR*, volume 2, pages 39–64, Stockholm, 1948.

[36] H. Middelkoop. *Twee Rivieren. Rijn en Maas in Nederland.* RIZA rapport 98.041, Arnhem, (in Dutch), 1998.

[37] H. Middelkoop and J.C.J. Kwadijk. Towards Integrated Assessment of the Implications of Global Change for Water Management - The Rhine Experience. *Physics and Chemistry of the Earth Part B: Hydrology Oceans and Atmosphere*, 26(7-8):553–560, 2001.

[38] M. G. Morgan and M. Henrion. *Uncertainty; A Guide to dealing with Uncertainty in Quantitative Risk and Policy Analysis.* Cambridge University Press, 1990.

[39] A. J. Odgaard. Transverse bedslope in alluvial channels bends. *Journal of the Hydraulic Division, ASCE*, 107, 1981.

[40] E.S. Pearson and M.G. Kendall. *Studies in the History of Statistics and Probability.* Griffin, London, 1970.

[41] Zentralkommission für die Rheinschifffahrt. Jahresbericht 2000/2001. *http://www.ccr-zkr.org/*, (in German), 2001.

[42] Zentralkommission für die Rheinschifffahrt. Wirtschaftliche Entwicklung der Rheinschifffahrt 2002, Rhein- und Binnenschifffahrtsstatistiken. *http://www.ccr-zkr.org/*, (in German), 2002.

[43] K. Shiono and Y. Muto. Complex flow mechanisms in compound meandering channels with overbank flow. *Journal of Fluid Mechanics*, 376:2221–2261, 1998.

[44] A. Siegfried. *Morphologische Reaktion der Waal auf Baggermaßnahmen.* Diplomarbeit, Arnheim, The Netherlands, (in German), 2000.

[45] C.J. Sloff. Tweedimensionale veranderingen in de vaarweg van de Waal. Technical Report Q3811.00, WL|Delft Hydraulics, Delft, The Netherlands, (in Dutch), 2004.

[46] A.M. Sorber. Oeversedimentatie tijdens de hoogwaters van 1993/1994 en 1995. Technical report, Ministerie van Verkeer en Waterstaat, Directoraat- Generaal Rijkswaterstaat, Notanr. 97.015, (in Dutch), 1997.

[47] H.N. Southgate. Guideline for error assessment in models of long-term coastal morphology. In *IAHR Symposium on River, Coastal and Estuarine Morphodynamics*, volume 2, pages 299–308, University of Genova, 1999.

[48] N. Struiksma, K.W. Olesen, C. Flokstra, and H.J. De Vriend. Bed deformation in curved alluvial channels. *Journal of Hydraulic Research*, 23(1):57–79, 1985.

[49] A.M. Talmon, M.C.L.M. Van Mierlo, and N. Struiksma. Laboratory measurements of the direction of sediment transport on transverse alluvial-bed slopes. *Journal of Hydraulic Research*, 33(4):495–517, 1995.

[50] W.B.M. Ten Brinke, M.M. Schoor, A.M. Sorber, and H.J.A. Berendsen. Overbank sand deposition in relation to transport volumes during large-magnitude floods in the Dutch sand-bed Rhine river system. *Earth Surface Processes and Landforms*, 23:809–824, 1998.

[51] L. Van Bendegom. Enige beschouwingen over riviermorfologie en rivierverbetering. *De Ingenieur*, 59(4):b1–b11 (in Dutch), English translation: Some considerations on river morphology and river improvement, Nat. Res. Council of Canada, Tech. Transl. 1054, 1963, 1947.

[52] H. Van der Klis. *Uncertainty Analysis applied to Numerical Models of River Bed Morphology.* Ph.D. dissertation, Delft University of Technology, The Netherlands, 2003.

[53] P.H.A.J.M. Van Gelder. *Statistical Methods for Risk-Based Design of Civil Structures.* Ph.D. Dissertation, Delft University of Technology, The Netherlands, 2000.

[54] L.C. Van Rijn. Sediment transport- Part 3: bedforms and alluvial roughness. *Journal of Hydraulic Engineering*, 110:1733–1754, 1984.

[55] L.C. Van Rijn. *Principles of sediment transport in rivers, estuaries and coastal seas.* Amsterdam Aqua Publications, 1993.

[56] L.C. Van Rijn. Estuarine and coastal sediment problems. In *Proceedings of the Ninth International Symposium on River Sedimentation*, pages 105–120, Yichang, China, 2004.

[57] B.G. Van Vuren. *Stochastic modelling of lowland river morphology.* Ph.D. dissertation, Delft University of Technology, The Netherlands, 2005 (in press).

[58] S. Van Vuren. *Stochastic modelling of river morphology, Literature review.* Ph.D. research project, Delft University of Technology, The Netherlands, 2002.

[59] S. Van Vuren and H.J. Barneveld. Invloed basisalternatieven Ruimte voor de Rivier op de bevaarbaarheid van en onderhoudsbaggerwerk op de rivier: Een stochastische benadering. Technical Report PR748.10, Rijkswaterstaat, Directie Oost Nederland, (in Dutch), 2004.

[60] S. Van Vuren and H.J. De Vriend. River hydraulic and morphological response to navigation: a case study of the river Rhine in The Netherlands. In *Ninth International Symposium on River Sedimentation,*, pages 1645–1653, Yichang, China, 2004.

[61] S. Van Vuren, H. Van der Klis, and H.J. De Vriend. Large-scale floodplain lowering along the River Waal: a stochastic prediction of morphological impacts. In D. Bousmar and Y. Zech, editors, *River Flow 2002*, volume 2, pages 903–912, Louvain-la-Neuve, Belgium, 2002. Balkema Publisher.

[62] V.A. Vanoni and L.S. Wang. Relation between bed forms and friction in streams. *Journal of the Hydraulic Divisions*, 93(3):121–144, 1967.

[63] P.J. Visser. Bodemontwikkeling rijnszsteem: Een verkenning van omvang, oorzaken, toekomstige ontwikkelingen en mogelijke maatregelen. *Technische Universiteit Delft, Sectie Waterbouwkunde*, (in Dutch), 2000.

[64] P.J. Visser, H. Havinga, and W.B.M. Ten Brinke. Hoe houden we de rivier bevaarbaar? Daling zomerbed Rijntakken vraagt aandacht. *Land + Water*, 9(9):24–27 (in Dutch), 1999.

[65] S.S.Y. Wang and W. Weiming. River sedimentation and morphological modelling - the state of the art and future development. In *Ninth International Symposium on River Sedimentation*, volume I, pages 71–94, Yichang, China, 2004.

[66] Ministerie van Verkeer en Waterstaat. Waal Hoofdtransportas, Rivierkundige Maatregelen. *Rijkswaterstaat directie Gelderland, Notanr. RIZA 91.030, Arnhem*, (in Dutch), 1991.

[67] Ministerie van Verkeer en Waterstaat. Projectdirectie Nationaal Verkeers- en Vervoersplan - Nationaal Verkeers- en Vervoersplan 2001-2020. *ISBN 90-369-1941-x. http://www.minvenw.nl/nvvp/*, (in Dutch), 2001.

[68] S. Wieprecht. Manuskript zur Vorlesung Verkehrswasserbau, Institut für Wasserbau, Universität Stuttgart, Germany, (in German), 2004.

[69] A. Wilbers. *The development and hydraulic roughness of subaqueous dunes.* Netherlands Geographical Studies 323, ISSN 0169-4839, 227, Ph.D. dissertation, Utrecht University, The Netherlands, 2004.

[70] B.R. Winkley. The cause and cure of low water navigation problems on alluvial rivers. *Bulletin of the Permanent International Association of Navigation Congress*, 64:188–196, 1989.

[71] M.F.M. Yossef and G.J. Klaassen. Reproduction of groyne-induced river bed morphology using LES in a 2-D morphological model. In D. Bousmar and Y. Zech, editors, *River Flow 2002*, volume 2, pages 1099–1108, Louvain-la-Neuve, Belgium, 2002. Balkema Publishers.